Chemical and Isotopic Studies of Granitic Archean Rocks, Owl Creek Mountains, Wyoming

U.S. GEOLOGICAL SURVEY PROFESSIONAL PAPER 1388–A, B, C

Chemical and Isotopic Studies of Granitic Archean Rocks, Owl Creek Mountains, Wyoming

Geochemistry and Petrogenesis of an Archean Granite from the Owl Creek Mountains, Wyoming

By J. S. STUCKLESS, A. T. MIESCH, *and* D. B. WENNER

Geochronology of an Archean Granite, Owl Creek Mountains, Wyoming

By C. E. HEDGE, K. R. SIMMONS, *and* J. S. STUCKLESS

Uranium-Thorium-Lead Systematics of an Archean Granite from the Owl Creek Mountains, Wyoming

By J. S. STUCKLESS, I. T. NKOMO, *and* K. A. BUTT

U.S. GEOLOGICAL SURVEY PROFESSIONAL PAPER 1388–A, B, C

Isotopic and geochemical studies are used to determine the age and origin of an Archean granite in the Owl Creek Mountains, Wyoming

UNITED STATES GOVERNMENT PRINTING OFFICE, WASHINGTON : 1986

DEPARTMENT OF THE INTERIOR

DONALD PAUL HODEL, *Secretary*

U.S. GEOLOGICAL SURVEY

Dallas L. Peck, *Director*

Library of Congress Cataloging in Publication Data

Main entry under title:
Chemical and isotopic studies of granitic Archean rocks, Owl Creek Mountains, Wyoming.
(Geological Survey Professional Paper ; 1388)
Bibliography: p.
Supt. of Docs. no.: I 19.16: 1388A–C
Contents: Geochemistry and petrogenesis of an Archean granite from the Owl Creek Mountains, Wyoming / J.S. Stuckless, A. T. Miesch, D. B. Wenner—Geochronology of an Archean granite, Owl Creek Mountains, Wyoming / C. E. Hedge, K. R. Simmons, J. S. Stuckless—Uranium-thorium-lead systematics of an Archean granite from the Owl Creek Mountains, Wyoming / J. S. Stuckless, I. T. Nkomo, K. A. Butt.
1. Geology, Stratigraphic—Precambrian. 2. Radioactive dating. 3. Geochemistry—Wyoming—Owl Creek Mountains. 4. Geology—Wyoming—Owl Creek Mountains. I. Stuckless, John S. II. Series.
QE653.C49 1986 551.7'1 85–600130

For sale by the Branch of Distribution
Books and Open-File Reports Section
U.S. Geological Survey
Federal Center
Box 25425
Denver, CO 80225

CONTENTS

[Letters designate the chapters.]

Geochemistry and Petrogenesis of an Archean Granite from the Owl Creek Mountains, Wyoming

By J. S. STUCKLESS, A. T. MIESCH, *and* D. B. WENNER

CHEMICAL AND ISOTOPIC STUDIES OF GRANITIC ARCHEAN ROCKS, OWL CREEK MOUNTAINS, WYOMING

U.S. GEOLOGICAL SURVEY PROFESSIONAL PAPER 1388–A

CONTENTS

ILLUSTRATIONS

TABLES

CHEMICAL AND ISOTOPIC STUDIES OF GRANITIC ARCHEAN ROCKS, OWL CREEK MOUNTAINS, WYOMING

GEOCHEMISTRY AND PETROGENESIS OF AN ARCHEAN GRANITE FROM THE OWL CREEK MOUNTAINS, WYOMING

By J. S. STUCKLESS, A. T. MIESCH, and D. B. WENNER

ABSTRACT

Analytical data consisting of 37 oxides in 39 samples of granite from the Owl Creek Mountains, Wyo., have been examined by extended Q-mode factor analysis. The results show that 25 samples are cogenetic and that 29 oxides in these samples have retained a magmatically controlled distribution. For these samples and oxides, a five-factor model can account for most of the variance, and therefore the compositional data can be explained as the product of mixing (or unmixing) of five end members. The mixing (or unmixing) may have resulted entirely from fractional crystallization in two distinct stages, or alternatively, the first stage may have been mostly fractional fusion. Either interpretation can be correlated with variations in whole-rock values of $\delta^{18}O$. These variations reflect inhomogeneities in the protolith, which was probably similar to the highly diverse suite of metamorphic rocks intruded by the granite. The two-stage history indicated by either interpretation of the model is compatible with derivation of the granite or initial differentiation at approximately 3 kb and near water-saturated conditions, followed by differentiation at a lower pressure of perhaps 1.0–0.5 kb. Although extended Q-mode factor analysis cannot uniquely identify the exact end members that controlled evolution of the granite, it has identified the types of processes necessary to explain the chemical complexities observed for the pluton, and the model presented here is compatible with all available data.

INTRODUCTION

The major uranium deposits of Wyoming are located within sedimentary rocks derived from the Archean granites of central Wyoming (Seeland, 1976, 1978). Isotopic studies have shown that most of these granites lost large quantities of uranium (Rosholt and Bartel, 1969; Rosholt and others, 1973; Nkomo and others, 1978; Stuckless and Nkomo, 1978; Nkomo and others, 1979) at about the same time that the uranium deposits were formed (Ludwig, 1978, 1979). The genesis of these granites is therefore of economic interest. The granite of the Owl Creek Mountains (fig. 1) not only is closely associated with uranium deposits in overlying Tertiary sediments, but locally hosts near-economic deposits of uranium (Yellich and others, 1978).

The Owl Creek Mountains consist of a discontinuous series of east-west-striking fault blocks that are composed of Archean metamorphic rocks, granites, and diabase dikes (Thaden, 1980a, b, and c). The metamorphic rocks are a multiply-folded and petrologically complex assemblage of volcanic and sedimentary precursors that can be subdivided into three roughly east-west-striking groups (Hamil, 1971). The southern group is dominated by metasediments, with subordinate metavolcanic rocks that are preserved as biotite-muscovite schists. The middle group consists of diverse lithologies, including schists that contain biotite, garnet, hornblende, cummingtonite, cordierite, sillimanite, andalusite, and sericite, as well as quartzite, iron-formation, and minor siliceous marble. The northern group has the largest metavolcanic component. Rock types here include hornblende or biotite quartz-plagioclase gneisses and small amounts of crossbedded quartzite. Uralatized gabbroic dikes also occur in this group (Condie, 1967). The highest metamorphic grade observed in the three zones is the sillimanite-cordierite-muscovite-almandine subfacies of the Abukuma type of metamorphism (Winkler, 1967). Metabasalts and metadacites, which are presumably part of the northern group, are exposed in the Wind River Canyon (near locality 24, fig. 1). These yield a rubidium-strontium whole-rock age of 2,755±100 Ma (Mueller and others, 1981).

The metamorphic sequence is intruded by granitic rocks and associated pegmatites which have reported ages of 2,645±60 Ma (lead-lead whole-rock, Nkomo and others, 1978) and 2,663 and 2,584 Ma (rubidium-strontium for pegmatitic muscovite and microcline respectively, Giletti and Gast, 1961). The contact between the intrusive and the metamorphic rocks commonly forms a wide mixed zone (fig. 1). Within the mixed zone the metamorphic rocks and xenoliths of these rocks are generally migmatitic (Thaden, 1980b). Modal analyses (Nkomo and others, 1978) show that the intrusive rock is a granite according to the IUGS classification (Streckeisen, 1973).

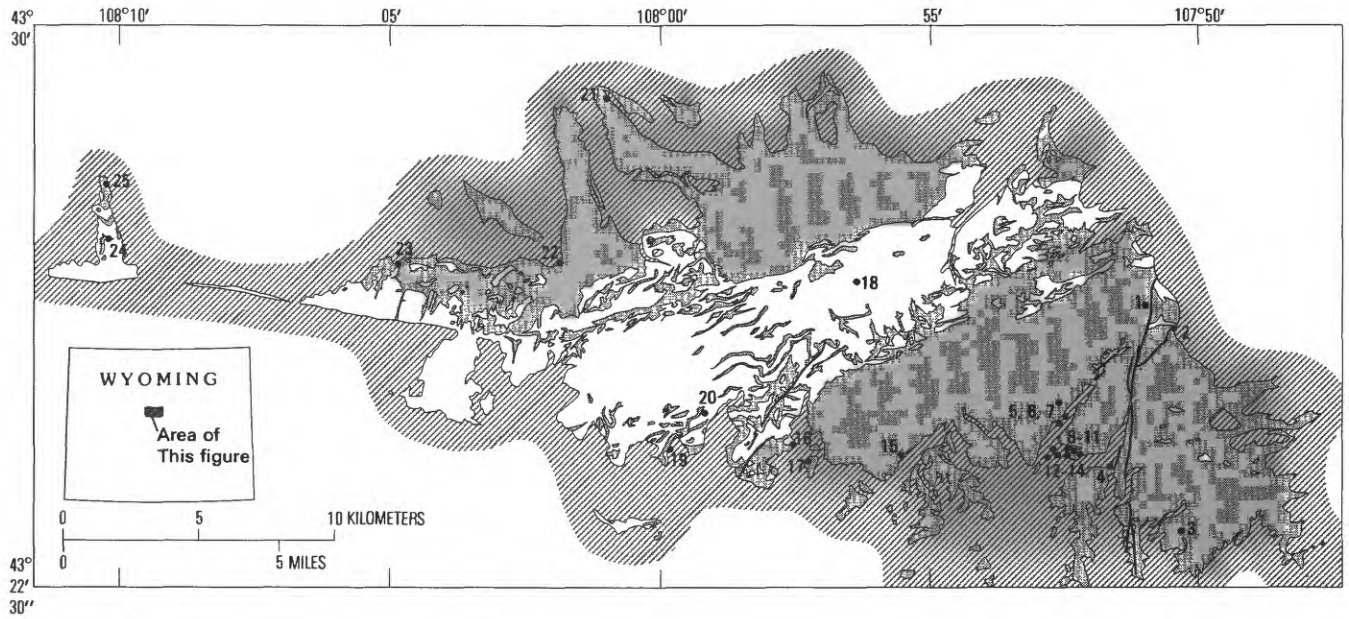

POST-PROTEROZOIC COVER

DIABASE DIKES

GRANITE

METAMORPHIC ROCKS

SAMPLE LOCALITY

1	TDG13	6	TDG44, TDG45	15	GP-4
2	TDG12, DP-1	7	4343	16	TD6
3	DP-8	8	DP-3	17	GP-3
4	DP-2	9	23432	18	DKCH-1
5	GP-5	10	58-66, 58-80, 58-98, 58180, 58188, 58317 58392, 58398	19	GP-1
				20	GP-2
		11	TDG46, TDG47	21	TD22
		12	41591, 41596	22	TDG21
		13	30501, 30511, 29394, 29467	23	TDG20
				24	TDG16
		14	32466, 32496	25	TDG24

FIGURE 1.—Generalized geologic map of the Owl Creek Mountains (modified from Thaden, 1980a, b, and c) showing sample localities. Locality numbers are used as identification numbers on subsequent plots, and where more than one sample were collected at a single locality, samples are distinguished by an alphabetic suffix that corresponds to the order shown on figure 1. For example, sample TDG12 has a plot identification of 2a.

The granite and metamorphic rocks are cut by diabase dikes that trend north to northeasterly. Potassium-argon whole-rock analyses for east-west-trending dikes just west of the area shown on figure 1 yield ages of 1,900–2,100 Ma (Condie and others, 1969).

The crystalline rocks were uplifted and eroded during late Precambrian time. Topographic highs formed on this erosional surface protrude 60–100 m into the Paleozoic sedimentary rocks (Nkomo and others, 1978). Periods of sedimentation continued through the Paleocene and attained a total thickness of more than 7000 m of shallow marine and coastal plain sediments. The Laramide orogeny, which began in Late Cretaceous time, was accompanied by faulting that uplifted the Owl Creek Mountains more than 5300 m (Keefer and Love, 1963) and caused a stratigraphic separation of more than 7000 m along the south side of the range (Nkomo and others, 1978). The faulting, which may have occurred along zones of weakness in the Precambrian basement, was probably responsible for the development of brecciated zones along the southern side of the range (Yellich and others, 1978; Bramlett and others, 1982). Brecciation was particularly intense near the north Canning area (sample localities 4–14, fig. 1). This brecciated zone was mineralized with uranium during the Cenozoic (Nkomo and others, 1978). Most recently, the Owl Creek Mountains were partly buried by volcanic detritus during the late Eocene and reexhumed during the Quaternary.

METHODS

ANALYTICAL PROCEDURES

Major-element concentrations (reported in weight percent, tables 1, 2, and 3) were obtained by two methods. Most samples were analyzed by the single so-

TABLE 1.—*Original chemical data and CIPW normative mineralogy (O) for 25 samples from the Owl Creek Mountains, Wyo., and corresponding data represented by the factor solution (R)*

Sample No.	DP-3		23432		29394		29467		30501		30511		32466		32496	
Plot I.D.	8		9		13c		13d		13a		13b		14a		14b	
	O	R	O	R	O	R	O	R	O	R	O	R	O	R	O	R
								Weight percent								
SiO_2	71.89	72.24	73.92	73.52	70.87	71.21	71.45	71.61	72.81	72.69	72.29	72.36	73.24	72.94	73.34	73.44
Al_2O_3	14.88	14.77	14.38	14.52	14.94	14.87	15.01	14.97	14.52	15.63	14.54	14.68	14.53	14.72	14.39	14.46
FeO(t)	2.07	2.07	1.53	1.40	2.92	2.80	2.41	2.31	1.89	1.93	2.24	2.14	1.65	1.58	1.53	1.52
MgO	.83	.59	.28	.35	1.01	.91	.78	.70	.68	.56	.67	.65	.30	.41	.25	.38
CaO	1.90	1.71	1.31	1.53	2.12	2.09	1.91	1.93	1.73	1.72	1.92	1.82	1.60	1.59	1.60	1.49
Na_2O	4.19	4.07	4.02	4.03	4.34	4.47	4.23	4.47	4.06	4.15	4.14	4.20	4.11	4.03	4.12	4.01
K_2O	3.69	4.09	4.22	4.32	3.23	3.04	3.73	3.53	3.86	3.89	3.74	3.68	4.21	4.37	4.43	4.36
TiO_2	.30	.25	.16	.14	.33	.36	.27	.26	.24	.23	.26	.27	.17	.17	.15	.16
								Parts per million								
MnO	366	360	234	242	537	539	447	439	326	352	321	393	214	265	329	273
Rb_2O	205	200	188	195	213	182	217	191	209	192	194	186	174	197	212	207
BaO	1137	931	797	785	693	818	722	802	811	808	788	838	904	885	720	753
SrO	314	267	233	233	281	309	276	296	289	259	296	273	238	251	227	224
ThO_2	43.80	41.15	28.05	26.91	48.55	45.68	29.03	31.44	39.29	35.49	41.97	40.16	27.48	30.58	27.84	28.85
La_2O_3	64.87	60.74	22.37	25.81	82.64	79.67	41.53	48.98	51.44	48.36	66.12	60.11	36.41	36.12	32.43	28.86
Ce_2O_3	122.8	103.5	37.66	41.59	133.5	132	67.75	76.80	81.80	80.25	105.7	101	55.96	59.94	53.56	46.79
Nd_2O_3	36.33	34.96	11.95	14.11	43.56	45.46	24.14	26.09	27.76	27.52	35.08	34.53	21.16	19.88	18.75	16.38
Sm_2O_3	4.96	4.81	1.71	2.02	5.65	6.32	3.63	3.70	3.86	3.87	4.57	4.75	3.03	2.71	2.52	2.56
Eu_2O_3	1.07	.866	.650	.707	.990	.979	.810	.806	.780	.817	.880	.889	.650	.753	.620	.687
Gd_2O_3	3.41	2.60	1.06	1.55	3.42	3.68	3.26	2.87	1.84	2.41	2.33	2.62	1.94	1.71	2.15	2.14
Tb_2O_3	.44	.36	.16	.23	.48	.51	.44	.43	.29	.34	.36	.36	.27	.25	.32	.33
Dy_2O_3	2.36	1.89	.93	1.34	2.57	2.80	2.37	2.50	1.73	1.90	2.07	1.92	1.35	1.36	1.80	1.91
Tm_2O_3	.140	.099	.070	.083	.150	.148	.120	.146	.120	.108	.110	.101	.060	.077	.110	.124
Yb_2O_3	.81	.52	.42	.46	.80	.76	.60	.78	.65	.57	.60	.52	.32	.41	.62	.69
Lu_2O_3	.110	.066	.060	.062	.100	.095	.080	.100	.090	.074	.070	.066	.040	.055	.090	.094
Ta_2O_5	2.04	.78	.44	.53	.69	.80	.59	.63	.87	.67	.39	.68	.31	.57	.72	.73
HfO_2	4.62	4.59	4.15	3.57	4.77	5.73	4.43	4.87	3.96	4.42	4.45	4.70	3.71	3.75	4.15	3.97
ZrO_2	223	203	187	155	263	253	207	224	182	192	235	205	169	169	181	169
Sc_2O_3	4.04	3.99	2.71	2.75	5.46	5.83	4.45	4.99	4.85	3.89	4.24	4.20	2.95	2.99	2.87	3.29
CoO	5.56	4.47	2.44	2.70	7.29	6.80	5.39	5.42	4.79	4.22	5.22	4.84	2.56	3.17	2.44	2.95
								Norms (weight percent)								
Q	26.58	26.88	30.00	28.71	25.02	25.67	25.49	25.21	28.33	27.71	27.16	27.46	28.13	27.59	27.50	28.54
C	.53	.55	.82	.43	.45	.43	.54	.29	.52	.46	.20	.50	.30	.47	.00	.44
Or	21.88	24.20	25.00	25.58	19.12	17.99	22.07	20.87	22.84	23.00	22.11	21.76	24.91	25.86	26.20	25.78
Ab	35.56	34.48	34.09	34.13	36.80	37.92	35.87	37.88	34.43	35.22	35.09	35.56	34.82	34.19	34.95	33.99
An	9.43	8.49	6.50	7.62	10.54	10.38	9.51	9.61	8.58	8.55	9.53	9.03	7.97	7.88	7.68	7.41
Wo	.00	.00	.00	.00	.00	.00	.00	.00	.00	.00	.00	.00	.00	.00	.13	.00
En	2.07	1.47	.70	.87	2.52	2.26	1.94	1.75	1.70	1.39	1.66	1.61	.75	1.02	.63	.96
Fs	3.38	3.46	2.59	2.38	4.92	4.65	4.07	3.89	3.13	3.24	3.74	3.57	2.80	2.68	2.63	2.60
Il	.57	.47	.31	.27	.63	.69	.52	.50	.46	.43	.50	.51	.32	.32	.29	.30

lution technique (Shapiro and Brannock, 1962; Suhr and Ingamells, 1966). Stated accuracies in terms of percent of amount present are ±1 percent for SiO_2, ±2 percent for Al_2O_3, and ±1 to 10 percent for the remaining major oxides. Sample numbers prefixed by TD were analyzed using high precision X-ray fluorescence spectrometry (Taggart and others, 1982), and ferrous/ferric ratios were determined by wet chemical methods (Peck, 1964). Precision for the X-ray fluorescence results is ±2 percent of the amount present (2σ).

Minor- and trace-element concentrations (those reported in parts per million, tables 1, 2, and 3, except for U, Th, Rb, Sr, and Zr) were determined by neutron activation analysis using methods modified from those of Gordon and others (1968). Estimated accuracies range from 5 to 20 percent of the amount present except for a few samples for which high uranium contents produced large interferences for a few rare earth elements (REE). For these samples, the data reported in tables 1 and 2 were obtained by extrapolation between the chondrite normalized abundances of the adjacent REE. Chondrite values of Evensen and others (1978) are used for normalization throughout this paper.

Most uranium and thorium concentrations were obtained by isotope dilution and mass spectrometry (Stuckless and others, this volume). These values were supplemented by delayed neutron determinations for uranium (Millard, 1976) and γ-ray spectrometry determinations for thorium (Bunker and Bush, 1966). The general accuracy of reported uranium and thorium concentrations is ±2 percent (2σ).

Most rubidium and strontium concentrations were

TABLE 1.—*Original chemical data and CIPW normative mineralogy (O) for 25 samples from the Owl Creek Mountains, Wyo., and corresponding data represented by the factor solution (R)*—Continued

Sample No. / Plot I.D.	GP-3 17		GP-5 5		4343 7		TDG12 2a		TD-13 1		TDG21 22		TD22 21		TDG47 11b		58180 10d	
	O	R	O	R	O	R	O	R	O	R	O	R	O	R	O	R	O	R
								Weight percent										
SiO_2	74.89	74.85	75.55	75.86	73.76	73.72	74.16	74.33	74.34	74.20	74.50	74.53	74.76	74.98	76.75	76.80	76.19	76.02
Al_2O_3	13.16	13.39	14.13	13.76	14.03	13.80	13.62	13.78	13.92	13.76	14.08	13.83	13.72	13.59	12.69	12.83	12.95	13.19
FeO(t)	1.17	1.39	.30	.61	1.71	2.06	2.11	1.58	1.55	1.71	1.46	1.35	1.53	1.36	1.50	1.20	.89	1.21
MgO	.21	.08	.10	.07	.32	.49	.20	.31	.30	.35	.31	.21	.20	.24	.30	.35	.27	.26
CaO	.32	.08	1.39	1.18	1.21	.99	.96	.89	.82	.88	.64	.78	.60	.80	1.25	1.23	.91	.98
Na_2O	2.49	2.73	3.68	3.67	3.13	3.13	3.03	3.31	3.33	3.17	3.27	3.11	3.17	3.04	3.65	3.68	3.19	3.30
K_2O	7.48	7.26	4.68	4.67	5.35	5.33	5.63	5.46	5.40	5.53	5.45	5.89	5.75	5.64	3.57	3.62	5.08	4.73
TiO_2	.08	.05	.05	.06	.23	.26	.12	.15	.14	.19	.11	.13	.10	.15	.16	.19	.36	.16
								Parts per million										
MnO	134	229	96	98	351	337	342	271	320	281	190	199	163	205	329	279	299	221
Rb_2O	429	394	202	193	274	274	303	280	275	280	279	282	232	268	169	191	231	229
BaO	776	697	556	588	978	940	606	746	762	844	909	879	726	840	263	203	682	545
SrO	49	5	122	156	147	140	98	121	104	123	88	116	85	109	136	107	130	104
ThO_2	50.97	49.91	21.18	23.23	69.00	69.80	35.13	48.48	57.42	57.86	59.01	51.11	55.40	56.78	39.85	39.88	56.76	48.99
La_2O_3	45.61	36.82	6.11	2.78	96.21	94.88	50.57	50.79	66.71	68.78	57.59	53.23	48.85	62.30	29.66	29.64	47.96	46.07
Ce_2O_3	87.95	72.24	11.10	5.51	190.6	175.4	84.92	93.31	128.8	127.7	102.6	100.7	95.13	118.4	50.88	53.31	84.30	86.98
Nd_2O_3	35.13	29.23	3.81	3.09	75.18	62.08	30.93	34.40	43.54	45.93	32.96	36.18	36.55	42.64	22.21	23.01	28.24	33.08
Sm_2O_3	7.23	6.78	.66	.72	11.78	9.54	5.72	6.02	7.37	7.48	5.27	6.04	6.50	6.85	4.45	4.21	4.48	5.52
Eu_2O_3	.300	.274	.730	.612	1.06	.873	.640	.627	.640	.725	.570	.651	.650	.733	.720	.728	.740	.736
Gd_2O_3	7.36	6.85	.690	.746	4.18	4.93	4.16	4.36	4.56	4.53	3.40	3.78	4.38	3.72	3.51	2.96	2.96	3.18
Tb_2O_3	1.25	1.11	.13	.12	.66	.67	.59	.66	.60	.65	.50	.55	.55	.52	.51	.44	.46	.45
Dy_2O_3	7.60	6.54	.79	.69	3.89	3.48	3.18	3.70	3.01	3.52	2.74	3.00	2.55	2.70	2.68	2.43	2.49	2.37
Tm_2O_3	.575	.472	.070	.058	.250	.209	.200	.251	.190	.228	.220	.200	.120	.175	.190	.174	.180	.161
Yb_2O_3	3.34	2.77	.44	.35	1.44	1.16	1.14	1.44	1.06	1.30	1.29	1.16	.61	1.01	1.01	.98	1.08	.92
Lu_2O_3	.480	.389	.070	.053	.200	.158	.150	.199	.140	.179	.190	.162	.080	.140	.140	.136	.160	.128
Ta_2O_5	3.59	3.09	.96	.51	1.86	2.03	2.28	1.83	2.07	1.94	1.63	1.79	.80	1.76	.93	1.06	2.29	1.40
HfO_2	7.20	6.25	2.68	2.69	7.23	5.91	4.68	5.21	5.17	5.41	4.73	4.72	4.35	4.78	4.24	4.52	4.27	4.51
ZrO_2	293	217	100	92.7	302	215	193	190	205	196	109	171	97.9	164	87.4	132	153	141
Sc_2O_3	5.32	5.50	1.16	1.08	5.26	4.48	3.42	4.15	4.39	4.10	3.00	3.24	2.93	3.01	2.38	3.07	3.46	2.77
CoO	1.15	.63	.40	.39	3.02	3.40	2.17	2.21	1.78	2.47	1.57	1.45	1.51	1.54	1.83	2.02	1.29	1.53
								Norms (weight percent)										
Q	29.90	29.82	32.90	33.58	30.80	30.81	31.00	30.60	30.96	30.90	31.71	30.94	31.53	32.63	37.56	37.55	35.42	35.37
C	.39	.90	.48	.53	.89	1.10	.81	.80	1.12	.96	1.65	.93	1.19	1.02	.54	.63	.56	.86
Or	44.28	42.94	27.67	27.61	31.67	31.54	33.32	32.32	31.94	32.73	32.26	34.86	34.00	33.38	21.13	21.40	30.06	27.99
Ab	21.13	23.12	31.20	31.09	26.53	26.50	25.65	28.10	28.21	26.90	27.68	26.34	26.90	25.79	30.95	31.14	27.01	27.95
An	1.59	.42	6.92	5.85	6.02	4.91	4.76	4.42	4.06	4.38	3.19	3.86	3.00	4.00	6.20	6.10	4.50	4.87
Wo	.00	.00	.00	.00	.00	.00	.00	.00	.00	.00	.00	.00	.00	.00	.00	.00	.00	.00
En	.52	.19	.25	.18	.81	1.22	.50	.77	.75	.88	.76	.52	.51	.60	.76	.87	.67	.65
Fs	2.04	2.52	.48	1.05	2.84	3.43	3.74	2.70	2.68	2.89	2.54	2.32	2.67	2.29	2.55	1.95	1.11	1.99
Il	.15	.09	.09	.11	.44	.49	.23	.29	.27	.36	.21	.24	.19	.29	.31	.36	.68	.31

measured by isotope dilution and mass spectrometry (Hedge and others, this volume). These determinations were supplemented by X-ray fluorescence analyses, which have a general accuracy of ±5 percent. All zirconium concentrations were obtained by X-ray fluorescence for which the estimated precision is ±5 percent (2σ).

Oxygen isotopic compositions (table 4) were determined according to the methods of Taylor and Epstein (1962). Results are reported relative to SMOW (standard mean ocean water) and are accurate to ±0.1 per thousand (2σ).

Q-MODE FACTOR ANALYSIS

The mathematical method used to develop the petrogenetic model for the granites of the Owl Creek Mountains is the extended form of Q-mode factor analysis (Miesch, 1976a, b, 1981). The main difference between conventional Q-mode factor analysis and the extended form is that the extended method allows conversion of the scaled analyses back to the original metric so that the final model can be more easily interpreted in petrologic terms.

For extended Q-mode factor analysis, the analytical data for each oxide variable are scaled so that each variable has the same mean and variance; this assures that the major oxides, especially SiO_2 and Al_2O_3, will have no greater influence than the minor constituents in model development. The scaled analytical data are conceptually represented as N vectors in M-dimensional space, where N is the number of samples

TABLE 1.—*Original chemical data and CIPW normative mineralogy (O) for 25 samples from the Owl Creek Mountains, Wyo., and corresponding data represented by the factor solution (R)*—Continued

Sample No. / Plot I.D.	41591 12a		41596 12b		DP-8 3		DP-2 4		TDG46 11a		58-66 10a		58-80 10b		58-98	
	O	R	O	R	O	R	O	R	O	R	O	R	O	R	O	R
								Weight percent								
SiO_2	71.36	71.88	74.65	74.50	73.25	73.09	73.83	73.71	75.36	75.19	76.21	76.46	77.29	76.84	76.38	76.44
Al_2O_3	15.00	14.87	14.10	14.32	14.87	14.44	14.43	14.41	13.62	13.73	13.07	13.35	12.95	12.99	13.51	13.29
FeO(t)	2.26	2.25	1.11	.89	1.23	1.78	1.04	1.38	1.50	1.16	.90	.64	.66	.89	.72	.83
MgO	.70	.68	.16	.14	.37	.46	.30	.32	.30	.28	.10	.05	.25	.19	.14	.19
CaO	2.01	1.87	1.26	1.28	1.32	1.50	1.39	1.40	1.10	1.28	.87	.93	1.10	1.02	1.19	1.22
Na_2O	4.33	4.26	3.57	3.76	4.45	4.16	3.98	3.85	3.73	3.80	3.42	3.43	3.41	3.41	3.77	3.71
K_2O	3.82	3.70	4.94	4.88	4.15	4.23	4.68	4.61	4.20	4.29	5.23	4.97	4.12	4.42	4.07	4.09
TiO_2	.28	.27	.05	.07	.18	.17	.17	.14	.06	.13	.08	.06	.10	.13	.12	.11
								Parts per million								
MnO	465	409	166	127	347	349	209	229	230	228	136	114	111	179	130	176
Rb_2O	208	188	205	202	188	226	172	209	193	205	253	222	216	207	181	187
BaO	897	894	793	800	677	629	937	814	553	515	466	493	414	396	309	377
SrO	300	288	260	198	203	217	184	214	131	162	112	105	113	97	119	133
ThO_2	36.65	39.79	23.72	24.19	28.44	25.79	30.13	31.52	33.25	29.93	33.27	29.95	33.27	40.44	29.71	29.06
La_2O_3	71.58	62.43	11.76	12.45	21.39	24.35	27.66	31.26	12.28	19.45	7.10	8.11	30.62	27.33	11.73	11.38
Ce_2O_3	112.5	104.2	20.29	21.29	38.16	35.63	49.30	53.36	17.24	32.93	14.25	17.35	63.96	52.65	23.71	20.47
Nd_2O_3	38.33	35.22	7.39	7.10	16.12	13.52	19.38	18.38	8.26	13.44	7.25	8.59	29.03	21.69	10.38	9.93
Sm_2O_3	4.83	4.79	1.47	1.06	3.57	2.63	2.67	2.74	1.86	2.50	1.74	2.03	4.61	3.87	2.14	1.99
Eu_2O_3	.990	.894	.610	.637	.650	.599	.740	.704	.630	.648	.570	.564	.730	.695	.580	.658
Gd_2O_3	2.76	2.68	1.16	.854	3.70	3.20	2.02	1.87	1.47	2.19	1.72	1.87	2.70	2.39	1.45	1.62
Tb_2O_3	.41	.37	.17	.13	.61	.52	.31	.28	.23	.34	.28	.30	.39	.35	.21	.25
Dy_2O_3	2.37	1.99	.95	.75	3.60	3.19	1.75	1.54	1.44	1.97	1.68	1.70	2.11	1.83	1.15	1.39
Tm_2O_3	.120	.103	.060	.052	.220	.218	.100	.097	.120	.140	.140	.134	.140	.134	.090	.107
Yb_2O_3	.62	.53	.31	.31	1.23	1.23	.58	.54	.70	.80	.82	.80	.82	.77	.52	.62
Lu_2O_3	.080	.066	.040	.045	.160	.167	.070	.074	.100	.111	.110	.115	.120	.109	.070	.088
Ta_2O_5	.90	.68	.26	.51	.69	.99	.61	.74	.62	.84	1.08	1.00	.83	1.09	.59	.69
HfO_2	45.11	4.77	2.30	2.83	3.89	4.69	4.55	3.72	5.83	3.87	2.22	3.35	4.00	3.92	3.65	3.43
ZrO_2	189	215	107	118	164	198	154	156	131	139	89.4	103	144	112	126	106
Sc_2O_3	4.06	4.43	1.08	1.52	6.08	4.60	2.97	2.74	2.27	2.76	1.88	1.67	2.06	2.07	2.12	1.88
CoO	5.63	5.16	1.17	1.12	3.10	3.61	2.40	2.44	1.89	1.88	.72	.15	1.11	.91	.81	1.06
								Norms (weight percent)								
Q	24.51	26.31	31.21	30.32	27.22	27.46	28.64	29.15	33.59	32.67	33.63	34.97	38.50	37.04	35.59	35.72
C	.08	.47	.61	.51	.67	.30	.29	.53	.94	.51	.20	.64	.87	.75	.72	.55
Or	22.64	21.88	29.21	28.90	24.55	25.01	27.68	27.30	24.83	25.36	30.93	29.39	24.35	26.13	24.08	24.22
Ab	36.69	36.07	30.22	31.86	37.72	35.27	33.73	32.65	31.62	32.20	28.96	29.03	28.91	28.84	31.96	31.40
An	10.00	9.28	6.26	6.37	6.53	7.43	6.92	6.96	5.46	6.36	4.34	4.62	5.48	5.07	5.92	6.05
Wo	.00	.00	.00	.00	.00	.00	.00	.00	.00	.00	.00	.00	.00	.00	.00	.00
En	1.76	1.69	.40	.36	.93	1.16	.74	.80	.75	.69	.25	.14	.63	.46	.35	.47
Fs	3.78	3.77	2.00	1.54	2.02	3.06	1.67	2.34	2.70	1.97	1.55	1.11	1.07	1.46	1.14	1.38
Il	.54	.52	.10	.14	.35	.32	.32	.27	.12	.25	.15	.11	.19	.25	.23	.22

and M is the number of oxide variables. Dividing each scaled analysis by the square root of the sum of the squared values adjusts each vector to unit length. The M-reference axes for the vector system (each representing one of the oxide variables) are then replaced by the principal-component axes. The first principal-component axis represents the average composition of all samples and lies at the center of the sample-vector cluster. The second principal-component axis lies at a right angle to the first and is oriented so that the sample vectors have as high a projection on it as possible. Similarly the third principal-component axis lies at right angles to the first two, but again is so oriented that the sample vectors have as high a projection on it as possible. There are M principal-component axes in all, the same as the number of oxide variables.

The coordinates (projections) of the sample vectors with respect to the principal-component axes constitute a new data set that describes the composition of samples in terms of the principal components rather than in terms of the M oxides. The advantage here is that the successive principal components are of decreasing importance in terms of explaining compositional variation in the sample set. Commonly the compositional variability represented by the first few principal components (denoted by m) is almost as great as that represented by all M components. Consequently, elimination of all but the first several principal components will yield a data set that is not drastically different from that represented by all the principal components. The simplification thus attained greatly facilitates the development of a petrogenetic model that will account

TABLE 2.—*Chemical data and CIPW normative mineralogy for 14 samples not accounted for by the factor solution*

Sample No.	58188	58317	58392	58398	DP-1	GP-1	GP-2	GP-4	TD-6	TDG16	TDG20	TDG24	TDG44	TDG45
Plot I.D.	10e	10f	10g	10h	2b	19	20	15	16	24	23	25	6a	6b
							Weight percent							
SiO_2	71.06	76.35	49.90	52.82	75.22	75.79	70.54	71.35	74.10	76.09	73.69	74.58	75.55	50.97
Al_2O_3	15.05	13.29	15.38	15.30	14.20	14.92	18.21	17.33	14.11	14.00	15.08	14.11	12.96	13.46
FeO(t)	2.62	.59	11.44	10.38	.49	.51	.36	.89	.29	.64	1.20	1.29	1.34	14.68
MgO	1.32	.15	8.05	8.06	.04	.04	.04	.20	.05	.05	.05	.20	.20	5.90
CaO	3.56	1.20	9.57	7.75	.87	.23	.14	6.05	.03	.91	.32	.73	.34	10.91
Na_2O	3.76	3.80	2.65	2.89	4.60	5.81	10.31	3.53	2.32	4.26	4.42	4.13	2.41	1.83
K_2O	2.13	4.50	1.32	1.65	4.50	2.50	.29	.42	9.00	4.00	4.96	4.84	6.94	.84
TiO_2	.30	.06	1.43	.86	.02	.01	0.00	.09	.01	.01	.01	.05	.07	1.13
							Parts per million							
MnO	416	86	1630	1706	147	898	940	125	57	71	2042	104	841	2379
Rb_2O	131	227	62	86	217	725	22	37	598	148	403	191	521	26
BaO	801	112	356	570	40	131	6	136	142	77	114	296	273	162
SrO	345	69	236	175	12	9	8	703	29	44	19	56	52	135
ThO_2	13.30	30.16	1.75	2.18	9.30	5.94	3.23	44.03	2.44	6.04	8.27	19.01	33.26	2.40
La_2O_3	23.52	3.95	12.24	9.44	5.31	1.71	.53	34.51	2.48	5.18	2.22	20.67	9.99	9.30
Ce_2O_3	36.98	8.80	25.10	19.67	10.04	4.49	1.41	67.52	5.03	6.78	4.39	35.15	20.04	19.20
Nd_2O_3	12.65	5.23	13.87	11.27	3.59	3.34	1.04	23.04	2.70	2.91	2.53	13.72	9.48	11.40
Sm_2O_3	2.19	1.36	3.64	2.95	.72	1.06	.34	3.63	.63	.67	.56	2.65	2.19	3.12
Eu_2O_3	.616	.471	1.30	1.04	.059	.042	.037	.445	.175	.197	.100	.289	.291	.909
Gd_2O_3	1.61	1.59	3.44	3.29	.807	1.37	.438	2.24	.965	1.23	.811	2.55	2.43	3.66
Tb_2O_3	.25	.29	.59	.63	.14	.25	.08	.41	.21	.30	.25	.39	.49	.63
Dy_2O_3	1.35	1.93	3.74	4.33	.92	1.69	.54	2.59	1.43	2.35	1.67	2.36	3.54	4.15
Tm_2O_3	.104	.183	.326	.472	.081	.155	.051	.219	.127	.233	.155	.150	.557	.431
Yb_2O_3	.65	1.14	2.02	3.10	.50	.96	.33	1.32	.88	1.50	.98	.83	4.16	2.88
Lu_2O_3	.097	.173	.301	.482	.075	.139	.050	.188	.138	.226	.147	.108	.754	.450
Ta_2O_5	.56	.81	.45	.38	.32	58.2	23.6	1.60	2.14	.52	17.4	.87	8.58	.30
HfO_2	3.38	2.24	2.73	2.01	3.00	1.46	2.83	4.33	.24	.69	4.87	2.45	4.24	2.40
ZrO_2	189	65.7	155	105	76.2	42.7	59.5	183	27.0	49.7	75.6	17.6	28.1	47.2
Sc_2O_3	5.84	.98	28.7	64.6	.97	1.03	.08	4.03	.34	1.12	.40	3.23	6.91	61.2
CoO	7.57	.51	70.7	52.8	.08	.25	.10	.94	.63	.71	.96	1.13	1.56	46.4
							Norm (weight percent)							
Q	29.47	33.82	0.00	0.00	28.91	31.42	8.74	35.32	25.80	33.45	27.07	29.15	32.82	0.00
C	.08	.00	.00	.00	.18	2.24	.69	.08	.50	1.00	1.85	.76	.86	.00
Or	12.63	26.59	7.83	9.78	26.61	14.81	1.71	2.50	53.24	23.63	29.30	28.61	41.06	4.94
Ab	31.88	32.15	22.43	24.52	38.95	49.19	87.22	29.88	19.64	36.07	37.45	34.99	20.42	15.53
An	17.68	5.94	26.19	23.89	4.32	1.14	.70	30.04	.15	4.53	1.60	3.60	1.70	26.02
Wo	.00	.00	8.91	6.10	.00	.00	.00	.00	.00	.00	.00	.00	.00	11.74
En	3.30	.37	6.26	12.14	.10	.10	.10	.50	.13	.13	.13	.50	.50	13.80
Fs	4.39	1.00	5.92	10.86	.90	1.09	.84	1.50	.53	1.17	2.57	2.30	2.50	23.96
Fo	.00	.00	9.67	5.58	.00	.00	.00	.00	.00	.00	.00	.00	.00	.63
Fa	.00	.00	10.08	5.50	.00	.00	.00	.00	.00	.00	.00	.00	.00	1.21
Il	.58	.11	2.71	1.63	.04	.02	.00	.17	.02	.02	.02	.10	.13	2.15

for suitably large proportions of the variations in all M oxides.

Retention of only the first m principal components projects the sample vectors from an M-dimensional space into an m-dimensional space (where M is greater than m). Because projection moves vectors, the sample vectors will represent slightly different compositions before and after projection. Methods described in reports cited previously can be used to derive the compositions represented by the vectors after projection, and comparison of these recomputed compositions with the original compositions is used to judge the degree to

TABLE 3.—*Miscellaneous chemical data for 39 samples from the Owl Creek Mountains, Wyo.*

Sample No.	Weight percent				Parts per million			
	Fe_2O_3	H_2O	P_2O_5	CO_2	U	Cs	Sb	Cr
58-66	0.95	1.06	0.07	0.02	5.29	4.82	0.058	0.89
58-80	.62	1.46	.05	.01	11.80	3.25	.071	1.76
58-98	.69	.67	.08	.01	5.37	2.90	.038	1.28
58180	.42	.65	.10	.02	160.5	2.16	.050	1.50
58188	.86	2.60	.13	.43	5.77	3.03	.030	11.6
58317	.50	.66	.07	.11	2008	4.73	.090	.50
58392	2.70	1.61	.16	.06	1.87	.61	.030	181
58398	2.60	2.65	.15	.02	1.09	1.79	.030	247
DP-1	.46	.57	.07	.02	2.87	3.00	.048	.71
DP-2	.83	.76	.11	.01	14.58	2.47	.020	3.21
DP-3	1.50	.91	.15	.01	3.39	6.41	.050	18.8
GP-1	.30	.94	.16	.02	.99	46.9	.380	1.90
GP-2	.09	.57	.14	.02	.29	1.62	.950	1.90
GP-3	.80	.83	.10	.01	9.22	11.4	.020	1.83
GP-4	.80	1.24	.11	.01	17.00	1.72	.020	.35
GP-5	.11	.56	.06	.01	3.45	12.70	.220	.67
23432	.47	.37	.09	.04	21.88	1.96	.103	23.9
29394	.88	.68	.16	.02	11.94	4.54	.100	41.5
29467	.77	.46	.17	.05	8.42	3.81	.115	34.7
30501	.40	.50	.12	.04	9.30	2.72	.103	30.0
30511	.24	.53	.13	.04	9.16	2.82	.102	34.3
32466	.50	.40	.08	.06	6.15	1.77	.020	25.9
32496	.36	.33	.09	.06	14.44	2.68	.118	24.7
41591	.61	.49	.12	.04	11.90	3.94	.103	35.7
41596	1.23	.21	.05	.03	12.80	1.68	.098	19.5
4343	.11	.74	.12	.02	16.80	5.74	.082	2.90
DP-8	.46	.61	.12	.02	4.16	1.83	.020	6.11
TD-6	.32	.04	.05	.00	.40	34.30	.176	32.1
TDG12	2.32	.24	.05	.00	11.54	5.10	.248	57.4
TD-13	1.71	.49	.05	.00	3.72	3.21	.106	20.9
TDG16	.70	.30	.05	.00	3.77	1.95	.086	23.3
TDG20	1.33	.08	.05	.00	2.42	3.60	.128	39.9
TDG21	1.59	.75	.05	.00	2.29	5.18	.056	15.8
TD22	1.66	.66	.05	.00	2.44	2.02	.081	27.3
TDG24	1.42	.22	.05	.00	4.68	1.84	.205	45.1
TDG44	1.48	.10	.05	.00	14.08	7.87	.214	5.78
TDG45	16.00	.19	.05	.00	2.78	.42	.300	101
TDG46	1.65	.20	.05	.00	71.79	2.29	.275	14.8
TDG47	1.64	.02	.05	.00	78.41	1.74	.197	5.47

which the projection distorts the data. The effect of projections for different m's is examined on factor-variance diagrams. If large proportions of the variances in the oxide variables can be retained only by setting m to some value near M, little reduction in the complexity of the problem is possible; however, if the recomputed data derived for small m's are nearly the same as the original data, the problem may be greatly simplified. By convention, the value of m is referred to as the number of factors and is equal to the number of end members that must be mixed and (or) unmixed in a petrologic mixing model.

Commonly, m end members will be sufficient to account for the variation in all but a few of the oxide variables or in all but a few of the samples. It is always possible to account for the remaining unexplained variance in the oxides or samples by increasing m, but doing so may also obscure a simple underlying compositional structure and greatly complicate the process of developing an acceptable mixing model that accounts for most of the oxides or samples or both.

TABLE 4.—*Oxygen isotope compositions for granitic and metamorphic rocks from the Owl Creek Mountains, Wyo.*

[Values reported in parts per thousand relative to standard mean ocean water]

Sample	$\delta^{18}O$	Sample	$\delta^{18}O$
DP-3	6.9	4343	7.4
23432	7.5	TDG13	8.1
29394	7.7	TDG21	7.5
29467	8.2	TD22	7.2
30501	7.6	TDG47	8.1
30511	7.8	58180	7.6
32466	7.5	58188	5.2
32496	7.9	58317	8.1
41591	8.0	58392	7.8
41596	7.4	58398	4.9
DP-8	7.8	TD-6	6.5
DP-2	7.3	DP-1	5.8
TDG46	8.6	GP-2	7.3
58-66	7.6	DKCH-167	6.7
58-80	8.0	DKCH-207	5.1
58-98	8.0	DKCH-263	6.9
GP-3	7.8	DKCH-274	6.4
GP-5	7.8	DKCH-279	6.5

The oxide variables not adequately accounted for by m end members are easily identified on the factor-variance diagram. Samples not well accounted for are identified by comparatively large values of a badness-of-fit measure which is here defined as equal to the average absolute value of $(X_{comp}-X_{obs})/X_{obs}$ across the M oxide variables, where X_{obs} is the observed (raw) oxide value and X_{comp} is the corresponding value after projection of the sample vectors into m-dimensional space.

The badness-of-fit measure has a second application, which is used in the current study. Methods described in the reports cited previously can be used to project sample vectors not included in the original analysis into the m-dimensional vector system. After projection, the badness-of-fit measure can be used to test samples of doubtful relation to the main body or sequence for compositional compatibility with the main sequence.

Once the m-dimensional system of sample vectors has been established, the task is then to select m reference vectors that represent m petrologic phases that are thought to have been involved in the processes of mixing and (or) unmixing (precipitation). Methods that can be used to find m petrologically meaningful reference axes have been summarized previously (Miesch, 1981), but they consist in general of either using compositions represented by hypothetical vectors in selected positions within the vector cluster, or using compositions of actual sample vectors providing that the compositions are adequately represented in the m-dimensional cluster. One of the reference (end-member) vectors used in the current study is an actual sample vector. The others were hypothetical, and therefore it is

improbable that they represent the exact compositions that controlled evolution of the granite. The hypothetical vectors do, however, represent the types of compositions needed to explain the observed data.

Finally, the derived model consists of m end-member compositions, each composition represented by one of the selected reference axes, and N sets of m mixing proportions. The end-member compositions are in the metric of the original data (weight percent), and the m mixing proportions for each of the N samples sum to unity. Positive mixing proportions indicate addition of the respective end member to the compositional system, whereas negative proportions indicate subtraction (fractionally crystallized solidus or residuum of fractional fusion). Mathematical mixing of the end-member compositions in the quantities indicated by the mixing proportions yields an approximation of the original data; the closeness of the approximation for each oxide and for a given value of m is given by the factor-variance diagram.

A Q-MODE MODEL FOR GRANITES OF THE OWL CREEK MOUNTAINS

Q-mode factor analysis was used for two different purposes. The first purpose was to identify cogenetic samples and oxides in these samples that had been little affected by postmagmatic processes. Non-cogenetic samples and oxides known to have been affected by postmagmatic events were included as a test to insure that the method correctly identified misfit data. The second purpose was to develop a petrogenetic model. It should be pointed out that end members used in the model are not unique, but are analogous to describing plagioclase compositions in terms of An_5 and An_{95}. Such compositions would be as mathematically accurate as conventionally used end members and could be used if the true end members were unknown.

ANOMALOUS OXIDES AND SAMPLES

The total data set available for the study consisted of analyses for 37 oxides in 39 samples. Although it was known beforehand that a few of the oxide concentrations were controlled in large part by late-magmatic and weathering processes, that some of the samples were hydrothermally altered, and that others were of doubtful relation to the main bodies of granite, the entire data set was used to derive a factor-variance diagram. The data for the diagram (not shown) are given in table 5 and indicate that although most of the oxides can be accounted for by five or six factors, there are at least nine notable exceptions (Fe_2O_3, FeO, H_2O, P_2O_5, CO_2, UO_2, Sb_2O_3, Cr_2O_3 and Cs_2O). H_2O and CO_2 contents and the oxidation state of iron are known to be strongly affected by postmagmatic processes in most igneous rocks; therefore, H_2O and CO_2 were eliminated as variables, and ferrous and ferric iron were combined as total FeO (FeO(t)). Similarly, many of the samples used in this study either gained or lost uranium (Stuckless and others, this volume); therefore, UO_2 was eliminated from the data. Cs_2O has been found to be poorly explained in at least one other study (Stuckless and Miesch, 1981) and was readily removed in leaching experiments of the Proterozoic Sherman Granite (Zielinski and others, 1981). It is apparently also lost during devitrification of volcanic rocks (Zielinski and others, 1977). Cs_2O was therefore not used in further factor analyses. Also eliminated were P_2O_5, Sb_2O_3, and

TABLE 5.—*Proportions of the variances of 37 oxides in 39 samples accounted for by factor models with 2 through 10 factors*

	Number of factors								
Oxide	2	3	4	5	6	7	8	9	10
SiO_2	0.16	0.92	0.93	0.94	0.96	0.96	0.95	0.96	0.96
Al_2O_3	.09	.07	.54	.74	.75	.82	.83	.83	.88
Fe_2O_3	.08	.43	.53	.60	.61	.70	.69	.80	.95
FeO	.03	.55	.60	.59	.76	.79	.86	.90	.95
MgO	.15	.93	.93	.92	.96	.97	.99	.99	.99
CaO	.10	.91	.92	.93	.91	.90	.90	.98	.99
Na_2O	.08	.30	.64	.89	.89	.89	.94	.97	.97
K_2O	.15	.35	.72	.81	.84	.87	.86	.92	.95
H_2O	.01	.23	.32	.38	.44	.73	.78	.78	.85
TiO_2	.04	.88	.88	.88	.90	.90	.92	.93	.94
P_2O_5	.00	.08	.38	.41	.63	.76	.82	.82	.83
CO_2	.00	.01	.18	.38	.39	.56	.56	.60	.84
MnO	.31	.58	.60	.72	.74	.74	.73	.73	.78
Rb_2O	.00	.32	.60	.61	.90	.91	.91	.92	.92
BaO	.58	.62	.66	.66	.72	.73	.73	.78	.79
SrO	.10	.25	.57	.58	.57	.63	.81	.95	.96
ThO_2	.84	.85	.87	.87	.88	.88	.88	.89	.89
UO_2	.01	.02	.03	.18	.41	.44	.74	.82	.85
La_2O_3	.74	.78	.79	.85	.88	.87	.89	.90	.91
Ce_2O_3	.75	.79	.79	.86	.89	.88	.90	.92	.92
Nd_2O_3	.72	.78	.78	.86	.88	.87	.91	.93	.93
Sm_2O_3	.63	.72	.77	.85	.87	.86	.92	.93	.94
Eu_2O_3	.20	.73	.77	.79	.80	.86	.88	.88	.88
Gd_2O_3	.31	.50	.72	.80	.81	.86	.90	.90	.91
Tb_2O_3	.16	.38	.71	.79	.81	.91	.94	.94	.94
Dy_2O_3	.06	.31	.69	.76	.78	.94	.95	.95	.95
Tm_2O_3	.01	.25	.74	.77	.78	.95	.95	.95	.95
Yb_2O_3	.04	.24	.74	.76	.76	.91	.91	.91	.91
Lu_2O_3	.05	.22	.70	.71	.72	.85	.86	.86	.86
Cs_2O	.09	.30	.35	.35	.78	.79	.81	.94	.94
Ta_2O_5	.21	.39	.39	.53	.72	.75	.79	.84	.90
HfO_2	.57	.58	.58	.71	.71	.73	.74	.77	.78
ZrO_2	.57	.65	.72	.73	.77	.82	.83	.83	.83
Sb_2O_3	.24	.34	.35	.74	.75	.77	.80	.80	.81
Sc_2O_3	.15	.89	.92	.92	.93	.93	.92	.93	.94
Cr_2O_3	.12	.73	.72	.71	.80	.83	.86	.87	.90
CoO	.14	.92	.91	.91	.95	.95	.98	.98	.98

Cr_2O_3. Variations in content of these oxides are fairly well accounted for by five- and six-factor models; however, many of the determinations were at or slightly below the detection limits of the analytical methods.

Of the 39 samples, 14 had badness-of-fit measures that were distinctly poorer than the other 25 and were not used in derivation of the final model. For geologic reasons 12 of the 14 samples were suspected of having little or no genetic relationship to the main granite body. Samples 58392, 58398, and TDG45 are banded, mafic drill-core samples and, on the basis of the Q-mode factor analysis, are interpreted to be xenoliths of the older metamorphic sequence rather than mafic segregates. Samples GP–2 and GP–4 are albitized and silicified-epidotized granite respectively. They have apparently been too severely altered to preserve any recognizable genetic relationship to the granite. Samples DP–1, GP–1, and TDG20 are garnetiferous and show metamorphic textures; sample TD–6 is a graphic granite; sample TDG16 is a tourmaline-bearing granite; sample 58188 is a gneissic granite; and sample 58317 is a mineralized aplite. Samples TDG24 (the only seemingly normal sample from the Wind River Canyon) and TDG44 (a drill-core sample for which the REE pattern is similar to that of the garnetiferous samples) were eliminated solely on the basis of factor-analysis results. The combined adjustments to the original data set resulted in a matrix of 29 oxides by 25 samples. This matrix was used to develop the petrogenetic model.

TABLE 6.—*Proportions of the variances of 29 oxides in 25 samples accounted for by factor models with 2 through 10 factors*

	Number of factors								
Oxide	2	3	4	5	6	7	8	9	10
SiO_2	0.56	0.81	0.93	0.98	0.99	0.99	0.99	0.99	0.99
Al_2O_3	.69	.70	.90	.92	.93	.93	.95	.95	.98
FeO(t)	.31	.79	.79	.82	.84	.95	.98	.99	.99
MgO	.47	.81	.83	.86	.88	.88	.89	.89	.91
CaO	.87	.92	.93	.92	.92	.93	.95	.98	.98
Na_2O	.84	.88	.89	.92	.92	.94	.97	.97	.98
K_2O	.65	.74	.96	.96	.96	.97	.97	.97	.97
TiO_2	.29	.63	.70	.70	.75	.91	.91	.97	.97
MnO	.33	.76	.80	.85	.87	.87	.87	.88	.89
Rb_2O	.47	.68	.78	.86	.88	.89	.96	.97	.97
BaO	.14	.30	.82	.84	.84	.91	.91	.94	.94
SrO	.89	.88	.89	.89	.90	.89	.90	.90	.92
ThO_2	.17	.79	.79	.88	.88	.90	.90	.94	.94
La_2O_3	.02	.92	.92	.96	.96	.97	.97	.98	.98
Ce_2O_3	.00	.90	.90	.96	.95	.98	.98	.99	.99
Nd_2O_3	.01	.88	.88	.93	.93	.95	.96	.99	.99
Sm_2O_3	.11	.92	.92	.93	.93	.94	.95	.98	.98
Eu_2O_3	.37	.62	.68	.80	.79	.87	.88	.91	.95
Gd_2O_3	.26	.78	.78	.91	.92	.92	.94	.95	.95
Tb_2O_3	.31	.73	.74	.94	.94	.95	.96	.97	.97
Dy_2O_3	.29	.65	.66	.93	.93	.96	.96	.97	.97
Tm_2O_3	.41	.63	.64	.92	.91	.96	.96	.96	.96
Yb_2O_3	.44	.63	.64	.90	.90	.95	.96	.96	.96
Lu_2O_3	.46	.63	.64	.88	.88	.95	.95	.95	.95
Ta_2O_5	.43	.66	.67	.71	.75	.86	.93	.93	.96
HfO_2	.06	.60	.60	.64	.91	.92	.95	.97	.98
ZrO_2	.03	.54	.57	.67	.71	.82	.91	.94	.99
Sc_2O_3	.02	.65	.65	.85	.84	.91	.95	.95	.95
CoO	.56	.91	.91	.95	.96	.96	.96	.97	.97

DETERMINATION OF END MEMBERS

Although the factor-variance diagram (fig. 2) shows that three factors account for much of the variance in the 29 oxides in the 25 samples, five factors are required to account for the variance in some of the minor elements. (See also table 6.) The approach used was therefore to first derive a plausible three-factor (end-member) model and then refine it into the final five-factor model. Consequently, the sample vectors were first projected from the original 29-dimensional space ($M=29$) into a three-dimensional space. The three-dimensional vector cluster is represented by the stereographic projection in figure 3.

The vector configuration (fig. 3) reveals two separate compositional trends, one that extends from the upper-right portion of the diagram to the lower-central part (trend A) and the other that extends from the lower-central to the upper-left part (trend B). Judging from the differentiation indices of Thornton and Tuttle (1960) calculated for the compositions represented by the vectors, magma evolution proceeded along trend A towards the lower-central part of the diagram and then towards the upper left along trend B. Therefore, the composition of the initial parent material, liquid or solid, is probably represented best by a vector near the upper-right portion of trend A, possibly near the vector that represents sample 29394 (13c on fig. 3), which has the lowest differentiation index of all 25 samples.

Compositional changes along trend A could have resulted by subtraction of a primary solid (S) from the parent material (L). Possible compositions of this solid can be represented by vectors near the intersection of trend A with the dashed line (fig. 3) that outlines the area of entirely positive compositions. If the parent material were a liquid, the material would have had to have been subtracted by fractional crystallization and settling, but if the parent material were solid crust, then the subtraction could have been by partial fusion and residual accumulation of more mafic phases. The mathematical model provides no means for distinguishing between these two possible processes. In either case, differentiation could have proceeded along trend A until a liquid evolved with a composition near that of a vector at the intersection of trends A and B.

Differentiation along trend B could have been

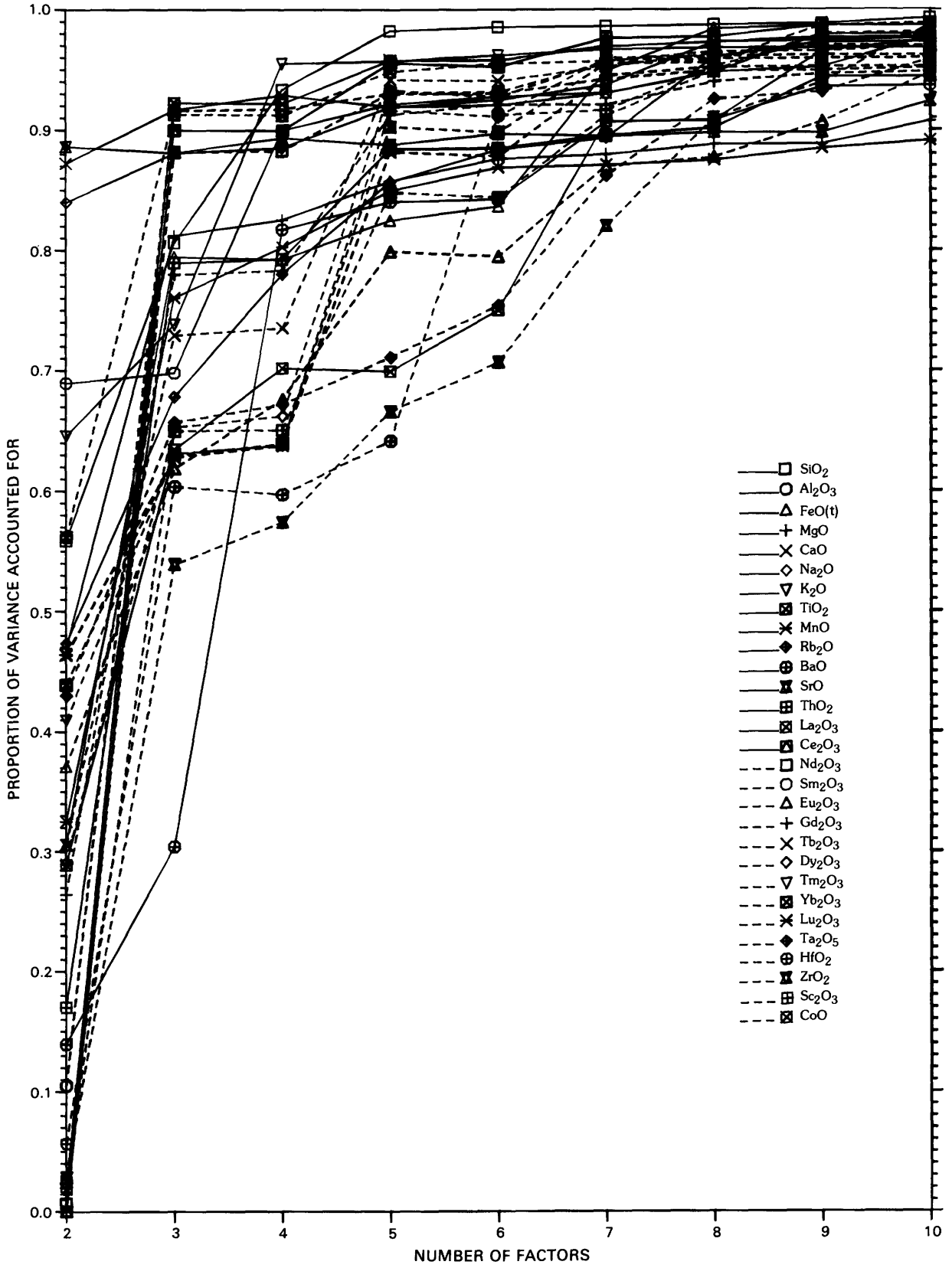

FIGURE 2.—Factor-variance diagram for 29 oxides in 25 samples.

brought about by fractional crystallization of this liquid and separation of a material for which the composition would be like that of sample GP–5 represented by the vector S_3 on figure 3. Sample GP–5 has a low REE content and a strongly positive europium anomaly (fig. 4) and may represent a cumulate from the magma.

The three-end-member process just outlined accounts for the observed compositional data to the degree indicated in the factor-variance diagram (fig. 2) for a three-factor model. In order to account for some of the minor oxide constituents, however, two additional end members must be used. Inasmuch as the three-end-member process accounts for the observed data in at least a general way, we decided to derive the two additional end members by simply modifying the three-end-member model. The most realistic modification that could be introduced was to allow some variability in the compositions of the initial parent material (L), liquid or solid, and in the compositions of the materials separated from it (S). The vector representing the parent material (L) was then replaced by vectors L_1 and L_2, which represent two extremes in a range of parent materials. The vector representing the material subtracted from the parent material (S) was replaced by vectors S_1 and S_2, which represent the extremes in a range of separated materials. (For illustration purposes

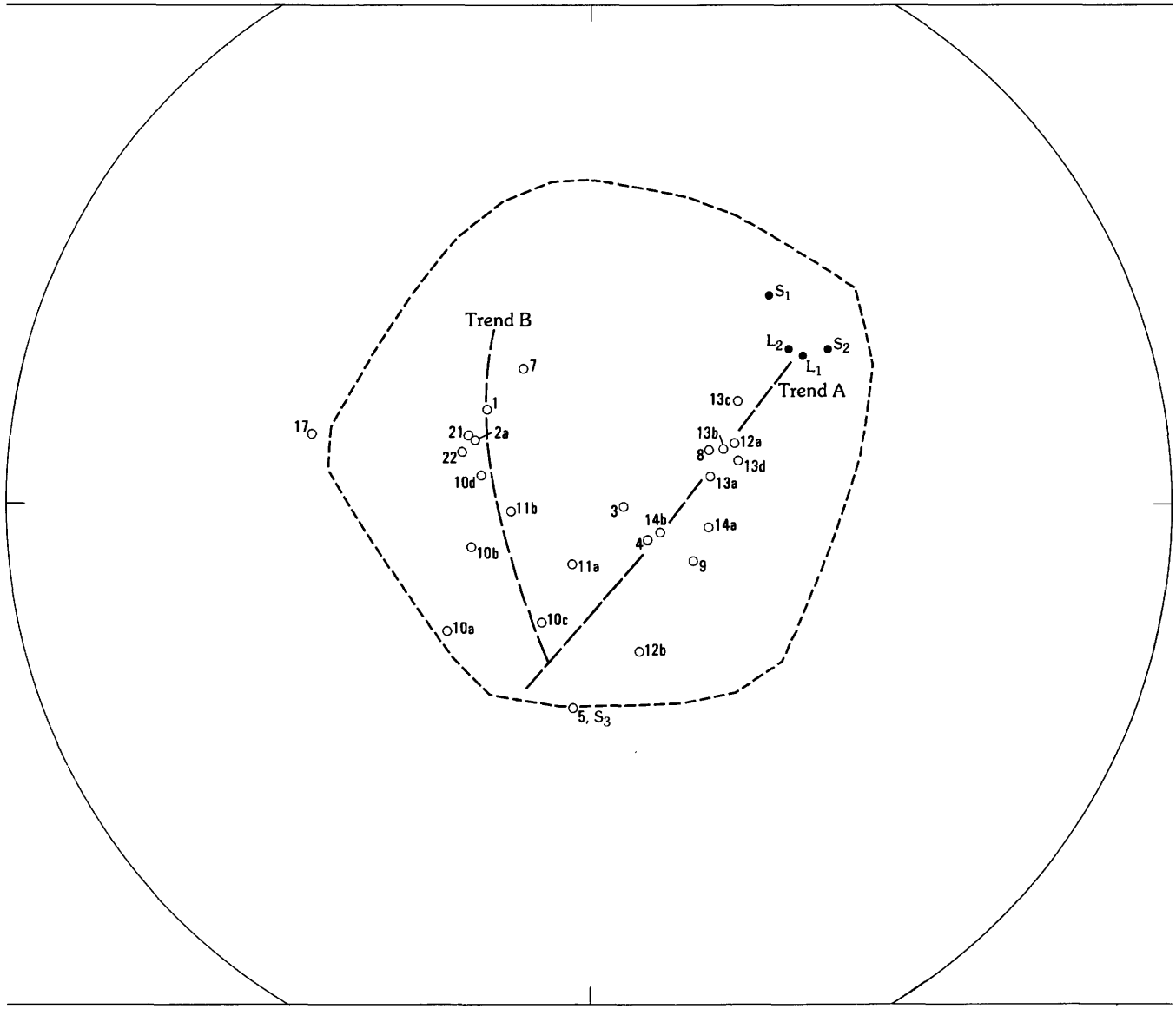

FIGURE 3.—Stereographic projection of the three-factor Q-mode vector solution derived from the data for 29 oxides in 25 samples from the Owl Creek Mountains. The dashed line outlines the area within which the vectors represent compositions that are entirely positive. Also shown are the projected positions for the starting liquids (L_1 and L_2), the initial crystallizing solids (S_1 and S_2), and the final crystallizing solid (S_3). Samples are identified by Plot I.D. (table 1 and fig. 1).

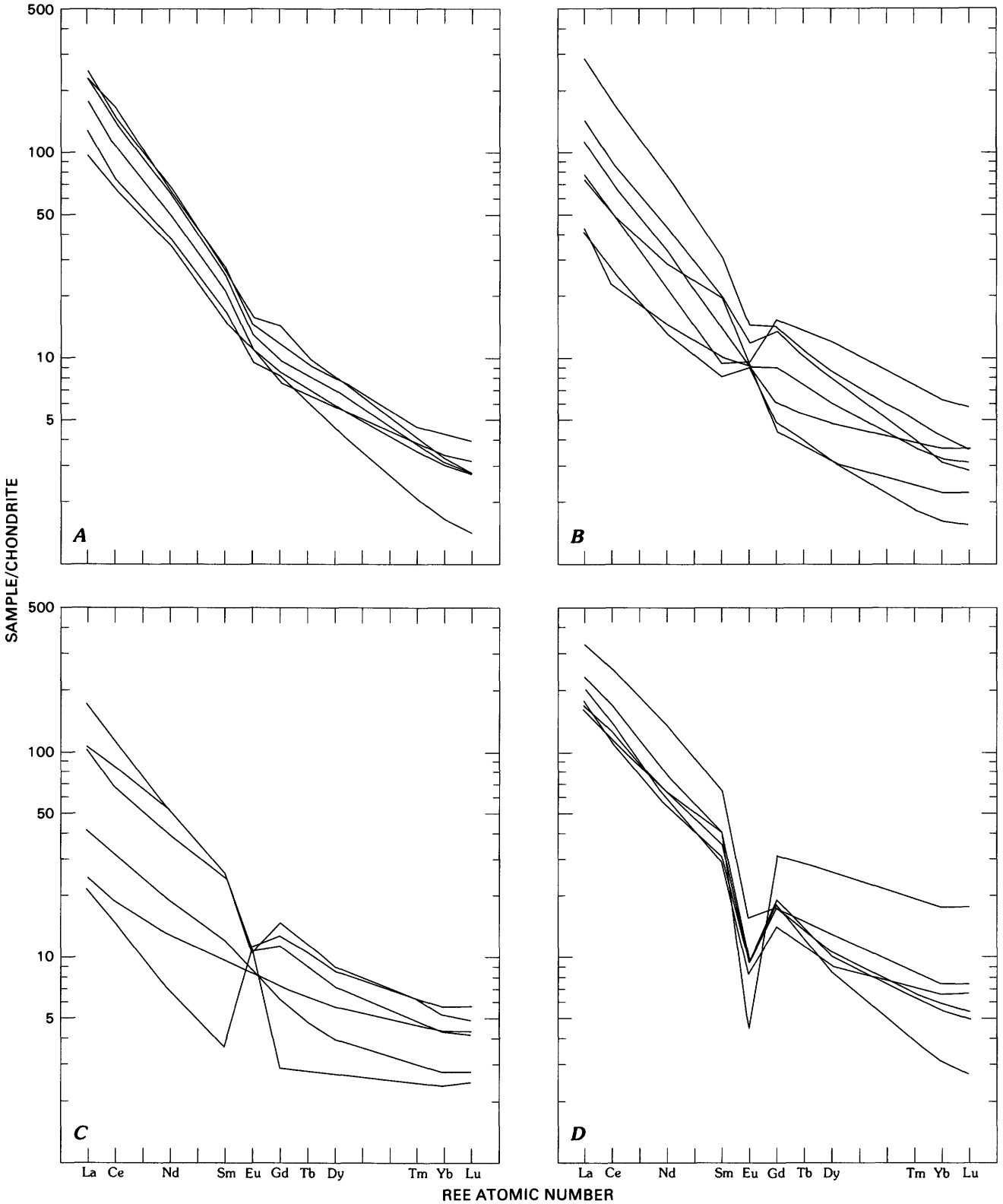

FIGURE 4.—Chondrite-normalized, rare-earth-element diagrams for the 25 granite samples used in the factor analysis. Diagrams *A* and *B* show the patterns of trend A (fig. 2): *A*, steep patterns with little or no europium anomaly (samples 41591, DP–3, DP–2, 30511, 30501, and 32466), and *B*, steep patterns with minor europium anomalies (23432, TDG46, 41596, 32496, 39294, and 39467, and DP–8). Diagrams *C* and *D* show patterns of trend B (fig. 2): *C*, strongly positive through weakly negative europium anomalies (GP–5, TDG47, 58180, 58–80, 58–98, and 58–66), and *D*, moderately to strongly negative europium anomalies (4343, TDG13, TDG12, TDG21, TD22, and GP–3).

only, vectors L_1, L_2, S_1, and S_2 were projected back into the three-dimensional vector cluster and are shown on figure 3 together with sample vectors and composition S_3.)

The search for vectors L_1, L_2, S_1, and S_2 was made using the assumption that a series of liquids had been generated by partial melting under fairly constant physical conditions and that therefore major-element concentrations would be fairly uniform. However, minor-element concentrations would be controlled by partitioning coefficients of phases existing in an inhomogeneous source and would therefore be more variable. The search for vectors S_1 and S_2 was made using similar assumptions. In a fractional-fusion interpretation, as discussed at the end of the next section, the compositions represented by vectors L_1 and L_2 would be less constrained than in a partial melting model and could encompass the full range of compositions observed for the metamorphic assemblage. Similarly, compositions S_1 and S_2 could be more variable, but without independent constraints, mathematically valid end-member compositions are too numerous to evaluate.

The compositions represented by the five selected reference vectors—the five end-member compositions—are given in table 7. Combining these compositions mathematically, according to the mixing proportions given in table 8, produces the recomputed data as given in table 1. The proportional differences between the original and recomputed data for each oxide in each sample are given in tables 9 and 10.

The mixing proportions in table 8 indicate that all but 3 of the 25 samples could have been derived from a mixture of compositions L_1 and L_2 by subtraction of some composition intermediate between compositions S_1 and S_2, plus the addition or subtraction of relatively small amounts of composition S_3. The other three samples require either the subtraction of material outside the range of compositions S_1 and S_2 (sample 58–80) or negative quantities of the starting material (samples 58–98 and TDG47).

EVALUATION OF THE MODEL

For most samples, the average agreement between the original and recomputed data is within 15 percent (table 9). A similar comparison for the 14 rejected samples is given in table 10. The recomputed data for the rejected samples were obtained by projecting vectors that represented the original compositions into the five-dimensional vector system. All of these recomputed compositions are in poor agreement with the original compositions. Thus the five-factor model accounts for

TABLE 7.—*Compositions of the end members for the factor model*

Oxides	End member L_1	L_2	S_1	S_2	S_3
	Weight percent				
SiO_2	66.95	66.31	64.39	64.97	75.86
Al_2O_3	16.26	16.32	16.34	16.91	13.76
FeO(t)	4.30	4.71	6.24	4.99	.61
MgO	1.47	1.62	2.22	1.74	.07
CaO	2.87	3.00	3.45	3.28	1.18
Na_2O	5.22	5.41	5.63	5.65	3.67
K_2O	2.04	1.68	.44	1.44	4.67
TiO_2	.55	.60	.85	.63	.06
	Parts per million				
MnO	818	919	1240	956	98.0
Rb_2O	165	172	167	155	193
BaO	1161	1086	1114	1272	588
SrO	466	478	528	542	156
ThO_2	53.46	54.32	85.38	53.78	23.23
La_2O_3	126.0	132.1	205.3	142.0	2.78
Ce_2O_3	205.1	212.9	341.0	228.0	5.51
Nd_2O_3	67.94	71.20	116.2	74.71	3.09
Sm_2O_3	8.81	9.52	15.9	9.49	.72
Eu_2O_3	1.22	1.22	1.58	1.31	.612
Gd_2O_3	4.84	5.82	8.61	5.35	.746
Tb_2O_3	.66	.82	1.17	.73	.12
Dy_2O_3	3.58	4.58	6.31	4.03	.69
Tm_2O_3	.160	.226	.303	.174	.058
Yb_2O_3	.76	1.12	1.48	.80	.35
Lu_2O_3	.083	.131	.171	.085	.053
Ta_2O_5	.66	.83	1.39	.54	.51
HfO_2	7.25	8.05	10.7	7.94	2.69
ZrO_2	364	399	504	416	92.7
Sc_2O_3	8.73	10.1	13.4	10.2	1.08
CoO	11.4	12.5	16.8	13.5	.39
	Norms (weight percent)				
Q	17.27	16.04	14.65	13.24	33.58
C	.25	.15	.35	.09	.53
Or	12.07	9.95	2.60	8.56	27.61
Ab	44.25	45.93	47.77	47.94	31.09
An	14.29	14.90	17.15	16.30	5.85
En	3.67	4.05	5.55	4.34	.18
Fs	7.16	7.85	10.30	8.33	1.05
Il	1.05	1.14	1.63	1.20	.11

TABLE 8.—*Mixing proportions for the factor model*

Sample	End member				
	L_1	L_2	S_1	S_2	S_3
DP-3	4.9193	0.8773	-0.7261	-3.6972	-0.3733
23432	1.9963	.8379	-.5650	-1.5585	.2892
29394	.0782	.0645	.2909	.0000	.5663
29467	.4517	1.3172	-.3913	-.7226	.3451
30501	1.8175	.5829	-.2887	-1.4031	.2914
30511	1.6091	.0000	-.0443	-.9482	.3833
32466	3.8449	.9678	-.8382	-2.8440	-.1305
32496	2.9678	1.8039	-.8156	-2.9294	-.0267
41591	2.4510	.3367	-.2966	-1.6225	.1315
41596	3.8435	.9832	-.9080	-2.9256	.0069
DP-8	2.6332	3.8947	-1.1908	-4.0625	-.2747
DP-2	4.6932	1.5443	-.9658	-3.9800	-.2918
TDG46	.0001	1.1258	-.0000	-.9262	.8003
58-66	2.8789	1.8496	-.4870	-3.5200	.2786
GP-3	27.5097	14.6323	-6.1028	-28.8249	-6.2143
GP-5	.0000	-.0000	.0000	-.0000	1.0000
4343	17.2184	4.4041	-2.2856	-15.3472	-2.9896
TDG12	13.7561	6.0112	-2.5642	-13.6872	-2.5160
TD-13	15.9529	5.4194	-2.5629	-14.9546	-2.8548
TDG21	16.6719	5.6296	-2.9129	-15.3889	-2.9997
TD22	15.0054	4.1247	-2.1754	-13.5233	-2.4316
58180	5.3650	1.5566	-.2858	-5.4684	-.1673
58-80	.1490	.1230	.6220	-.9745	1.0805
58-98	-3.7071	-.6311	.9866	2.4947	1.8570
TDG47	-5.3798	-.6756	1.6794	3.1401	2.2358

most of the variance in all of the 25 samples and discriminates against altered and unrelated samples.

The five-factor model also accounts for more than 64 percent of the variance in all 29 oxides used and more than 80 percent of the variance in all but four oxides (table 5 and fig. 2). All four of the oxides that show low percentages of variance accounted for are suspected to have large analytical errors relative to geologic variation and are therefore poorly explained.

Standard petrologic diagrams and isotopic data can be used to evaluate the petrogenetic model. The pronounced break in differentiation trend indicated by Q-mode factor analysis suggests a marked change in physical conditions during crystallization. A different crystallization pressure for samples from trends A and B is suggested by a plot of the normative data in both the Q-Ab-Or (fig. 5) and the An-Ab-Or systems (fig. 6). If the whole-rock compositions are interpreted as equilibrium liquids, both ternary systems indicate crystallization at lower water pressure for trend B.

Three samples (58–80, 58–98, and TDG47) that plot near the junction of trends A and B (fig. 3, points 10b, 10c, and 11a) and that are not explained by the petrologic model as simple differentiates plot as a group above the polybaric minimum (fig. 5). These compositions cannot be derived by equilibrium crystal fractionation if a probable starting liquid from trend A is assumed as parental to these samples. The position of these data points on figure 5 is probably due to a small amount of alteration during which potassium was lost, or quartz and albite were gained. Because the shift from a probable equilibrium liquid is small and may only involve a few elements, these samples still fit the five-factor model reasonably well (that is, the average difference between the original and recomputed data is less than 15 percent).

The interpretation of the five-factor model reveals a surprising relationship to oxygen isotopic data, even though these data were not used in the development of the model. Figure 7 shows a plot of whole-rock $\delta^{18}O$ values versus percent of composition L_1 in the total starting material ($100L_1/(L_1+L_2)$ for each sample. The very good correlation between these two variables for all but three samples suggests that the starting magma is well represented by a mixture of two materials. A similar correspondence between oxygen isotopic and elemental compositions has been noted for the Carboniferous Elberton Granite, Georgia (Wenner, 1980). However, in that granite the trace-element and oxygen isotopic data yield a geographic pattern that is interpreted to reflect a similar pattern in the protolith. No geographic pattern is noted for the granite of the Owl Creek Mountains. However, if the protolith for the granite is as lithologically complex as the metamorphic sequence intruded by the granite, a simple geographic pattern for variables that preserve a protolith imprint would be unlikely.

Although the interpretation of the five-factor model is reasonable in light of petrologic data, the same end members could be interpreted differently. The data permit the generation of trend A as a series of fractional melts. In this interpretation, end members L_1 and L_2 would represent a series of protolith compositions and end members S_1 and S_2 would represent a series of residuum compositions. In the alternate hypothesis, the difference in pressures suggested for trends A and B represents derivation at an intermediate pressure followed by differentiation at a slightly lower pressure. The generation of trend A by fractional fusion would also account for the correlation between starting liquid compositions and $\delta^{18}O$ values.

PROTOLITH CONSIDERATIONS

The wide range of $\delta^{18}O$ values, which appears to be a primary magmatic feature; the apparent range in initial $^{87}Sr/^{86}Sr$ ratios (Hedge and others, this volume) and $^{208}Pb/^{204}Pb$ ratios (Stuckless and others, this vol-

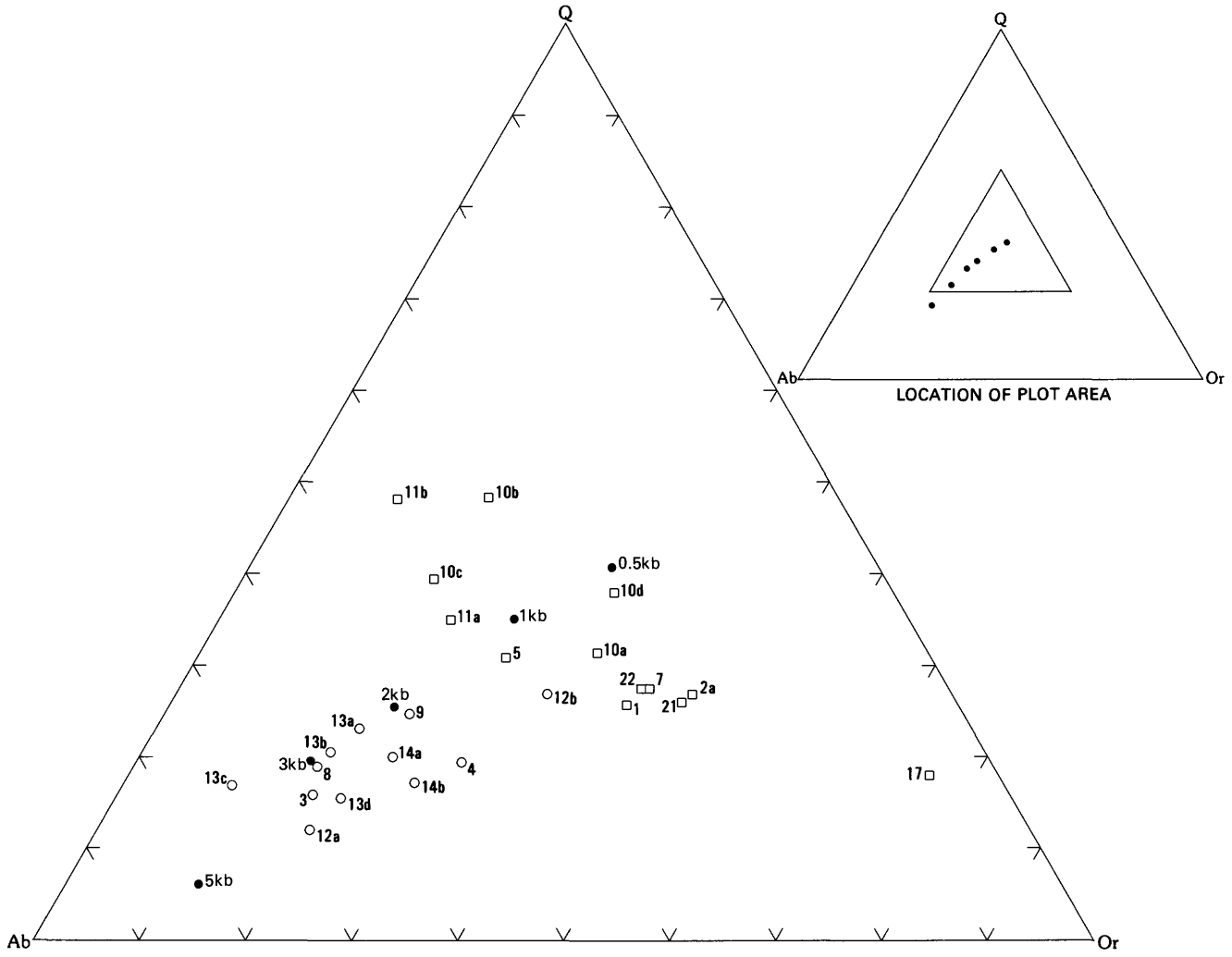

FIGURE 5.—Normative data for quartz, albite, and orthoclase for granite samples from the Owl Creek Mountains, Wyo. Trend-A samples indicated by circles; trend-B samples indicated by squares; polybaric, water-saturated minimum (Tuttle and Bowen, 1958; Luth and others, 1964) indicated by solid dots. The expanded portion of the diagram (shown on the inset) is bounded by quartz 25 to 60 percent, albite 20 to 55 percent, and orthoclase 20 to 55 percent.

ume); and the correlation of these variables with one another—all suggest that the magma genesis involved some sort of mixing process that did not proceed to homogenization. Although the isotopic data could be explained by assimilation and contamination of a homogeneous magma, chemical data favor derivation from a heterogeneous protolith. This conclusion is based on the facts that the samples from trend A indicate a higher pressure history than those from trend B and that samples from trend A exhibit the entire range of $\delta^{18}O$ values. Furthermore, the samples from trend A are less evolved than those of trend B. In contrast, a contamination-assimilation model would most reasonably predict increasing contamination with increasing degree of magma evolution and increasing contamination with decreasing pressure because assimilation is most likely to occur during intrusion or final crystallization. Thus the isotopic data seem to reflect protolithic characteristics, which became primary features of the initial magma.

Oxygen isotope data provide some constraints on the nature of the protolith. Few $\delta^{18}O$ values are greater than 8.0 per mil (table 4), which by comparison to Paleozoic source regions suggests a low pelitic component in the protolith (O'Neil and Chappell, 1977). This suggestion is supported by both the low values for normative corundum (generally less than 1.1 percent, table 1) and the low pelitic component in the metamorphic complex intruded by the granite (Hamil, 1971). The few metamorphic rocks analyzed yield low $\delta^{18}O$ values (table 4, samples with prefix DKCH). The isotopic fraction for oxygen at the temperature required for granite

TABLE 9.—*Proportional differences between the original chemical data and the data represented by the factor solution for the 25 samples used to develop the solution*

[Average is the average of the absolute values]

Sample No.	DP-3	23432	29394	29467	30501	30511	32466	32496	41591	41596	DP-8	DP-2	TDG46
SiO_2	0.00	0.01	0.00	0.00	0.00	0.00	0.00	0.00	-0.01	0.00	0.00	0.00	0.00
Al_2O_3	.01	-.01	.00	.00	-.01	-.01	-.01	-.01	.01	-.02	.03	.00	-.01
FeO(t)	.00	.09	.04	.04	-.02	.04	.04	.01	.00	.20	-.45	-.32	.22
MgO	.29	-.25	.10	.10	.18	.03	-.35	-.53	.04	.11	-.24	-.07	.09
CaO	.10	-.17	.02	-.01	.00	.05	.01	.07	.07	-.02	-.14	.00	-.17
Na_2O	.03	.00	-.03	-.06	-.02	-.01	.02	.03	.02	-.05	.07	.03	-.02
K_2O	-.11	-.02	.06	.05	-.01	.02	-.04	.02	.03	.01	-.02	.01	-.02
TiO_2	.18	.10	-.09	.04	.06	-.02	.02	-.03	.03	-.42	.07	.17	-1.18
MnO	.02	-.03	.00	.02	-.08	-.22	-.24	.17	.12	.23	.00	-.10	.01
Rb_2O	.03	-.04	.15	.12	.08	.04	-.13	.02	.10	.01	-.20	-.22	-.06
BaO	.18	.02	-.18	-.11	.00	-.06	.02	-.05	.00	-.01	.07	.13	.07
SrO	.15	.00	-.10	-.07	.11	.08	-.05	.02	.04	.24	-.07	-.16	-.23
ThO_2	.06	.04	.06	-.08	.10	.04	-.11	-.04	-.09	-.02	.09	-.05	.10
La_2O_3	.06	-.15	.04	-.18	.06	.09	.01	.11	.13	-.06	-.14	-.13	-.58
Ce_2O_3	.16	-.10	.01	-.13	.02	.04	-.07	.13	.07	-.05	.07	-.08	-.91
Nd_2O_3	.04	-.18	-.04	-.08	.01	.02	.06	.13	.08	.04	.16	.05	-.63
Sm_2O_3	.03	-.18	-.12	-.02	.00	-.04	.11	-.02	.01	.28	.26	-.03	-.34
Eu_2O_3	.19	-.09	.01	.00	-.05	-.01	-.16	-.11	.10	-.04	.08	.05	-.03
Gd_2O_3	.24	-.46	-.08	.12	-.31	-.12	.12	.00	.03	.26	.13	.07	-.49
Tb_2O_3	.19	-.46	-.07	.02	-.19	.00	.09	-.03	.10	.22	.14	.11	-.48
Dy_2O_3	.20	-.44	-.09	-.06	-.10	.07	.00	-.06	.16	.21	.12	.12	-.37
Tm_2O_3	.29	-.18	.01	-.22	.10	.08	-.28	-.12	.14	.13	.01	.03	-.17
Yb_2O_3	.36	-.09	.05	-.30	.12	.13	-.30	-.12	.14	.00	.00	.06	-.14
Lu_2O_3	.40	-.03	.05	-.25	.17	.06	-.37	-.04	.17	-.12	-.04	-.06	-.11
Ta_2O_5	.62	-.21	-.16	-.08	.23	-.75	-.85	-.01	.25	-.98	-.43	-.21	-.36
HfO_2	.01	.14	-.20	-.10	-.12	-.06	-.01	.04	.07	-.23	-.20	.18	.34
ZrO_2	.09	.17	.04	-.09	-.05	.13	.00	.07	-.14	-.10	-.21	-.02	-.05
Sc_2O_3	.01	-.01	-.07	-.12	.20	.01	-.01	-.15	-.09	-.40	.24	.08	-.21
CoO	.20	-.11	.07	-.01	.12	.07	-.24	-.21	.08	.04	-.16	-.02	.00
Average:	.14	.13	.07	.09	.09	.08	.13	.08	.08	.15	.13	.09	.26

melting is expected to be small (O'Neil and others, 1977), such that the melt fraction should have the same or slightly greater $\delta^{18}O$ values than the source rock. Thus, at least a part of the exposed metamorphic complex could be similar to one end member in the protolith.

Either a fractional-crystallization or fractional-fusion interpretation as an explanation for trend A (fig. 3) can provide constraints on magma genesis because both interpretations indicate a starting liquid that can be used to estimate a minimum pressure for magma genesis. A unique starting liquid (or series of liquids) cannot be defined in a fractional crystallization interpretation, but presumably a series of liquids could have been found that included the composition of the least evolved sample (29394). In a fractional-fusion interpretation, this sample and others along trend A suggest a minimum pressure of 3 kb and approximately water-saturated conditions (fig. 5). A pressure of 3 kb and a temperature near that required for granite melting approach conditions indicated by the grade of metamorphism observed for the volcanic-sedimentary sequence.

TABLE 9.—*Proportional differences between the original chemical data and the data represented by the factor solution for the 25 samples used to develop the solution*—Continued

Sample No.	58-66	58-80	58-98	GP-3	GP-5	4343	TDG12	TD-13	TDG21	TD22	TDG47	58180
SiO_2	0.00	0.01	0.00	0.00	0.00	0.00	0.00	0.00	0.00	0.00	0.00	0.00
Al_2O_3	-.02	.00	.02	-.02	.03	.02	-.01	.01	.02	.01	-.01	-.02
FeO(t)	.29	-.35	-.16	-.19	-1.06	-.20	.25	-.10	.07	.11	.20	-.35
MgO	.46	.26	-.36	.63	.27	-.52	-.53	-.17	.32	-.16	-.14	.03
CaO	-.06	.08	-.02	.73	.15	.18	.07	-.08	-.21	-.33	.02	-.08
Na_2O	.00	.00	.02	-.09	.00	.00	-.10	.05	.05	.04	-.01	-.04
K_2O	.05	-.07	-.01	.03	.00	.00	.03	-.02	-.08	.02	-.01	.07
TiO_2	.27	-.31	.05	.41	-.13	-.11	-.27	-.32	-.11	-.50	-.17	.54
MnO	.16	-.61	-.35	-.72	-.03	.04	.21	.12	-.05	-.26	.15	.26
Rb_2O	.12	.04	-.03	.08	.05	.00	.08	-.02	-.01	-.16	-.13	.01
BaO	-.06	.04	-.22	.10	-.06	.04	-.23	-.11	.03	-.16	.23	.20
SrO	.06	.14	-.12	.91	-.28	.05	-.23	-.18	-.31	-.28	.21	.20
ThO_2	.10	-.22	.02	.02	-.10	-.01	-.38	-.01	.13	-.02	.00	.14
La_2O_3	-.14	.11	.03	.19	.55	.01	.00	-.03	.08	-.28	.00	.04
Ce_2O_3	-.22	.18	.14	.18	.50	.08	-.10	.01	.02	-.25	-.05	-.03
Nd_2O_3	-.18	.25	.04	.17	.19	.17	-.11	-.05	-.10	-.17	-.04	-.17
Sm_2O_3	-.17	.16	.07	.06	-.09	.19	-.05	-.02	-.15	-.05	.05	-.23
Eu_2O_3	.01	.05	-.13	.09	.16	.18	.02	-.13	-.14	-.13	-.01	.01
Gd_2O_3	-.09	.12	-.11	.07	-.08	-.18	-.05	.01	-.11	.15	.16	-.07
Tb_2O_3	-.06	.11	-.18	.12	.07	-.02	-.11	-.09	-.10	.05	.14	.02
Dy_2O_3	-.01	.13	-.21	.14	.13	.11	-.16	-.17	-.09	-.06	.09	.05
Tm_2O_3	.04	.05	-.18	.17	.17	.17	-.25	-.20	.09	-.46	.09	.11
Yb_2O_3	.03	.06	-.19	.17	.20	.19	-.26	-.22	.10	-.65	.03	.15
Lu_2O_3	-.04	.09	-.25	.19	.25	.21	-.33	-.28	.15	-.75	.03	.20
Ta_2O_5	.07	-.31	-.17	.14	.47	-.09	.20	.07	-.10	-1.20	-.14	.39
HfO_2	-.51	.02	.06	.13	.00	.18	-.11	-.05	.00	-.10	-.07	-.06
ZrO_2	-.15	.22	.16	.26	.08	.29	.01	.04	-.57	-.67	-.51	.08
Sc_2O_3	.11	-.01	.11	-.03	.07	.15	-.21	.07	-.08	-.03	-.29	.20
CoO	.79	.18	-.31	.46	.01	-.13	-.02	-.39	.07	-.02	-.10	-.19
Average:	.15	.14	.13	.22	.18	.12	.15	.10	.11	.25	.10	.13

MAGMA GENESIS

The initial liquids from which the granite may have been derived were probably formed at approximately 3 kb pressure and near water-saturated conditions. (A somewhat higher pressure would be possible for a fractional-crystallization interpretation because of the unconstrained composition of the initial liquids.) The protolith was heterogeneous in composition, most likely similar to the observed metamorphic sequence, but at a greater depth than currently exposed. Metamorphism apparently predates granite intrusion (Mueller and others, 1981; Hedge and others, this volume). Therefore at the time of intrusion, the currently exposed metamorphic rocks were probably under less pressure than that indicated by maximum metamorphic grade. Thus for a fractional-crystallization interpretation, the compositional variations along trend A would be the result of differentiation prior to intrusion. Following the generation of the compositions along trend A (by either fractional crystallization or fractional fusion), the magma was intruded to its current level of exposure,

TABLE 10.—*Proportional differences between the original chemical data and the data represented by the factor solution, for the 14 samples not used to develop the solution*

[Average is the average of the absolute values. Leaders (--) indicate indeterminate value due to division by zero]

Sample No.	58188	58317	58392	58398	DP-1	GP-1	GP-2	GP-4	TD-6	TDG16	TDG20	TDG24	TDG44	TDG45
SiO_2	0.01	-0.01	0.83	38.16	-0.01	-0.02	-0.06	-0.03	-0.03	-0.01	-0.02	-0.01	-0.01	-2.85
Al_2O_3	-.03	.02	-1.14	-37.17	.05	.13	.23	.15	.02	.05	.10	.03	-.01	2.35
FeO(t)	.01	.08	-1.56	-80.35	-.28	.53	-1.76	-.88	.79	.12	.02	.18	.31	4.57
MgO	.33	.58	-.48	-40.09	-1.13	5.93	-4.89	-1.73	8.01	-.22	-3.14	.05	.89	4.60
CaO	.30	.17	-.95	-56.93	-.31	-.32	-9.36	.66	-4.83	-.16	-1.96	-.46	-.06	3.53
Na_2O	-.37	.06	-8.17	-197.68	.16	.50	.59	-.33	-.21	.10	.16	.11	-.31	18.72
K_2O	-.09	.02	24.16	517.33	.02	-1.53	-12.58	-5.81	.17	-.09	.00	.01	.12	-75.60
TiO_2	.00	-.01	-1.65	-113.60	-1.00	4.83	---	-1.19	13.36	-2.07	-6.85	-.73	.78	6.70
MnO	-.26	-.53	-3.06	-111.20	.00	.98	.76	-1.80	2.25	-1.11	.88	-1.01	.77	6.11
Rb_2O	-.06	.10	8.27	79.39	.05	.60	-7.77	-2.79	.46	-.43	.34	-.24	.36	-30.78
BaO	.12	-1.28	.62	19.96	-7.18	-2.70	-63.60	-2.91	-5.02	-1.61	-2.34	-.65	-.21	-17.03
SrO	-.10	-.31	11.28	-414.84	-10.24	-.43	-21.80	.59	-.59	-1.43	-4.66	-1.33	.73	32.63
ThO_2	-.27	.19	19.11	994.57	-.50	-4.34	-1.44	.68	-8.84	-1.11	-1.92	-.41	.08	-53.95
La_2O_3	-.53	2.21	-38.38	>999.99	4.22	3.19	34.08	.66	6.50	5.51	-.08	.56	1.07	85.39
Ce_2O_3	-.23	1.84	-22.43	-685.59	4.35	.71	29.10	.88	4.23	7.59	.75	.58	.95	47.89
Nd_2O_3	-.14	.74	-12.66	-386.18	3.43	-.28	12.14	.87	2.61	4.98	-.59	.44	.40	27.39
Sm_2O_3	.26	.12	-5.04	-207.82	1.45	-1.15	3.70	.92	-.28	1.67	-2.86	.19	-.50	14.55
Eu_2O_3	-.36	-.13	-1.77	-44.67	-6.64	-7.59	-10.83	-.68	-.27	-1.05	-2.98	-.77	.21	4.27
Gd_2O_3	-.24	-.14	-7.30	-326.26	-.90	-1.14	-2.53	.51	-1.35	-.50	-3.71	-.09	-1.14	19.25
Tb_2O_3	-.27	-.06	-6.74	-283.64	-1.09	-.97	-2.85	.54	-.94	-.18	-1.61	-.18	-.81	18.47
Dy_2O_3	-.48	.05	-6.76	-265.09	-1.08	-.73	-2.88	.53	-.77	.02	-1.41	-.18	-.54	17.94
Tm_2O_3	-.07	.15	-3.51	-141.29	-1.00	-.49	-2.32	.65	-.63	.16	-1.02	-.38	.26	10.40
Yb_2O_3	.18	.21	-2.52	-110.61	-.89	-.50	-1.92	.70	-.49	.24	-.79	-.45	.41	8.19
Lu_2O_3	.37	.24	-1.61	-87.01	-.68	-.49	-1.69	.74	-.37	.29	-.64	-.53	.54	6.56
Ta_2O_5	1.12	-.07	10.98	73.88	-1.10	.97	.98	1.03	.20	-.50	.91	-.32	.73	-9.18
HfO_2	-.36	-.49	-12.37	-551.06	-.05	-1.44	-.18	.17	-10.81	-3.76	.04	-.65	-.22	29.34
ZrO_2	-.24	-.39	-13.15	-637.81	-.37	-1.24	-1.22	.10	-2.59	-1.04	-1.20	-7.19	-4.93	85.80
Sc_2O_3	.07	-.78	-.82	-33.63	-1.15	-.60	-35.63	.14	-2.16	-1.02	-9.41	.04	.36	3.27
CoO	.09	.83	-.33	-49.25	-5.29	7.81	-17.00	-3.45	4.89	.63	-.58	-.18	.95	4.62
Average:	.24	.41	7.86	271.11	1.90	1.78	9.87	1.11	2.89	1.30	1.75	.62	.64	22.48

where pressure may have been as low as 0.5–1.0 kb (fig. 5), and compositions along trend B were generated by the separation of the feldspar-dominated solid (S_3). Compositions along trend A were modified by minor addition or subtraction of this solid. Minor modifications of some sample compositions may have occurred as a result of deuteric or post-crystallization hydrothermal alteration. Such alterations may explain the 2–20 percent of the variance in the oxides not accounted for by the five-factor solution (table 6) and are supported by isotopic data in the rubidium-strontium and thorium-lead systems (Hedge and others, this volume; Stuckless and others, this volume).

SUMMARY AND CONCLUSIONS

Q-mode factor analysis has been used to identify 25 granitic samples from the Owl Creek Mountains, Wyo., for which 29 oxide variables can be well represented by a five-factor model. The five-factor model serves to identify samples of doubtful geologic relation to the main granite intrusion, including suspected xenoliths and rocks that have been strongly affected by hydrothermal alteration. The model also identifies oxide variables (H_2O, CO_2, UO_2, Cs_2O, and the oxidation state of iron) that have been controlled in large part by post-magmatic effects. The model presented here explains

more than 80 percent of the observed variance for 25 of the 29 oxides (table 6) and yields excellent agreement between recomputed and original (adjusted to 100 percent) compositions for all 25 samples.

End members that provide an explanation for the observed compositional variations were identified within the five-dimensional space defined by the sample compositions. These end members can be used in either a purely fractional-crystallization interpretation or a fractional-fusion and fractional-crystallization interpretation. According to either interpretation, the protolith is similar to the inhomogeneous metamorphic sequence that the granite intrudes, and the final compositions reflect a polybaric history. Both interpretations can also be reconciled with the wide range of whole-rock $\delta^{18}O$ values (6.9–8.6).

Two of the five end members in the model represent either the extremes in a range of starting liquids generated at a pressure equal to or greater than 3 kb, or the extremes in a series of protolith compositions. Two additional end members may represent either the extremes in a series of early separated solids at a pressure of approximately 3 kb, or the extremes in a series of residuum compositions from fractional fusion. The fifth end member is a feldspar-dominated solid that is either subtracted or added to account for minor variations in the least evolved compositions and major variations along a second trend defined by the most evolved compositions. This solid is interpreted to have crystallized at pressures of approximately 1.0–0.5 kb. The five-end-member model and the selected end members do not explain all of the observed variances in the 29

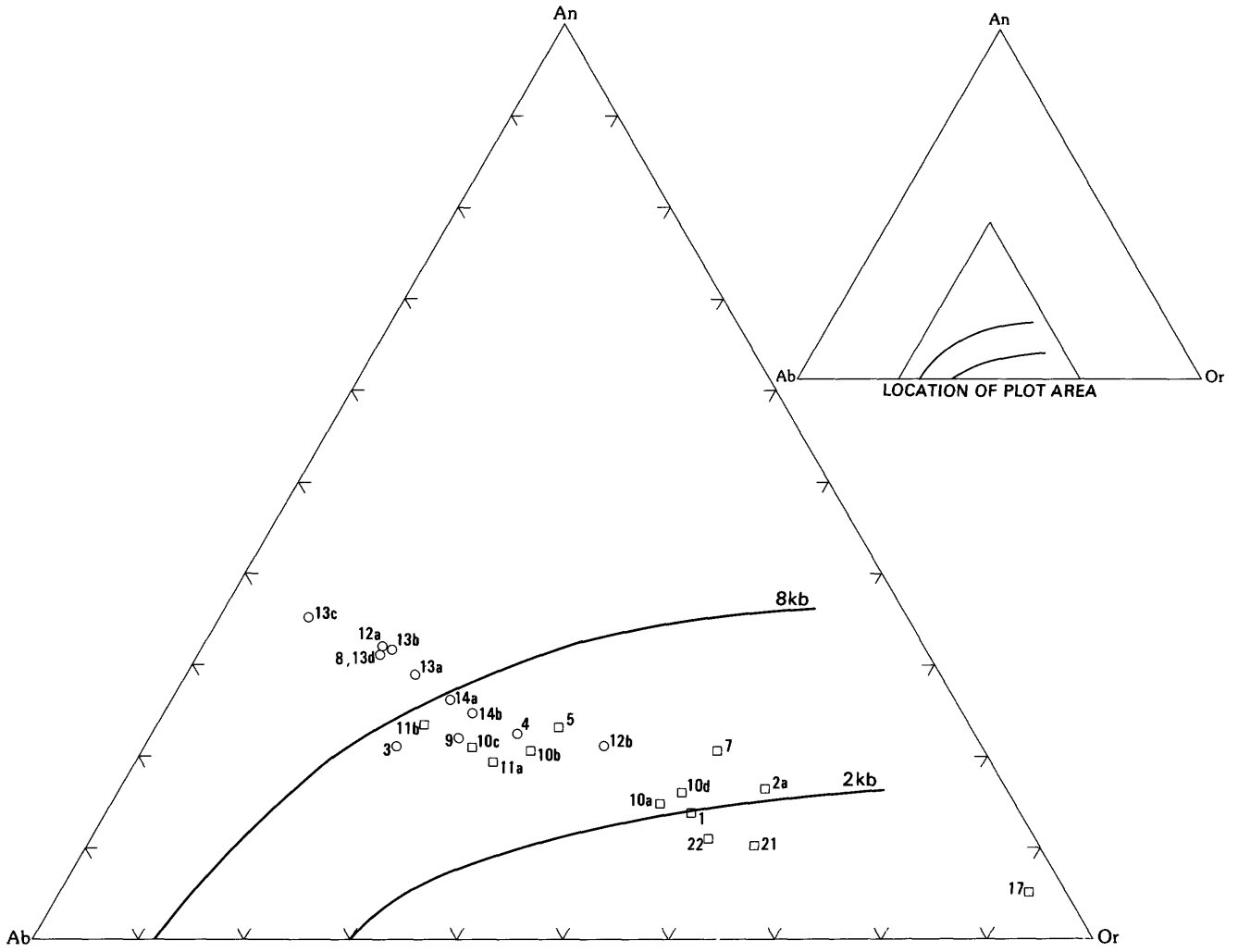

FIGURE 6.—Normative An-Ab-Or for granites from the Owl Creek Mountains, Wyo. Samples of trend A are shown by circles; samples of trend B shown by squares; 2- and 8-kb eutectic curves from Whitney (1975). The expanded portion of the diagram (shown on the inset) is bounded by anorthite 0 to 45 percent, albite 30 to 75 percent, and orthoclase 25 to 70 percent.

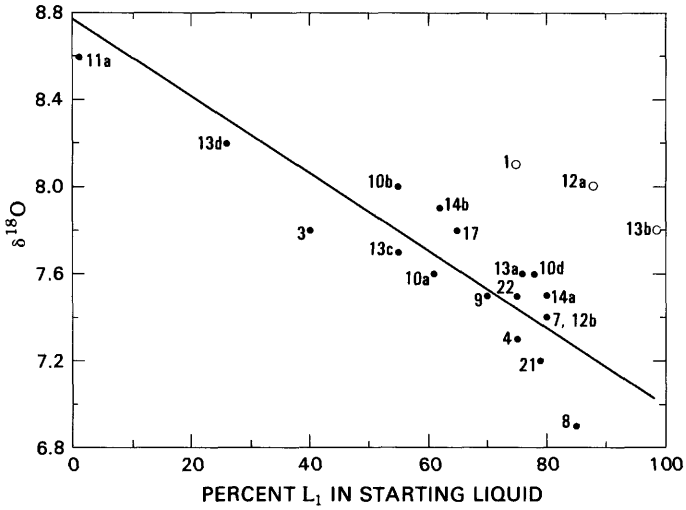

FIGURE 7.—Plot of whole-rock $\delta^{18}O$ values versus percent of end member L_1 in the total starting material. The best-fit line showing data correlation was determined using data points plotted as solid dots.

oxides. Although analytical error may account for some of the unexplained variance, hydrothermal or deuteric alteration probably redistributed some elements to a small extent such that variance within the data set is no longer purely magmatic.

REFERENCES

Bramlett, L. B., Reyher, S. L., and Southard, G. G., 1982, Uranium geology and geochemistry, Copper Mountain, Wyoming: Transactions of the American Institute of Mining Engineers, v. 272, p. 1891–1901.

Bunker, C. M., and Bush, C. A., 1966, Uranium, thorium, and radium analyses by gamma-ray spectrometry (0.184–0.352 million electron volts), *in* Geological Survey Research 1966: U.S. Geological Survey Professional Paper 550–B, p. B176–B181.

Condie, K. C., 1967, Petrologic reconnaissance of the Precambrian rocks in Wind River Canyon, central Owl Creek Mountains, Wyoming: University of Wyoming Contributions to Geology, v. 6, p. 123–129.

Condie, K. C., Leech, A. P., and Baadsgaard, H., 1969, Potassium-argon ages of Precambrian mafic dikes in Wyoming: Geological Society of America Bulletin, v. 80, p. 899–906.

Evensen, N. M., Hamilton, P. J., and O'Nions, R. K., 1978, Rare earth abundances in chondritic meteorites: Geochimica et Cosmochimica Acta, v. 42, p. 1199–1212.

Giletti, B. J., and Gast, P. W., 1961, Absolute age of Precambrian rocks in Wyoming and Montana, *in* Kulp, J. L., ed., Geochronology of rock systems: Annals of the New York Academy of Sciences, v. 91, p. 454–458.

Gordon, G. E., Randle, K., Goles, G., Corliss, J., Beeson, M., and Oxley, S., 1968, Instrumental activation analysis of standard rocks with high resolution gamma-ray detectors: Geochimica et Cosmochimica Acta, v. 32, p. 369–396.

Hamil, M. M., 1971, Metamorphic and structural environment of Copper Mountain, Wyoming: Columbia, Mo., University of Missouri Ph.D. thesis, 121 p.

Keefer, W. R., and Love, J. D., 1963, Laramide vertical movements in central Wyoming: University of Wyoming Contributions to Geology, v. 2, p. 47–56.

Ludwig, K. R., 1978, Uranium daughter migration and U-Pb isotope apparent ages of uranium ores, Shirley Basin, Wyoming: Economic Geology, v. 73, p. 29–49.

———1979, Age of uranium mineralization in the Gas Hills and Crooks Gap districts, Wyoming, as indicated by U-Pb isotope apparent ages: Economic Geology, v. 74, p. 1654–1668.

Luth, W. C., Jahns, R. H., and Tuttle, O. F., 1964, The granite system at pressures of 4 to 10 kilobars: Journal of Geophysical Research, v. 69, p. 759–773.

Miesch, A. T., 1976a, Interactive computer programs for petrologic modeling with extended Q-mode factor analysis: Computers and Geosciences, v. 2, p. 439–492.

———1976b, Q-mode factor analysis of geochemical and petrologic data matrices with constant row-sums: U.S. Geological Survey Professional Paper 574–G, 47 p.

———1981, Computer methods for geochemical and petrologic mixing problems, *in* Merriam, D. F., ed., Computer applications in the earth sciences: New York, Plenum Publishing Corporation, p. 243–265.

Millard, H. T., Jr., 1976, Determinations of uranium and thorium in USGS standard rocks by the delayed neutron technique: U.S. Geological Survey Professional Paper 840, p. 61–65.

Mueller, P., Peterman, Z. E., and Granath, J., 1981, An Archean bimodal volcanic series, Owl Creek Mountains, Wyoming: Geological Society of America Abstracts with Programs, v. 13, p. 515–516.

Nkomo, I. T., Rosholt, J. N., and Dooley, J. R., Jr., 1979, U-Th-Pb systematics in surface and drill core samples of a Precambrian basement rock from Laramie, Wyoming: Earth Science Bulletin, v. 12, p. 1–14.

Nkomo, I. T., Stuckless, J. S., Thaden, R. E., and Rosholt, J. N., 1978, Petrology and uranium mobility of an early Precambrian granite from the Owl Creek Mountains, Wyoming: Wyoming Geological Association Guidebook, 30th annual field conference, p. 335–348.

O'Neil, J. R., and Chappell, B. W., 1977, Oxygen and hydrogen isotope relations in the Berridal batholith: Journal of the Geological Society of London, v. 133, p. 559–571.

O'Neil, J. R., Shaw, S. E., and Flood, R. H., 1977, Oxygen and hydrogen isotope compositions as indicators of granite genesis in the New England Batholith, Australia: Contributions to Mineralogy and Petrology, v. 62, p. 313–328.

Peck, L. C., 1964, Systematic analysis of silicates: U.S. Geological Survey Bulletin 1170, 89 p.

Rosholt, J. N., and Bartel, J. A., 1969, Uranium, thorium and lead systematics in the Granite Mountains, Wyoming: Earth and Planetary Science Letters, v. 7, p. 141–147.

Rosholt, J. N., Zartman, R. E., and Nkomo, I. T., 1973, Lead isotope systematics and uranium depletion in the Granite Mountains, Wyoming: Geological Society of America Bulletin, v. 84, p. 989–1002.

Seeland, D. A., 1976, Relationship between early Tertiary sedimentation patterns and uranium mineralization in the Powder River Basin, Wyoming: Wyoming Geological Association Guidebook, 28th annual field conference, p. 53–64.

———1978, Sedimentology and stratigraphy of the lower Eocene Wind River Formation, central Wyoming: Wyoming Geological Association Guidebook, 30th annual field conference, p. 181–198.

Shapiro, Leonard, and Brannock, W. W., 1962, Rapid analysis of silicate, carbonate, and phosphate rocks: U.S. Geological Survey Bulletin 1144–A, 56 p.

Streckeisen, A. L., 1973, Plutonic rocks, classification and nomenclature recommended by the IUGS Subcommission on the Systematics of Igneous Rocks: Geotimes, v. 18, p. 26–30.

Stuckless, J. S., and Miesch, A. T., 1981, Petrogenetic modeling of a potential uranium source rock, Granite Mountains, Wyoming: U.S. Geological Survey Professional Paper 1225, 34 p.

Stuckless, J. S., and Nkomo, I. T., 1978, Uranium-lead isotope systematics in uraniferous alkali-rich granites from the Granite Mountains, Wyoming: Implications for uranium source rocks: Economic Geology, v. 73, p. 427–441.

Suhr, N. H., and Ingamells, C. O., 1966, Solution technique for analysis of silicates: Analytical Chemistry, v. 38, p. 730–734.

Taggart, J. E., Jr., Lichte, F. E, and Wahlberg, J. S., 1982, Analysis of samples using X-ray fluorescence and induction coupled plasma spectroscopy, *in* The 1980 eruptions of Mount St. Helens, Washington: U.S. Geological Survey Professional Paper 1250, p. 683–687.

Taylor, H. P., Jr., and Epstein, S., 1962, Principles and experimental results, part 1 *of* Relationship between O^{18}/O^{16} ratios in coexisting minerals of igneous and metamorphic rocks: Geological Society of America Bulletin, v. 73, p. 461–480.

Thaden, R. E., 1980a, Geologic map of the De Pass quadrangle, Fremont and Hot Springs Counties, Wyoming: U.S. Geological Survey Geologic Quadrangle Map GQ–1526, scale 1:24,000.

———1980b, Geologic map of the Guffy Peak quadrangle, showing chromolithofacies in the Wind River Formation, Fremont and Hot Springs Counties, Wyoming: U.S. Geological Survey Geologic Quadrangle Map GQ–1527, scale 1:24,000.

———1980c, Geologic map of the Birdseye Pass quadrangle, showing chromolithofacies and coal beds in the Wind River Formation, Fremont and Hot Springs Counties, Wyoming: U.S. Geological Survey Geologic Quadrangle Map GQ–1537, scale 1:24,000.

Thornton, C. P., and Tuttle, O. F., 1960, Differentiation index, *in* Chemistry of igneous rocks: American Journal of Science, v. 258, p. 664–684.

Tuttle, O. F., and Bowen, N. L., 1958, Origin of granites in the light of experimental studies in the system $NaAlSi_3O_8$–$KAlSi_3O_8$–$CaAl_2Si_2O_8$–H_20: Geological Society of America Memoir 74, 153 p.

Wenner, D. B., 1980, Oxygen isotope variations within the Elberton Pluton, *in* Stormer, J. C., Jr., and Whitney, J. A., eds., Guidebook 19, Geological, geochemical, and geophysical studies of the Elberton Batholith, eastern Georgia: A guidebook to accompany the 15th annual Georgia Geological Society field trip, p. 31–43.

Whitney, J. A., 1975, The effects of pressure, temperature and X_{H_2O} on phase assemblages in four synthetic rock compositions: Journal of Geology, v. 83, p. 1–27.

Winkler, H. G. F., 1967, Petrogenesis of metamorphic rocks, rev. 2d ed.: New York, Springer–Verlag, 237 p.

Yellich, J. A., Cramer, R. J., and Kendall, R. G., 1978, Copper Mountain, Wyoming, Uranium deposit—rediscovered: Wyoming Geological Association Guidebook, 30th annual field conference, p. 311–327.

Zielinski, R. A., Lipman, P. W., and Millard, H. T., Jr., 1977, Minor-element abundances in obsidian, perlite, and felsite of calc-alkalic rhyolites: American Mineralogist, v. 62, p. 426–437.

Zielinski, R. A., Peterman, Z. E., Stuckless, J. S., Rosholt, J. N., and Nkomo, I. T., 1981, The chemical and isotopic record of rock-water interaction in the Sherman Granite, Wyoming and Colorado: Contributions to Mineralogy and Petrology, v. 78, p. 209–219.

Geochronology of an Archean Granite, Owl Creek Mountains, Wyoming

By C. E. HEDGE, K. R. SIMMONS, *and* J. S. STUCKLESS

CHEMICAL AND ISOTOPIC STUDIES OF GRANITIC ARCHEAN ROCKS, OWL CREEK MOUNTAINS, WYOMING

U.S. GEOLOGICAL SURVEY PROFESSIONAL PAPER 1388–B

CONTENTS

ILLUSTRATIONS

TABLES

CHEMICAL AND ISOTOPIC STUDIES OF GRANITIC ARCHEAN ROCKS, OWL CREEK MOUNTAINS, WYOMING

GEOCHRONOLOGY OF AN ARCHEAN GRANITE, OWL CREEK MOUNTAINS, WYOMING

By C. E. HEDGE, K. R. SIMMONS, and J. S. STUCKLESS

ABSTRACT

Rubidium-strontium analyses of whole-rock samples of an Archean granite from the Owl Creek Mountains, Wyo., indicate an intrusive age of 2640±125 Ma. Muscovite-bearing samples give results suggesting that these samples were altered about 2300 Ma. This event may have caused extensive strontium loss from the rocks as potassium feldspar was altered to muscovite. Alteration was highly localized in nature as evidenced by unaffected rubidium-strontium mineral ages in the Owl Creek Mountains area. Furthermore, the event probably involved a small volume of fluid relative to the volume of rock because whole-rock $\delta^{18}O$ values of altered rocks are not distinct from those of unaltered rocks. In contrast to the rubidium-strontium whole-rock system, zircons from the granite have been so severely affected by the alteration event, and possibly by a late-Precambrian uplift event, that the zircon system yields little usable age information.

The average initial $^{87}Sr/^{86}Sr$ (0.7033±0.0042) calculated from the isochron intercept varies significantly. Calculated initial $^{87}Sr/^{86}Sr$ ratios for nine apparently unaltered samples yield a range of 0.7025 to 0.7047. These calculated initial ratios correlate positively with whole-rock $\delta^{18}O$ values; and, therefore, the granite was probably derived from an isotopically heterogeneous source. The highest initial $^{87}Sr/^{86}Sr$ ratio is lower than the lowest reported for the metamorphic rocks intruded by the granite as it would have existed at 2640 Ma. Thus, the metamorphic sequence, at its current level of exposure, can represent no more than a part of the protolith for the granite.

INTRODUCTION

The Owl Creek Mountains are located near the center of an extensive area of Archean rocks that includes most of Wyoming, much of southern Montana, and adjacent parts of Utah and South Dakota. Throughout this region, older gneiss and greenstone terranes were intruded by granitic rocks between 2500 and 2800 Ma. In the Teton Range to the west, Reed and Zartman (1973) assigned an age of metamorphism of 2820 Ma to the Webb Canyon Gneiss. Several studies of metasedimentary rocks (up to granulite grade) in the Beartooth Mountains to the northwest have provided an age of 3000–3400 Ma (Nunes and Tilton, 1971; Henry and others, 1981; Wooden and others, 1981). Ages of 2800–3000 Ma have been reported for the rocks of the Big Horn Mountains to the east (Arth and others, 1980). An amphibolite-grade sedimentary-volcanic sequence in the Granite Mountains to the south has a reported rubidium-strontium whole-rock age of 2860 Ma (Peterman and Hildreth, 1978); this age probably represents the most recent period of metamorphism, as other isotopic studies suggest that at least the original sediments are as old as 3200 Ma (L. B. Fischer and J. S. Stacey, unpub. data, 1982). Granites that intrude the metamorphic complex of the Granite Mountains have been dated by uranium-lead zircon at 2640 and 2595 Ma (Ludwig and Stuckless, 1978). Two plutons in the Wind River Range (southwest of the Owl Creek Mountains) yield uranium-lead zircon ages of 2640 and 2560 Ma (Naylor and others, 1970).

Previous geochronology of the Precambrian rocks of the Owl Creek Mountains is rather limited. Giletti and Gast (1961) presented rubidium-strontium ages for pegmatitic muscovite and microcline of 2663 Ma and 2584 Ma, respectively. Lead-lead whole-rock data for the granites, reported by Nkomo and others (1978), indicate an age of 2645±60 Ma. Metamorphic rocks from Wind River Canyon gave a whole-rock rubidium-strontium age of 2755±100 Ma (Mueller and others, 1981). Diabase dikes are common throughout the Precambrian of Wyoming, and Condie and others (1969) reported potassium-argon whole-rock ages of 1900–2100 Ma for six dikes in the Owl Creek Mountains.

ANALYTICAL METHODS

Rubidium and strontium concentrations were measured on separate aliquots of whole rock using ^{87}Rb and ^{84}Sr tracers. All $^{87}Sr/^{86}Sr$ ratios (table 1) have been normalized to a $^{86}Sr/^{88}Sr$ of 0.1194, and the mass spectrometer used in this study yielded a value of

0.70802 ± 0.00006 (2σ) for the Eimer and Amend $SrCO_3$ standard. Replicate analyses of granitic samples indicate an analytical accuracy of ±1.0 percent (2σ) for concentrations and ±0.02 percent (2σ) for the strontium isotopic composition. These errors were used for data regression because they include splitting errors that can be significant for granitic materials.

Zircon separates were sized and magnetically separated. Before dissolution, the separates were leached first in 8N HCl and then in 7N HNO_3. The attack procedure is similar to that given in Krogh (1973), and the extraction procedure is that described by Ludwig and others (1981). Lead was run on a single rhenium filament using H_3PO_4-silica gel. Uranium and thorium were run together on a single filament using H_3PO_4 and aquadag. Analytical uncertainties for zircon ages were calculated according to the methods of Ludwig (1980). The determination of best-fit lines was made using the methods of Ludwig (1979), and the decay constants used are those recommended by the IUGS Subcommission on Geochronology (Steiger and Jäger, 1977).

DATA AND DISCUSSION

The rubidium-strontium analytical data are presented in table 1. On the basis of field evidence, petrography, and Q-mode analyses of chemical data (Stuckless and others, this volume), the first nine samples listed in the table are deemed to represent unaltered and cogenetic samples of the main granitic intrusion. These samples are from the North Canning area. The nine unaltered granite samples give a rubidium-strontium age of 2640 ± 125 Ma and an initial $^{87}Sr/^{86}Sr$ of 0.7033 ± 0.0042 (all errors 2σ). The scatter of data points (fig. 1) is greater than would be expected from analytical uncertainty alone, and the age and initial $^{87}Sr/^{86}Sr$ are calculated from a model-3 fit to the data (Ludwig, 1979).

A possible cause for the observed scatter in the rubidium-strontium data, as suggested by the model-3 fit, might be variable initial $^{87}Sr/^{86}Sr$ ratios. To test this hypothesis, we calculated initial $^{87}Sr/^{86}Sr$ ratios (assuming an age of 2640 Ma) and plotted them against the $\delta^{18}O$ values for those samples for which both types of data were available. A positive correlation results (fig. 2). The variable initial $^{87}Sr/^{86}Sr$ ratios cannot be an artifact of assuming the wrong age because the two samples with the highest and lowest apparent initial ratios (29467 and 41596, respectively) have nearly identical rubidium-strontium ratios. Similar correlative variations between initial $^{87}Sr/^{86}Sr$ values and whole-rock $\delta^{18}O$ values have been noted for Paleozoic granites of the southeastern Piedmont (Wenner, 1980), and the observed variability in these two parameters has been interpreted as reflecting variations within the source region of the granite (Wenner, 1981). By analogy, we conclude that the age of 2640 ± 125 Ma is correct (to the

TABLE 1.—*Rubidium-strontium data for whole-rock samples from the Owl Creek Mountains, Wyo.*

Sample number	Rb (ppm)	Sr (ppm)	$^{87}Rb/^{86}Sr$	$^{87}Sr/^{86}Sr$
		Unaltered granite		
41596	185.9	218.0	2.491	0.7982
29394	193.2	235.3	2.396	.7947
23432	171.3	190.2	2.630	.8030
41591	188.8	252.3	2.184	.7871
29467	196.6	232.1	2.474	.7993
30511	175.6	247.7	2.067	.7820
23496	193.3	190.8	2.964	.8166
30501	187.5	241.2	2.267	.7898
32466	159.0	201.2	2.307	.7916
		Altered granite		
TDG12	292.1	79.5	11.049	1.1068
TDG47	144.9	116.8	3.637	.8339
58-80	196.7	95.4	6.087	.9162
58-66	230.1	93.6	7.293	.9649
58-98	166.5	101.3	4.839	.8780
GP-1	735.0	8.58	1807.5	65.04
GP-4	34.3	590.1	.1682	.7104
		Metamorphic rocks		
DKCH-207	88.0	193.6	1.322	0.7582
DKCH-254	98.1	99.2	2.894	.8246
DKCH-263	94.3	132.5	2.076	.7932
58188	117.6	286.7	1.193	.7580

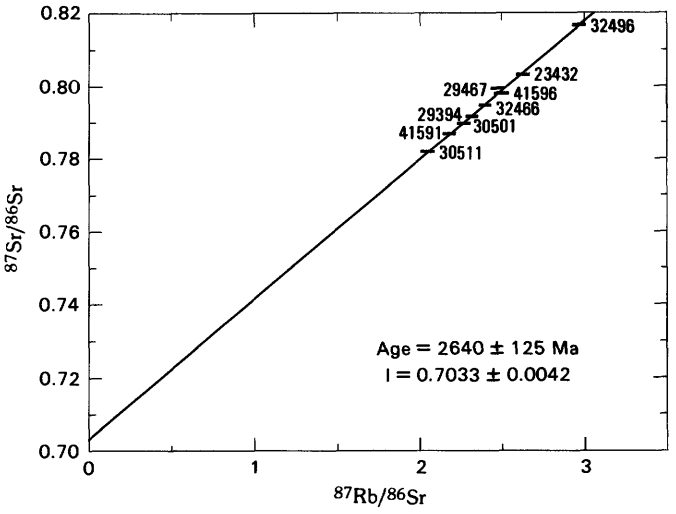

FIGURE 1.—Rubidium-strontium isochron diagram for unaltered granite samples from the North Canning area, Owl Creek Mountains, Wyo. Symbol size corresponds to ±2σ analytical error.

extent that the data fit the mathematical assumptions of model 3) and that the scatter of the rubidium-strontium data for the granite of the Owl Creek Mountains (fig. 1) is a function of variable $^{87}Sr/^{86}Sr$ caused by melting of an isotopically heterogeneous source and crystallization prior to homogenization of the magma. Assimilation of metasedimentary wall rock might also explain the variable initial $^{87}Sr/^{86}Sr$; however, the $\delta^{18}O$ values of the metamorphic rocks are low, and the $^{87}Sr/^{86}Sr$ ratios of the metamorphic rocks at the time of intrusion were high. Hence, assimilation of these rocks would produce a negative trend of $\delta^{18}O$ versus initial $^{87}Sr/^{86}Sr$. Also, such a mechanism would be incompatible with the Q-mode analyses of the chemical data (Stuckless and others, this volume).

The remaining seven granite samples in table 1 show various types of evidence for alteration. Sample GP–4 is a silicified-epidotized granite, sample GP–1 is an albitized and garnetiferous granite, and the other five samples contain abundant (secondary?) muscovite. These seven samples do not define a precise rubidium-strontium isochron (fig. 3) but give an apparent age of 2463 Ma. For reasons that are not totally understood, rubidium-rich and strontium-poor samples like GP–1 frequently yield low apparent rubidium-strontium ages relative to samples of lower Rb/Sr from the same rock unit. For geologic (Gilluly, 1933) and isotopic reasons (Stuckless and others, 1981), albitized samples such as GP–1 are thought to be the product of postmagmatic hydrothermal alteration. Samples similar to GP–4 have been interpreted to have been altered hydrothermally after crystallization of a granite (Peterman and Hildreth, 1978; Stuckless and others, 1981). The remaining five samples, which are all from the North Canning area, seem to represent an event that is separate from the two types of hydrothermal alteration noted for samples GP–1 and GP–4.

The altered samples from the North Canning area have distinctly different rubidium-strontium systematics relative to the unaltered samples from the same area. The unaltered samples have very limited ranges of rubidium and strontium contents (rubidium range from 159 to 197, average 183; strontium range from 190 to 252, average 223). The altered samples from this same area have similar rubidium contents (range from 145 to 230, average 185) but markedly lower strontium contents (range from 94 to 116, average 102). The alteration process appears, therefore, to have had little effect on the rubidium, but to have lowered the strontium contents to something less than half of the original values. This postulated expulsion of strontium is consistent with the petrographic observation that, during alteration, potassium feldspar was partially transformed to muscovite. Potassium feldspar accepts appreciable strontium, whereas muscovite does not. Assuming that such is indeed the mechanism of strontium loss and that the altered samples originally had strontium contents like those of the unaltered samples, we can calculate that the time of alteration was approximately 2300 Ma. According to this interpretation, the "age" of 2463 Ma, shown in figure 2, results either from multiple types of alteration that may be of different ages or from scatter indicative of a resetting process that was less than perfect.

The mechanism and driving force needed to locally transform potassium feldspar to muscovite are not un-

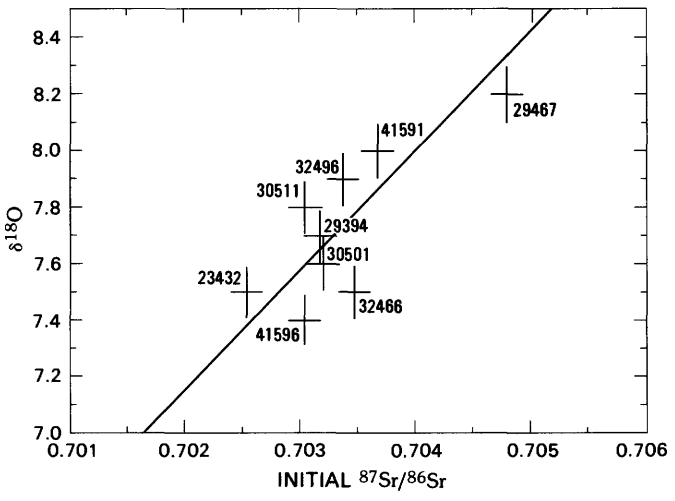

FIGURE 2.—Plot showing correlation of initial $^{87}Sr/^{86}Sr$ with whole-rock $\delta^{18}O$ values for unaltered granite samples from the Owl Creek Mountains, Wyo. Symbol sizes correspond to $\pm 2\sigma$.

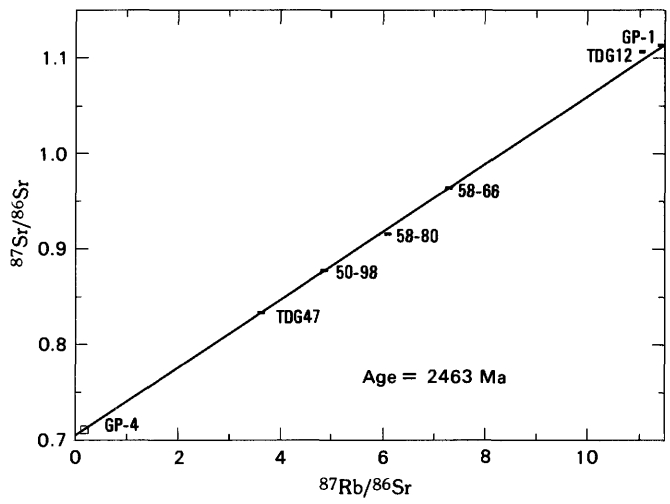

FIGURE 3.—Rubidium-strontium isochron diagram for altered granite samples. Data for sample GP–1 (indicated by arrow) plot well beyond the boundaries of the diagram, but on the isochron. Symbol size corresponds to $\pm 2\sigma$ except data for GP–4 which plot as a dot in the center of the square.

derstood, but it is noteworthy that the alteration was patchy and that samples separated by less than 100 m could exhibit very different rubidium-strontium whole-rock systematics. The event was probably not accompanied by regional heating (as documented for granites approximately 80 km to the south by Peterman and Hildreth, 1978) because rubidium-strontium ages for pegmatitic minerals were not reset (Giletti and Gast, 1961). It also appears that the alteration did not affect whole-rock $\delta^{18}O$ values because values for four of the altered samples from North Canning are within the range of values for unaltered samples from the same area (Stuckless and others, this volume). This similarity in $\delta^{18}O$ suggests that the volume of fluid was small relative to the volume of rock. Alternatively, the fluid had a fortuitously appropriate isotopic composition relative to temperature of alteration, or possibly alteration occurred at too high a temperature to cause isotopic fractionation. The latter seems unlikely in view of the evidence against significant regional heating. Finally, even the whole-rock chemistry of samples identified as altered by rubidium-strontium systematics and supported by petrographic observations is apparently unaffected because at least some of the altered samples are well accounted for by Q-mode factor analysis (Stuckless and others, this volume). Although the specifics of alteration are not understood, the conclusion that subtle changes in mineralogic assemblages can indicate large effects on rubidium-strontium systematics of individual, closely spaced samples without concomitant evidence from major-element chemistry or oxygen isotope data has significant implications for rubidium-strontium geochronology.

Six zircon fractions from two hydrothermally altered rocks and one apparently unaltered rock were analyzed for uranium and lead isotopic compositions (table 2). The results yield little information about the age of the granite. The data fail to define a unique line on a concordia diagram (fig. 4), and all that can be said with complete certainty is that the zircons indicate an age in excess of 2514 Ma (the oldest observed lead-lead age).

If the intrusive age for the granite is 2640 Ma, as indicated by the rubidium-strontium data for the unaltered samples, the zircon data points should lie along a line whose upper intercept is 2640 Ma and whose lower intercept approximates the time of the Tertiary uplift (for example, the heavy solid line on fig. 4). By assuming that only one Precambrian event has affected the samples since crystallization, we can place some limits on when that event occurred. It must have happened after 2393 Ma, because this is the youngest lead-lead age, but before 1700 Ma, which is the age calculated by passing a line from 2640 Ma through the data point for the zircon closest to concordia (GP–5–3). The former case requires that the Precambrian event totally reset sample 58–80–2, whereas the latter requires that no lead has been lost recently from GP–5–3. Neither extreme seems particularly appealing, and the second case is the more unlikely. We, therefore, conclude that the resetting of the zircons occurred between 2393 and 1700 Ma, and perhaps nearer the upper than the lower part of the range. In other words, the zircons may have been partly reset at the same time as the rubidium-strontium systems of the altered rocks (about 2300 Ma), and the zircons may also have been disturbed during the Tertiary uplift or mineralization event.

TABLE 2.—*Uranium-lead isotopic data for zircon separates from granites of the Owl Creek Mountains, Wyo.*

Sample number	Concentrations U (ppm)	Concentrations Pb (ppm)	Atomic ratios $^{206}Pb/^{238}U$	Atomic ratios $^{207}Pb/^{235}U$	Atomic ratios $^{207}Pb/^{206}Pb$	Ages $^{206}Pb/^{238}U$	Ages $^{207}Pb/^{235}U$	Ages $^{207}Pb/^{206}U$
GP-5-1	3124	2161	0.4033	9.211	0.1657	2184	2359	2514
GP-5-2	2701	1321	.2970	6.642	.1622	1676	2065	2479
GP-5-3	3965	2776	.4264	9.3561	.1591	2290	2375	2446
58-80-1	4128	1468	.3024	6.494	.1558	1703	2045	2410
58-80-2	4562	1733	.3182	6.766	.1542	1789	2081	2393
41596	719	204	.1482	3.226	.1579	891	1463	2433

In addition to an early and recent lead loss, there may have been a lead loss from the zircons during the late-Precambrian unroofing. Lead loss at that time would not greatly alter the above interpretation, but the upper limit for the earlier Proterozoic event would be increased to about 2460 Ma. A lead loss during the late Precambrian eliminates the paradox of a zircon (41596) that was affected by the 1700- to 2300-Ma event in a sample for which the rubidium-strontium whole-rock system was unaffected (fig. 5).

The mechanism by which most of the zircons were reset is not clear, but some of the salient features are noteworthy. The alteration event was local and not regional. No Early Proterozoic resetting was encountered for zircons in the studies (cited in the introduction) of the surrounding Precambrian exposures except for small hydrothermally altered outcrops (Ludwig and Stuckless, 1978).

The zircon data are unusual in that the common-lead and uranium contents of these zircons are exceptionally high. Uranium analyses for 963 zircons from granitic rocks yield a geometric mean of 636 ppm with a standard deviation of +934 and −379 ppm (Stuckless and VanTrump, 1982). All of the uranium contents for zircons from the altered rock are more than two standard deviations greater than this mean, and three of the five are more than three standard deviations greater than this mean. In contrast, the uranium content for the one zircon from an apparently unaltered granite is indistinguishable from that of an average granitic zircon. Also

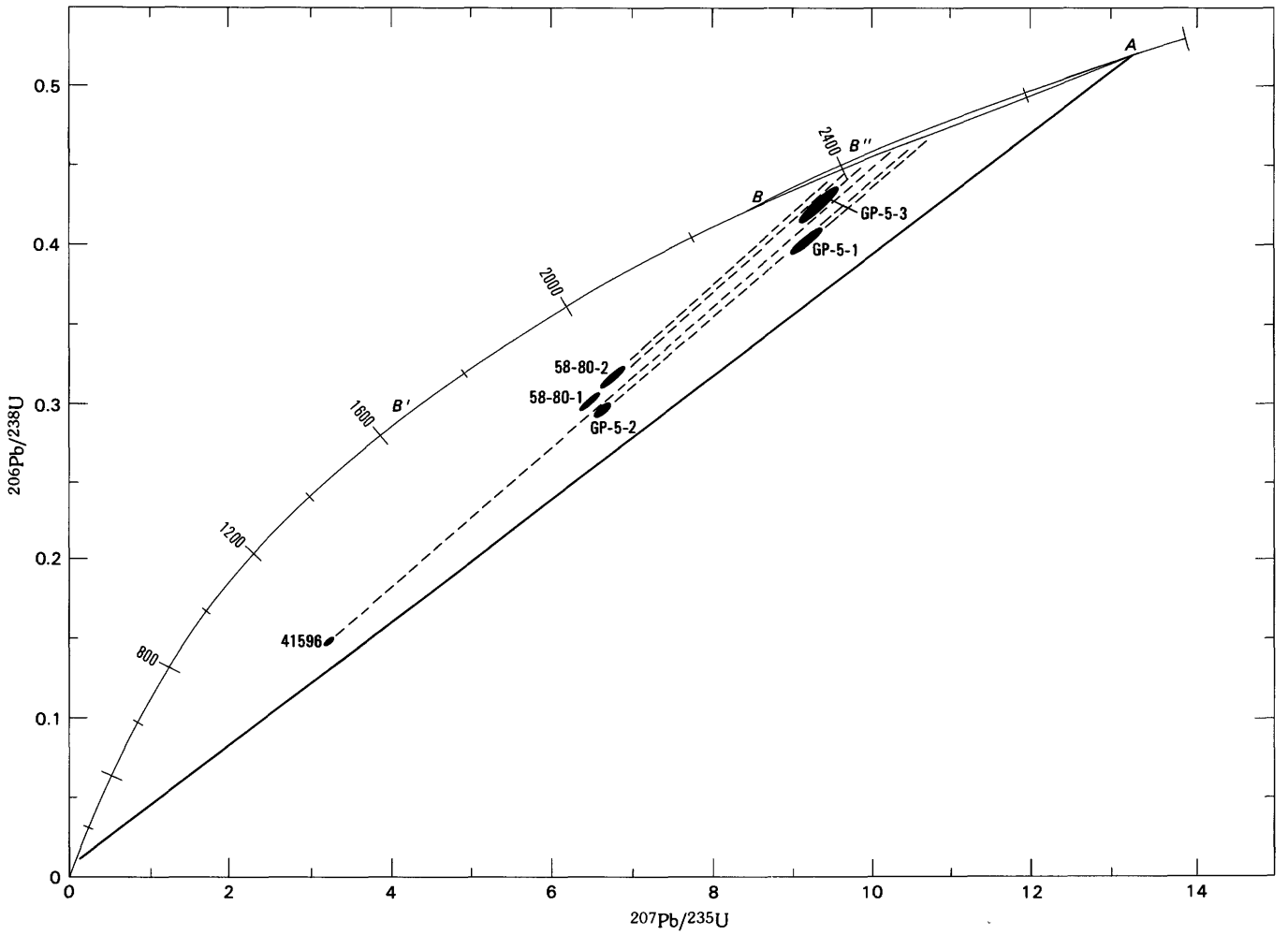

FIGURE 4.—Concordia plot for uranium-lead data from zircons. Symbol sizes represent analytical error at the 2σ level. The point labeled A represents the intrusive age, and B represents the time of alteration as indicated by the rubidium-strontium data. The possible limits for B are indicated by B'and B''. The line from A to near the origin indicates where the data would have plotted if they had not been affected by the event at time B'. According to this interpretation, at time B data points were displaced from A towards B and would have plotted along line A–B had no further lead loss occurred. In response to the Tertiary uplift and uncovering, the zircons again lost lead such that data points were displaced from line A–B to their current positions along paths indicated by the dashed lines.

exceptional is the fact that the frequently observed relationships of increasing degree of discordance with increasing uranium content of the zircons is only partly true for the zircons from the altered rock. If all the data are considered, no such correlation is seen because the zircon with the lowest uranium content is the most discordant. Whether these features represent cause or effect of the zircon resetting is unknown, but the problem merits further study.

No real effort was made to determine the age of the metamorphic complex; however, a few drill-core samples were analyzed in order to test the possibility that the granitic magma was derived from the metamorphic complex. Mueller and others (1981) reported an initial $^{87}Sr/^{86}Sr$ for metadacite of the Owl Creek Mountains of 0.7037 ± 0.0015 at 2755 Ma; they pointed out that although the age was probably applicable to all of the metavolcanic rocks, the initial ratio need not be. The average metadacite would have been too radiogenic at 2640 Ma to account for all but the highest calculated initial $^{87}Sr/^{86}Sr$ of the granite. At 2640 Ma, the $^{87}Sr/^{86}Sr$ ratios calculated for three metagraywackes and one granitic gneiss analyzed as part of this study (table 1, the last four samples) range from 0.7077 to 0.7140. These analyzed metamorphic rocks were, therefore, too radiogenic to have been a source material for a granite for which calculated initial $^{87}Sr/^{86}Sr$ ratios range from 0.7025 to 0.7047. This conclusion is valid even though our samples of the metamorphic sequence do not yield an isochronal relationship if it is assumed that these

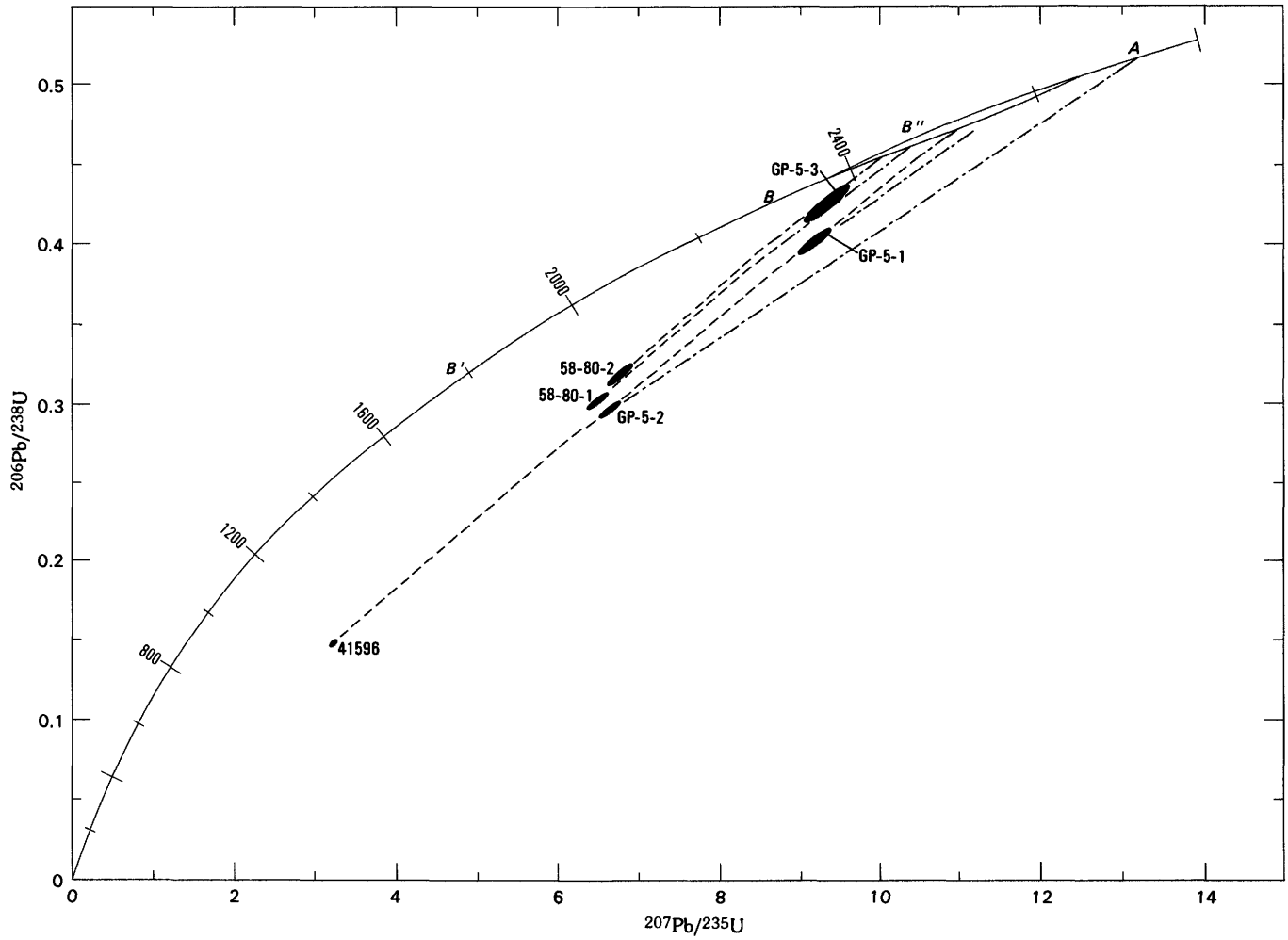

FIGURE 5.—Concordia plot for uranium-lead data from zircons assuming the added complexity of lead loss at 600 Ma. Symbol sizes represent analytical error at the 2σ level. Points A and B represent the time of intrusion and alteration, respectively, and B′ and B″ represent the maximum limits of B. In this alternate interpretation, data for all of the zircons except 41596 would plot along the line A–B at time B. All of the zircons would have then responded to the late Precambrian uplift and unroofing such that data points were displaced along the dot-dash vectors. Finally, data points were moved along the dash lines in response to the Tertiary uplift event.

samples behaved as a closed system from 2640 Ma ago to the present. Thus, the metamorphic sequence as presently exposed is not a suitable source for the granitic magma. A suitable protolith would have lower rubidium-strontium ratios and consequently lower $^{87}Sr/^{86}Sr$ values. Such a protolith may have been more mafic than the exposed metamorphic sequence. Alternatively, the protolith could be similar to the metamorphic sequence if rubidium-strontium ratios were lowered at least 300 Ma before generation of the granite.

Earlier depletion of rubidium in deeper parts of the metamorphic sequence by granulite facies metamorphism (Heier, 1960; Lambert and Heier, 1968) could have created a source for the granite of the Owl Creek Mountains that had low and inhomogeneous $^{87}Sr/^{86}Sr$ ratios of 2640 Ma. A source region that had experienced granulite facies metamorphism could also account for the relatively low $\delta^{18}O$ whole-rock values for a granite as evolved as the granite of the Owl Creek Mountains (Hoefs, 1980) and for such low initial $^{206}Pb/^{204}Pb$ ratios which could persist as a result of uranium depletion (Gray and Oversby, 1972).

CONCLUSIONS

Rubidium-strontium analyses of whole-rock samples of an Archean granite from the Owl Creek Mountains indicate an age of 2640 Ma. Results for altered samples can be interpreted as indicating an alteration age of about 2300 Ma and further suggest extensive strontium loss during alteration. Zircons from the granite were so severely affected that they give little usable age information. The resetting of the zircons may have occurred about 2300 Ma, but a second resetting in re-

sponse to unroofing at the end of the Precambrian cannot be ruled out. Measured and published strontium isotopic data for the intruded metamorphic complex indicate that the granite could not have been derived by melting of these rocks at their current level of exposure. However, if the same or similar rocks exist at depth and were metamorphosed to granulite facies at 3000 Ma or earlier, they could account for the low and variable initial $^{87}Sr/^{86}Sr$ ratios observed for the granite.

REFERENCES

Arth, J. B., Barker, Fred, and Stern, T. W., 1980, Geochronology of Archean gneisses in the Lake Helen area, southwestern Big Horn Mountains, Wyoming: Precambrian Research, v. 11, p. 11–22.

Condie, K. C., Leech, A. P., and Baadsgaard, Halfdan, 1969, Potassium-argon ages of Precambrian mafic dikes in Wyoming: Geological Society of America Bulletin, v. 80, p. 899–906.

Giletti, B. J., and Gast, P. W., 1961, Absolute age of Precambrian rocks in Wyoming and Montana, *in* Kulp, J. L., ed., Geochronology of rock systems: Annals of the New York Academy of Sciences, v. 91, p. 454–458.

Gilluly, James, 1933, Replacement origin of albite granite near Sparta, Oregon: U.S. Geological Survey Professional Paper 175–C, p. 65–81.

Gray, C. M., and Oversby, V. M., 1972, The behavior of lead isotopes during granulite facies metamorphism: Geochimica et Cosmochimica Acta, v. 36, p. 939–952.

Heier, K. S., 1960, Petrology and geochemistry of high-grade metamorphic and igneous rocks on Langoy, northern Norway: Norge Geologiska Undersokelse, v. 207, 246 p.

Henry, D. J., Mueller, P. A., and Wooden, J. L., 1981, Early Archean granulite supracrustal assemblages, eastern Beartooth Mountains, Wyoming: Geological Society of America Abstracts with Programs, v. 13, p. 471.

Hoefs, J., 1980, Stable isotope geochemistry, 2d ed.: Berlin, Springer–Verlag, 218 p.

Krogh, T. E., 1973, A low-contamination method for hydrothermal decomposition of zircon and extraction of U and Pb for isotopic age determinations: Geochimica et Cosmochimica Acta, v. 37, p. 485–494.

Lambert, I. B., and Heier, K. S., 1968, Geochemical investigations of high grade regional metamorphic and associated rocks in the Australian shield: Lithos, v. 1, p. 30–53.

Ludwig, K. R., 1979, A program in Hewlett–Packard BASIC for X-Y plotting and line-fitting of isotopic and other data: U.S. Geological Survey Open-File Report 79–1641, 33 p.

———1980, Calculations of uncertainties of U-Pb isotope data: Earth and Planetary Science Letters, v. 46, p. 212–220.

Ludwig, K. R., Nash, J. T., and Naeser, C. W., 1981, U-Pb isotope systematics and age of uranium mineralization, Midnite Mine, Washington: Economic Geology, v. 76, p. 89–110.

Ludwig, K. R., and Stuckless, J. S., 1978, Uranium-lead isotope systematics and apparent age of zircons and other minerals in Precambrian granitic rocks, Granite Mountains, Wyoming: Contributions to Mineralogy and Petrology, v. 65, p. 243–254.

Mueller, P. A., Peterman, Z. E., and Granath, J., 1981, An Archean bimodal volcanic series, Owl Creek Mountains, Wyoming: Geological Society of America Abstracts with Programs, v. 13, p. 515–516.

Naylor, R. S., Steiger, R. H., and Wasserburg, G. J., 1970, U-Th-Pb and Rb-Sr systematics of 2700×10^6 year old plutons from the southern Wind River Range, Wyoming: Geochimica et Cosmochimica Acta, v. 34, p. 1133–1159.

Nkomo, I. T., Stuckless, J. S., Thaden, R. E., and Rosholt, J. N., 1978, Petrology and uranium mobility of an early Precambrian granite from the Owl Creek Mountains, Wyoming: Wyoming Geological Association Guidebook, 30th annual field conference, p. 335–348.

Nunes, P. D. and Tilton, G. R., 1971, Uranium-lead ages of minerals from the Stillwater igneous complex and associated rocks, Montana: Geological Society of America Bulletin, v. 82, p. 2231–2250.

Peterman, Z. E., and Hildreth, R. A., 1978, Reconnaissance geology and geochronology of the Precambrian of the Granite Mountains, Wyoming: U.S. Geological Survey Professional Paper 1055, 22 p.

Reed, J. C., Jr., and Zartman, R. E., 1973, Geochronology of the Precambrian rocks of the Teton Range, Wyoming: Geological Society of America Bulletin, v. 84, p. 561–582.

Steiger, R. H. and Jäger, E., 1977, Subcommission geochronology: Convention on the use of decay constants in geo- and cosmochronology: Earth and Planetary Science Letters, v. 36, p. 359–362.

Stuckless, J. S., Nkomo, I. T., and Doe, B. R., 1981, U-Th-Pb systematics in hydrothermally altered granites from the Granite Mountains, Wyoming: Geochimica et Cosmochimica Acta, v. 45, p. 635–645.

Stuckless, J. S. and VanTrump, George, Jr., 1982, An evaluation of uranium contents in zircons from igneous rocks of the contiguous United States as an aid to exploration and resource assessment: Proceedings of the IAEA/OECD Symposium on Uranium Exploration Methods, Paris, June 1–4, 1982, p. 369–384.

Wenner, D. B., 1980, Oxygen isotope variations within the Elberton pluton, *in* Stormer, J. C., Jr., and Whitney, J. A., eds., Geological, geochemical and geophysical studies of the Elberton Batholith, eastern Georgia: A Guidebook to accompany the 15th annual Georgia Geological Society field trip, p. 31–43.

———1981, Oxygen isotopic compositions of the late orogenic granites in the southern Piedmont of the Appalachian Mountains, U.S.A., and their relationship to subcrustal structures and lithologies: Earth and Planetary Science Letters, v. 54, p. 186–199.

Wooden, J. L., Muellers, P. A., and Bowes, D. R., 1981, Archean crustal evolution in the Beartooth Mountains, Montana-Wyoming: Geological Society of America Abstracts with Programs, v. 13, p. 585.

Uranium-Thorium-Lead Systematics of an Archean Granite from the Owl Creek Mountains, Wyoming

By J. S. STUCKLESS, I. T. NKOMO, *and* K. A. BUTT

CHEMICAL AND ISOTOPIC STUDIES OF GRANITIC ARCHEAN ROCKS, OWL CREEK MOUNTAINS, WYOMING

U.S. GEOLOGICAL SURVEY PROFESSIONAL PAPER 1388–C

CONTENTS

ILLUSTRATIONS

TABLE

CHEMICAL AND ISOTOPIC STUDIES OF GRANITIC ARCHEAN ROCKS
OWL CREEK MOUNTAINS, WYOMING

URANIUM-THORIUM-LEAD SYSTEMATICS OF AN ARCHEAN GRANITE FROM THE OWL CREEK MOUNTAINS, WYOMING

By J. S. STUCKLESS, I. T. NKOMO, and K. A. BUTT

ABSTRACT

Isotopic analyses of apparently unaltered whole-rock samples of a granite from the Owl Creek Mountains, Wyo., yield a lead-lead isochron age of 2,730±35 Ma, which is somewhat older than the age obtained by the rubidium-strontium whole-rock method. Thorium-lead data for the same samples deviate markedly from an isochronal relation; however, calculated initial $^{208}Pb/^{204}Pb$ ratios correlate with whole-rock $\delta^{18}O$ values and lead to the conclusion that the ^{232}Th-^{208}Pb data are not colinear because of an originally heterogeneous granitic magma. This conclusion also has been drawn on the basis of chemical and other isotopic data and attributed to inhomogeneities in the protolith. Although the protolith apparently had a wide range in $^{232}Th/^{204}Pb$ ratios, the range for $^{238}U/^{204}Pb$ ratios (μ) was small. The μ values for the protolith are high relative to an average orogene, and thus the source region for the granite was anomalously uraniferous.

Relationships in the $^{207}Pb/^{235}U$-$^{206}Pb/^{238}U$ system show that uranium was mobilized during early Laramide time or shortly before, such that most surface and shallow drill-core samples lost 60–80 percent of their uranium, and some fractured, deeper drill-core samples gained from 50 to 10,000 percent uranium. Fission-track maps show that much uranium is located along edges and cleavages of biotite and magnetite where it is readily accessible to oxidizing ground water. Furthermore, qualitative comparisons of uranium distribution in samples with excess radiogenic lead and in samples with approximately equilibrium amounts of uranium and lead suggest that the latter contain more uranium in these readily accessible sites.

Unlike other granites that have uranium distributions and isotopic systematics similar to those observed in this study, the granite of the Owl Creek Mountains is not associated with economic uranium deposits. We attribute this to the small areal extent of the granite, the shallow depth of leaching, and the timing of uranium mobilization, which apparently predated the deposition of sediments that elsewhere in central Wyoming host uranium ore.

INTRODUCTION

The granite of the Owl Creek Mountains is overlain by Tertiary sedimentary rocks that contain uranium-mineralized areas, and the granite hosts moderate-sized areas of mineralized fractures (Yellich and others, 1978). The study of uranium-thorium-lead isotope systematics in the Granite Mountains to the south has proved useful in demonstrating a probable connection between Archean granite and Tertiary uranium deposits (Rosholt and others, 1973; Stuckless and Nkomo, 1978). A preliminary isotopic study of the granite of the Owl Creek Mountains has suggested that this granite may also be related to uranium mineralization (Nkomo and others, 1978).

Uranium-thorium-lead systematics can yield information on uranium gain or loss from a granite, the timing of uranium movement (including multiple events in certain circumstances), the age of the granite, and constraints on the source of the granite (Rosholt and others, 1973; Stuckless and Nkomo, 1978). The method consists of determining the concentrations of uranium, thorium, and lead and the isotopic composition of lead for cogenetic samples that were isotopically homogeneous at the time of crystallization. Isochronal relationships are examined in the ^{232}Th-^{208}Pb and ^{206}Pb-^{207}Pb systems for linear fits within the limits of analytical error and agreement of calculated ages. Internally precise isochrons and agreement between ages calculated from the two isochrons indicate that uranogenic lead concentrations can be used as a measure of uranium gain or loss. If the isotopic composition of lead at the time of intrusion can be measured or closely estimated, relationships within the $^{207}Pb/^{235}U$-$^{206}Pb/^{238}U$ system can be used to place limits on the amount and timing of uranium mobility.

Results reported in this study build on information gained from chemical and other isotopic studies. Oxygen and strontium isotopic studies and uranium-lead analyses in zircons (Stuckless and others, this volume; Hedge and others, this volume) show that the granite of the Owl Creek Mountains was isotopically inhomogeneous at the time of intrusion and that isotopic systems in at least some samples have been affected by one or more postmagmatic events. Furthermore, not all of the spatially associated granitic samples are genetically related. These results indicate that many samples will not fit a simple interpretation of the ura-

TABLE 1.—*Uranium, thorium, and lead concentrations and the isotopic compositions of lead for samples from the Owl Creek Mountains, Wyo.*

Sample	Plot I.D.	U (ppm)	Th (ppm)	Pb (ppm)	$^{206}Pb/^{204}Pb$	$^{207}Pb/^{204}Pb$	$^{208}Pb/^{204}Pb$
23432	9	21.88	24.51	52.83	27.645	17.570	38.245
41596	12b	12.80	20.69	45.47	23.573	16.837	37.451
29394	13c	11.94	42.26	46.09	22.244	16.568	42.824
DP-2	4	14.58	26.61	56.93	26.097	17.303	37.698
32496	14b	14.44	24.32	50.99	22.748	16.683	38.070
30511	13b	9.16	36.53	51.20	22.067	16.533	40.344
DP-3	8	3.39	38.55	46.41	22.163	16.542	41.229
29467	13d	8.42	25.32	38.12	22.126	16.520	40.283
GP-3	17	9.22	44.92	75.61	26.385	17.350	39.451
TD22	21	2.44	47.54	56.51	22.337	16.604	41.184
4343	7	16.08	59.49	61.41	22.723	16.669	42.861
TDG21	22	2.29	50.82	54.92	20.113	16.158	42.186
58180	10d	160.5	50.09	91.27	59.285	23.152	42.011
TD-13	1	3.72	50.03	67.01	22.980	16.741	41.131
TDG46	11a	71.79	28.97	60.66	31.268	18.102	39.140
GP-5	5	3.09	20.22	42.5	22.795	16.701	36.001
TDG47	11b	78.41	34.50	75.21	77.352	26.307	42.544
TDG12	2a	12.89	34.44	38.26	28.307	17.616	41.248
58-66	10a	5.29	29.08	56.33	26.172	17.299	36.310
58-80	10b	11.80	29.13	44.65	28.465	17.666	38.088
58-98	10c	5.37	26.29	46.41	26.091	17.299	36.754
DP-1	2b	2.87	8.17	62.45	17.159	15.673	34.338
TDG16	24	3.77	5.23	41.22	23.261	16.547	35.306
TDG20	23	2.42	7.23	8.15	34.811	19.191	39.501
58317	10f	1994	26.35	81.11	54.263	21.700	37.491
TDG45	6b	2.78	2.07	10.94	17.230	15.681	36.005
TDG24	25	4.68	16.58	36.03	19.551	16.070	37.119
TD-6	16	.40	2.13	42.26	15.200	15.389	34.470
TDG44	6a	14.50	35.02	70.48	23.199	16.745	37.291

nium-thorium-lead systematics. Thus, for isotopic purposes, the data are considered as three subsets: (1) the main granite intrusion, which is subdivided into (1a) samples apparently unaffected by postmagmatic hydrothermal alteration and (1b) hydrothermally altered samples, and (2) samples not genetically related to the main intrusion.

ANALYTICAL PROCEDURES

Uranium, thorium, and lead concentrations for 29 whole-rock samples were determined by isotope dilution and mass spectrometry. Compositions and concentrations were determined on separate dissolutions, and therefore a minimum of 1-g splits of −200 mesh powder was used for each sample in order to minimize splitting errors. Most samples were analyzed in duplicate and average results are reported in table 1. Examination of duplicate analyses indicates a precision of ±0.5 percent for elemental ratios (2σ) and ±0.2 percent for isotopic composition ratios (2σ). Details of chemical and mass spectrometric procedures are nearly the same as those described by Rosholt and others (1973) except that lead was analyzed using the silica gel-H_3PO_4 method.

Regression analysis of the data used the methods of York (1969). Decay and isotopic constants used are those recommended by the IUGS Subcommission on Geochronology (Steiger and Jäger, 1977). Reported errors are at the 95 percent confidence limit.

RESULTS

Data for the granite of the Owl Creek Mountains exhibit extremely large ranges in both elemental concentrations and isotopic compositions. Uranium concentrations range from 0.40 to 1,994 ppm. Exclusion of four obviously mineralized samples (TDG46, 58180, TDG47, and 58314) still leaves an upper limit of 21.88 ppm (sample 23432) and eight other samples that contain more than 10 ppm uranium. Thus the granite of the Owl Creek Mountains is anomalously uraniferous

relative to the typical range of 0.5–5.0 ppm uranium for silicic plutonic rocks (Rogers and Adams, 1969a). Thorium contents can be anomalously large and range from 2.07 to 59.49 ppm, which compares to a typical range of 10–20 ppm (Rogers and Adams, 1969b). Lead contents vary from 8.15 to 91.27 ppm and are generally greater than 40 ppm. These values contrast with an arithmetic mean lead content for granites of 23.6 ppm (Wedepohl, 1974) and reflect a large radiogenic lead component in the total lead.

The isotopic composition of lead shows a wide range of values ($^{206}Pb/^{204}Pb$, 15.200 to 77.352; and $^{208}Pb/^{204}Pb$, 34.338 to 42.861). Most compositions are generally much more radiogenic than that of the average modern orogene. Its composition isotopically approximates that of the average mantle, upper crust, and lower crust (Doe and Zartman, 1979), and is given as 18.70 for $^{206}Pb/^{204}Pb$ and 38.63 for $^{208}Pb/^{204}Pb$ (Stacey and Kramers, 1975). This radiogenic tendency is reasonable in view of the Archean age and high uranium and thorium contents. However, three samples (DP–1, TDG45, and TD–6) are less radiogenic than the average orogenic lead.

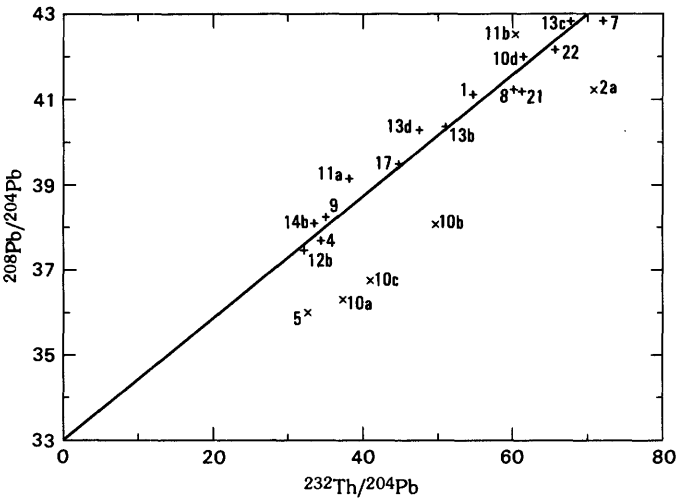

FIGURE 1.—Plot of $^{232}Th/^{204}Pb$ versus $^{208}Pb/^{204}Pb$ for apparently cogenetic samples from the granite of the Owl Creek Mountains. Reference line corresponds to an age of 2,700 Ma. Samples that are suspected to have been affected by postmagmatic alteration are shown by x's. Other samples are shown by crosses that correspond to $\pm 2\sigma$ analytical error.

DISCUSSION

SAMPLE SELECTION

Results of extended Q-mode factor analyses have shown that several of the analyzed samples are not related chemically to the main granite intrusion (Stuckless and others, this volume). Therefore, these samples (the last eight on table 1) were not used in the construction of isochron diagrams. Likewise, the rubidium-strontium system has been largely reset by a postmagmatic, hydrothermal alteration for five samples (Hedge and others, this volume). These samples (TDG47 through 58–98, table 1) were also not used in isochron regressions. Ten of the remaining sixteen samples could not be evaluated by this criterion because they were not analyzed isotopically for rubidium and strontium. However, three of these samples (TD–13, TDG46, and GP–5) are nearly colinear with the hydrothermally altered samples on a log-log plot of rubidium and strontium concentration data and, therefore, may be reset samples. The first 13 samples in table 1 are thought to be cogenetic and are apparently unaltered.

AGE RELATIONSHIPS

A plot of the thorium-lead isotopic data (fig. 1) for the 21 samples for which a probable genetic relationship has been established by extended Q-mode factor analysis reveals a marked deviation from linearity that is well in excess of that predicted by analytical error. Fifteen of the samples scatter about a trend with a slope that corresponds to an age of 2,700 Ma. Four of five hydrothermally altered samples (10a, 10b, 10c, and 2a, fig. 1) as defined by the rubidium-strontium system (Hedge and others, this volume) are displaced towards higher $^{232}Th/^{204}Pb$ values and form a second trend. A fifth sample (5, fig. 1) lies along this second trend and therefore was most likely affected by the postmagmatic hydrothermal alteration. Displacements from the first to the second trend are probably due to radiogenic lead loss as discussed later in this section. One sample (11b, fig. 1) that plots with the hydrothermally altered samples in the rubidium-strontium system has an anomalously high $^{208}Pb/^{232}Th$ value relative to either of the trends, which suggests that this sample may have gained some radiogenic lead long after crystallization of the granite.

Analysis of oxygen and strontium isotopic data has shown that the granite was isotopically inhomogeneous at the time of intrusion and that variations in oxygen and initial strontium isotopic compositions are correlative (Hedge and others, this volume). Figure 2 shows a similar correlation for $\delta^{18}O$ and calculated initial $^{208}Pb/^{204}Pb$ ratios. The good correlation between calculated initial-lead composition and $\delta^{18}O$ suggests (1) that the excess scatter about the reference 2,700-Ma isochron on figure 1 can be explained by isotopic inhomogeneities in the magma at the time of intrusion, and (2) that, for most samples, the thorium-lead system has remained closed throughout the history of the granite.

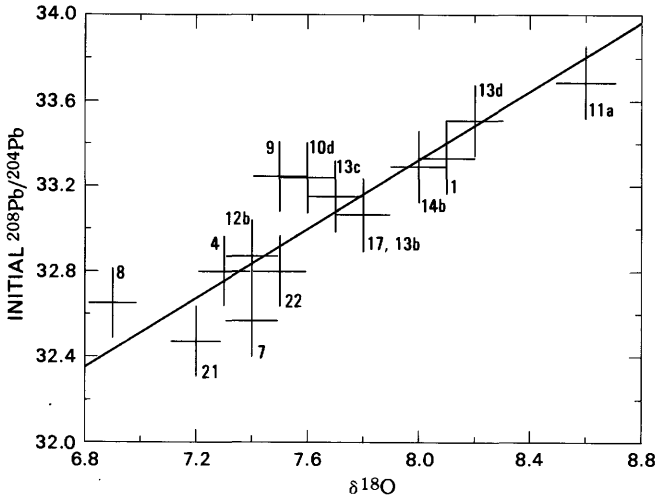

FIGURE 2.—Plot of whole-rock $\delta^{18}O$ values versus initial $^{208}Pb/^{204}Pb$ ratios assuming an intrusive age of 2,700 Ma. Symbol size corresponds to errors of ±1.2 percent for $\delta^{18}O$ and ±0.5 percent for initial $^{208}Pb/^{204}Pb$.

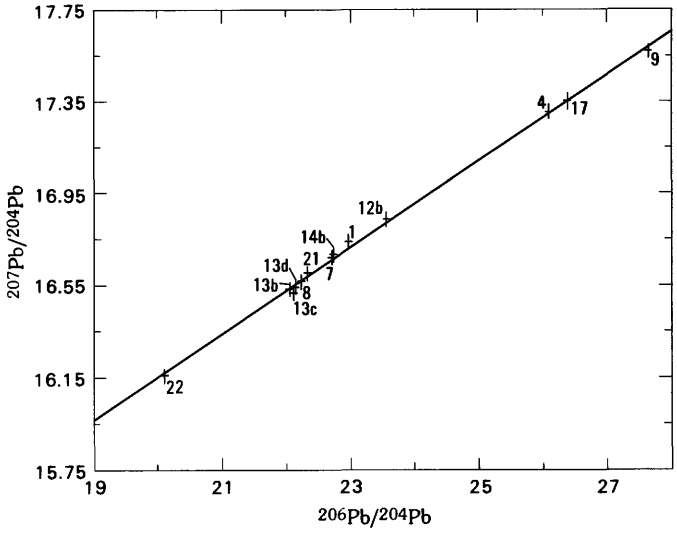

FIGURE 3.—Lead-lead isochron plot for granite samples from the Owl Creek Mountains. Symbol size corresponds to ±2σ errors. Slope of the isochron (0.18834±0.00380) corresponds to an age of 2730±35 Ma. Intercept is 12.382±0.089.

The range in calculated initial $^{208}Pb/^{204}Pb$ ratios is very large (32.472 to 33.689) relative to that observed for calculated initial $^{87}Sr/^{86}Sr$ ratios (0.7025 to 0.7047, Hedge and others, this volume). However, the range in initial lead compositions can be accounted for by a range of 11 to 59 for $^{232}Th/^{204}Pb$ in the source region. (The calculations assume an age of 3.2 Ga for the source region and an initial $^{208}Pb/^{204}Pb$ ratio of 32.202 from the model of Stacey and Kramers, 1975.) Ranges in $^{232}Th/^{204}Pb$ in excess of 200 have been noted for cogenetic suites of granite (for example, Stuckless and Nkomo, 1978), and thus, large variations in initial $^{208}Pb/^{204}Pb$ are reasonable for a heterogeneous source region.

The assumed age of the source region of 3.2 Ga is supported by the low initial $^{208}Pb/^{204}Pb$ calculated for sample TD22 (32.472) and a calculated initial $^{208}Pb/^{204}Pb$ for a feldspar (32.64, Nkomo and others, 1978). Such low values require a $^{232}Th/^{204}Pb$ in the source that is significantly lower than that of the average orogene of Stacey and Kramers (1975) for at least the time period of 3.1–2.7 Ga. Granulite facies rocks of approximately 3.2-Ga age are reported for the Beartooth Mountains to the northwest (Henry and others, 1981; Wooden and others, 1981), and therefore, 3.2 Ga has been used to calculate $^{232}Th/^{204}Pb$ ratios in the source region.

Data for all but two of the samples that scatter about the reference isochron in the thorium-lead system plot along a lead-lead isochron within the limits of analytical precision (fig. 3). The resulting age is 2,730±35 Ma, which is slightly older than (but not distinct from) that obtained by rubidium-strontium dating (2,640±125 Ma, Hedge and others, this volume). Not shown on figure 3 are two samples (58180 and TDG46) that plot along the trends for thorium-lead isotopic data (fig. 1) and the $\delta^{18}O$-initial $^{208}Pb/^{204}Pb$ data (fig. 2). These samples have been mineralized and plot below the lead-lead isochron. This direction of displacement from the lead-lead isochron indicates that mineralization occurred long after crystallization of the granite, as discussed in the next section.

Also excluded from figure 3 are data for the hydrothermally altered samples (TDG47 through 58–98, table 1). Most of these data points are displaced from the lead-lead isochron and plot along a trend for which slope corresponds to an age of about 2,600 Ma. This trend, if shown, would cross the isochron shown on figure 3 at a shallow angle, and therefore some samples (GP–5, 58–98, and 58–66) could be interpreted as belonging to either group.

The excellent linearity of data in the lead-lead system is somewhat surprising in view of the large degree of scatter in the thorium-lead system. Although the source region for the granite had highly variable $^{232}Th/^{204}Pb$ ratios, the variation in $^{238}U/^{204}Pb$ ratios must have been small. As a result, the initial $^{206}Pb/^{204}Pb$ and $^{207}Pb/^{204}Pb$ ratios were fairly similar throughout the granite, and an estimate of the isotopic composition from the intersection of the lead-lead isochron and the model lead-lead secondary isochron of Stacey and Kramers (1975) yield $^{206}Pb/^{204}Pb=14.156$ and $^{207}Pb/^{204}Pb=15.044$. These correspond to an average μ ($^{238}U/^{204}Pb$) of 11.64 for the second stage of the Stacey and Kramers (1975) lead evolution. Thus the average μ for the source material for the 1 b.y. prior to intrusion of the granite was greater than that calculated by

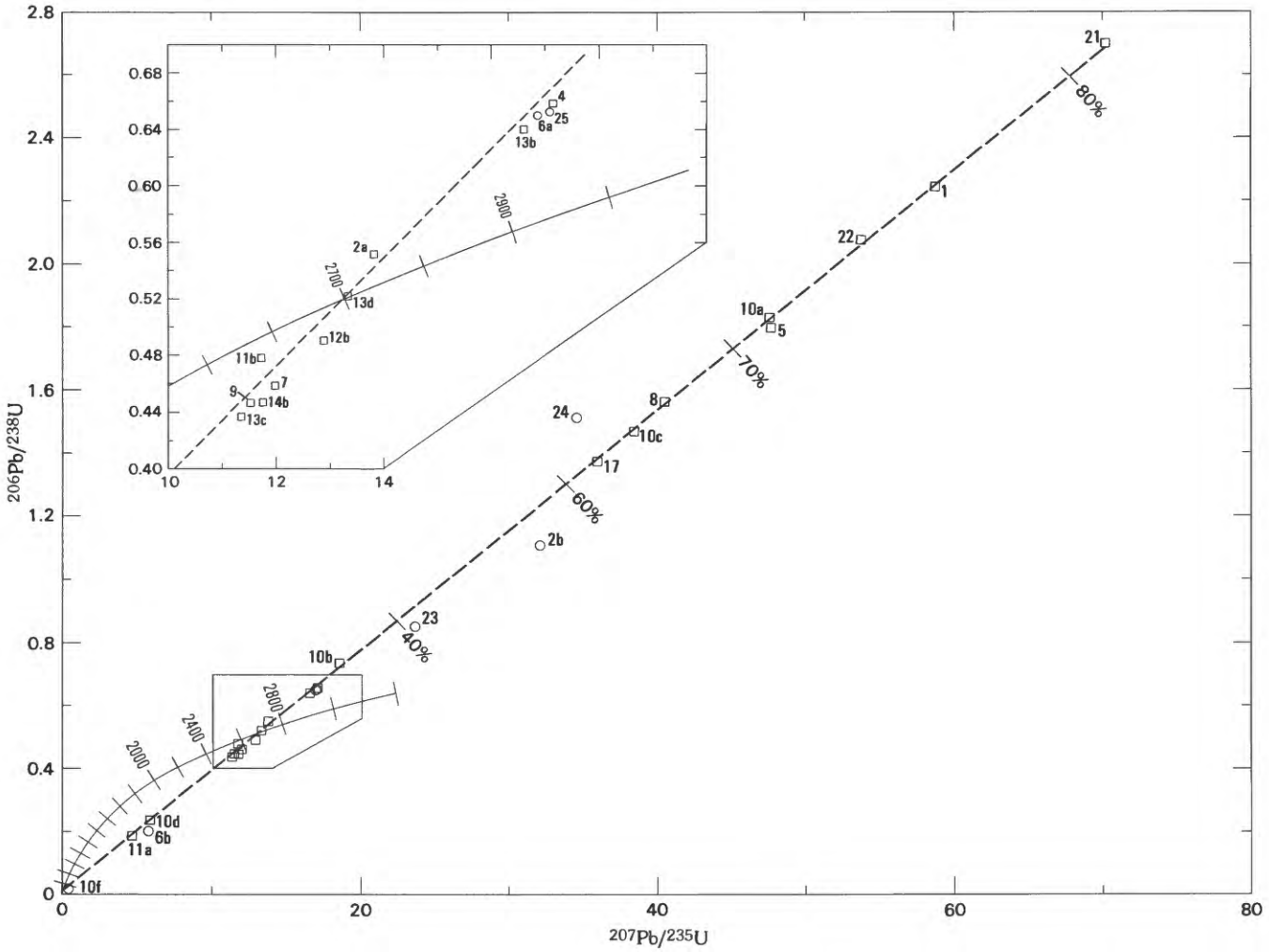

FIGURE 4.—Concordia diagram for all granitic samples from the Owl Creek Mountains. Data for genetically related samples (as defined by extended Q-mode analysis) are shown by squares. Data for apparently unrelated samples are shown by circles. The regressed chord uses data for the first 15 samples in table 1 (those that fit a trend in the thorium-lead system) and intersects concordia at 2,695±20 Ma and 120±40 Ma. The chord is marked to show data positions for Tertiary uranium losses of 40, 60, 70, and 80 percent. Inset shows detail around the upper intercept.

Stacey and Kramers (1975) for an average orogene (9.64). Furthermore, a μ of 11.64 is a minimum value if the metamorphic sequence (which is much less than 1 b.y. older than the granite) is the protolith for the granite. Therefore, the protolith for the granite must have been more strongly enriched in uranium than the average orogene.

The common-lead composition can be used to calculate the radiogenic component of the lead, and a concordia diagram (fig. 4) can then be constructed. Regression of the data for the apparently unaltered samples yields intercept ages of 2,695±20 and 120±40 Ma. Inclusion of data for samples that have been affected by the post-magmatic hydrothermal alteration changes the intercept ages to 2,680±30 and 120±100 Ma. Most of the data for the altered samples plots to the left of the chord for the unaltered samples and indicates at least a partial resetting some time after 2600 Ma.

The lower intercept ages calculated with or without the hydrothermally altered samples are distinctly older than the 20±10 Ma for whole-rock samples from the Granite Mountains (Stuckless and Nkomo, 1978). This difference suggests that the main episode of uranium mobility occurred prior to burial by volcanic detritus in early Tertiary time and prior to formation of the large uranium deposits of the Gas Hills district to the south which formed about 35 Ma (Ludwig, 1979). However, α-activity ratios for three drill-core samples (Nkomo and others, 1978) show marked disequilibrium within the uranium decay chain, which indicates that uranium or its daughter products or both have been mobile within the last hundred thousand years.

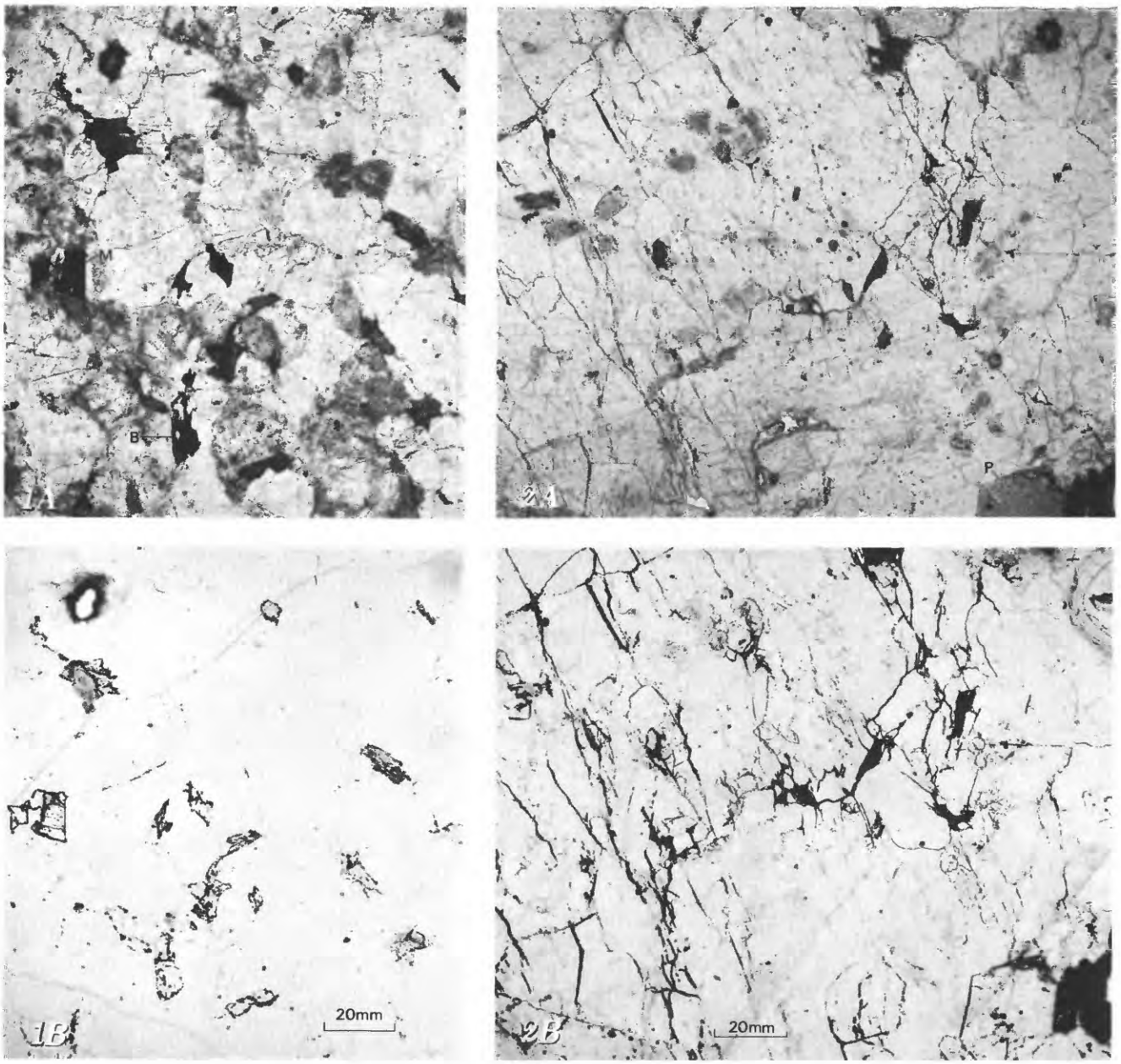

FIGURE 5 (above and facing page).—Photomicrograph (*A*) and fission-track detector (*B*) pairs for granite samples from the Owl Creek Mountains. Mica detectors, directly below corresponding photomicrographs, were photographed from the back side so that correspondence is not mirror image. Mineral abbreviations are M=magnetite, B=biotite, P=plagioclase, I=ilmenorutile, A=allanite, E=epidote, and H=hematite. Samples were irradiated with a total neutron dose of approximately 2×10^{16}/cm^2. Uranium concentrations in excess of 30 ppm appear as black areas.

URANIUM MOBILITY

Figure 4 shows that most of the samples gained or lost some uranium during or just before earliest Laramide time, and that most samples approximated closed-system behavior from the time of intrusion until the Laramide disturbance. These conclusions are supported both by the fit of the data (for the unaltered samples) to a chord within the limits of analytical precision, and by general agreement of the upper intercept age with that determined by rubidium-strontium and lead-lead methods.

Data for samples that are presumed to have been affected by the postulated hydrothermal alteration plot to the left of the chord on figure 4. This displacement can be caused by uranium gain or lead loss at the time of hydrothermal alteration (approximately 2,300 Ma ago, Hedge and others, this volume). The position of

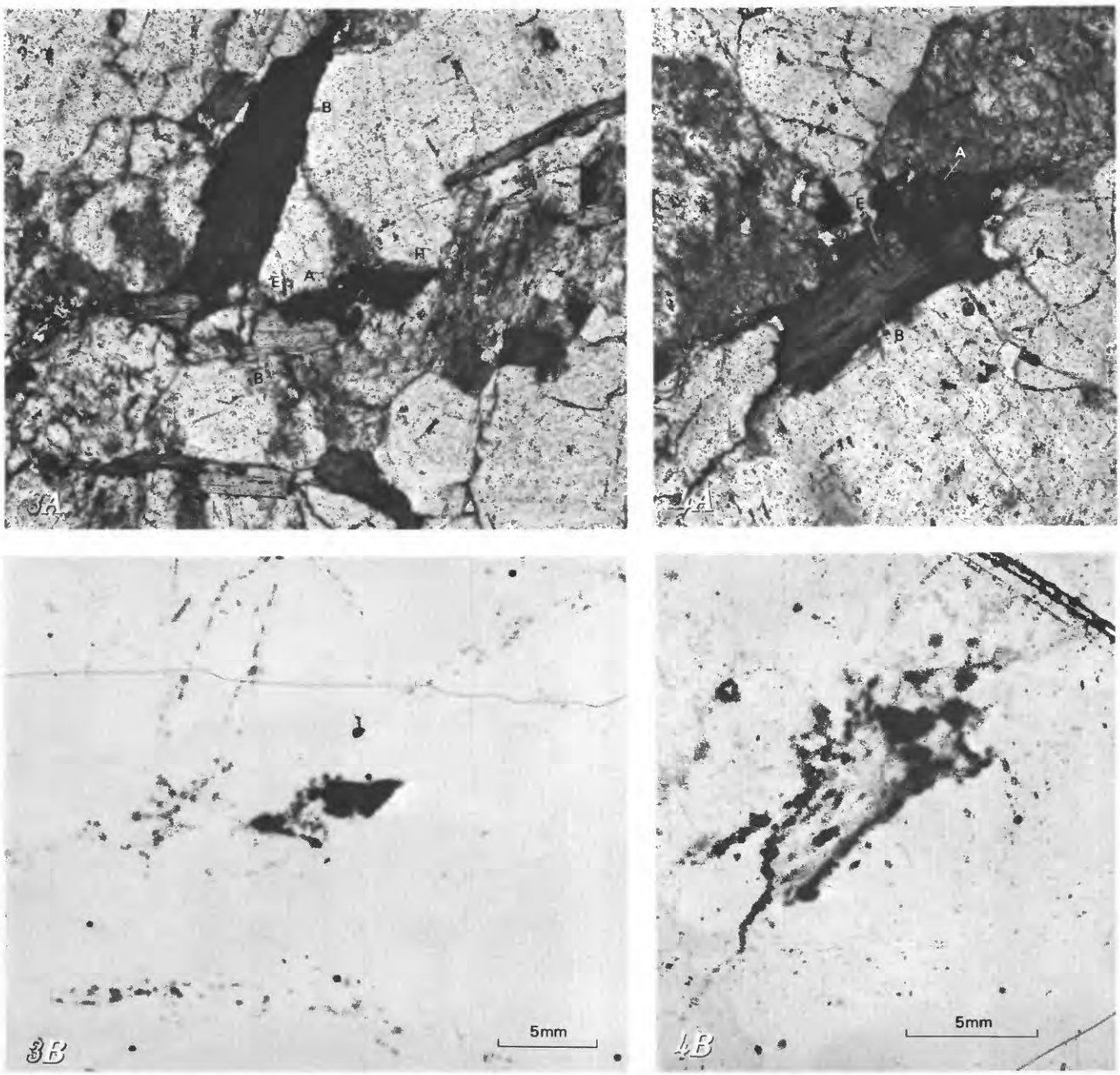

these samples relative to the thorium-lead reference isochron (fig. 1) can be explained by either lead loss or thorium gain. Many studies have shown that thorium is generally immobile in granitic rocks and that lead can be mobilized under many conditions (Manton, 1973; Zielinski and others, 1977; Stuckless and Nkomo, 1978; Doe and Delevaux, 1980; Stuckless, Nkomo and Doe, 1981; Zielinski and others, 1981; Doe and others, 1982). Furthermore, potassium feldspar, which forms a major site for lead in granite, has been altered in the hydrothermal event (Hedge and others, this volume). Thus, all lines of evidence suggest that the altered samples lost lead in response to postmagmatic hydrothermal activity.

The uranogenic portion of the lead and measured uranium contents can be used to estimate the amount and timing of uranium mobility (Stuckless and Nkomo, 1978). The apparent immobility of lead in the thorium-lead system for the unaltered samples (as suggested by the correlation between calculated initial $^{208}Pb/^{204}Pb$ ratios and $\delta^{18}O$ values) indicates that estimates of uranium mobility should be fairly accurate (± 10 percent), with most of the error attributed to the uncertainty in the initial $^{206}Pb/^{204}Pb$ and $^{207}Pb/^{204}Pb$ ratios. Because lead loss from the altered rocks probably occurred not too long after the time of intrusion (relative to the age of the granite), reasonable inferences about uranium mobility can be made for these samples; however, esti-

mates of uranium loss will be slightly low, and estimates of uranium gain will be slightly high. Estimates of uranium mobility have also been made for the eight samples that do not have a cogenetic relationship to the main granite intrusion on the assumptions that the common lead compositions and ages for these samples are not very different from the parameters used to calculate radiogenic leads for the other samples. Interpretation of uranium mobility for these samples is therefore much less certain.

The chord on figure 4 is marked for percent uranium loss. Nine of the data points suggest uranium loss in excess of 60 percent during Laramide time or later. Seven of these points are for surface samples and two are for drill-core samples from a depth of less than 30 m. In contrast, four drill-core samples from depths in excess of 60 m are mineralized and suggest uranium enrichments of 50 to nearly 10,000 percent. The fact that the data points both above and below concordia are colinear indicates that uranium loss from the surface and shallow drill-core samples occurred at the same time as uranium mineralization. Thus, the granite was the most likely source for, as well as host to, the uranium deposit. Samples that lost uranium are confined to the surface and near-surface environment, which suggests oxidizing ground water as a likely medium for uranium transport.

Both postulated uranium gain and loss for specific samples are consistent with the observed uranium distribution within the samples. Figure 5 shows uranium sites for samples that apparently gained or lost varying amounts of uranium. In general, the same primary and secondary uranium sites are present within samples that lost little or no uranium (such as DP–2, figs. 5–1 and 5–4) and those that lost considerable uranium (such as DP–3, fig. 5–3). Most of the uranium is located within zircon, apatite, allanite, and ilmenorutile. These minerals probably constitute the primary or magmatic uranium sites. Epidote, which is commonly enclosed within biotite or allanite (figs. 5–3 and 5–4), generally contains very little uranium. Epidote is paragenetically late, but is nonetheless considered to be a primary site for uranium. Secondary sites include uranium intimately associated with hematite and microscopic opaque inclusions that are titanium-rich. Secondary uranium also occurs along edges, cleavage traces, and fractures in magnetite and biotite. Qualitatively, there appears to be less uranium in secondary sites in samples that show isotopic evidence for more than 50 percent uranium loss (figs. 5–3 and 5–4) than in samples that contain near equilibrium amounts of uranium and radiogenic lead.

Samples for which there is isotopic evidence for uranium gain reveal the same primary and secondary sites for uranium as other samples; but, in addition, secondary uranium occurs along fractures and grain boundaries of felsic minerals (fig. 5–2). There is also a tendency towards replacement of biotite by iron oxides that are highly uraniferous. Leaching experiments of mineralized granite from the Owl Creek Mountains (Maysilles and others, 1977) show that most if not all of the secondary uranium is rapidly removed by either strong acids or bases.

The primary and secondary sites for uranium noted for the granite of the Owl Creek Mountains are similar to those noted for granites that are associated with uranium deposits. Uranium associated with biotite and magnetite has been postulated as a source for the deposits in central Wyoming (Stuckless and others, 1977) and at the Midnite Mine, Wash. (Nash, 1979). A significant difference in uranium distribution for samples from the Owl Creek Mountains is that epidote from the granite of the Granite Mountains has been shown to be uraniferous and to have lost much uranium in the near-surface environment (Stuckless and Nkomo, 1980).

Although both the results of Q-mode factor analysis and uranium-thorium-lead systematics indicate uranium mobility for the granite of the Owl Creek Mountains, comparison of radioelement ratios with those of granite from the Granite Mountains suggests a generally lesser degree of uranium mobility for the former (fig. 6). Both granites are enriched in thorium relative to potassium if compared to an average of 2,500 granites from the contiguous United States (Stuckless and VanTrump, 1982), but the granite of the Granite Mountains is depleted in uranium relative to thorium whereas the granite of the Owl Creek Mountains is enriched. This reflects, in part, the large proportion of drill-core samples for the latter, but Stuckless and Nkomo (1978) reported as much as 80 percent uranium loss for samples from as deep as 400 m for the Granite Mountains, and the deepest sample used in the current study is from 156 m. Thus, uranium in the granite of the Owl Creek Mountains seems to be less labile than that in the granite of the Granite Mountains, both in terms of depth of leaching and in amount of leaching from surface samples.

The lesser degree of uranium mobility, shallower depth of leaching, and smaller outcrop area may explain why the granite of the Owl Creek Mountains is not associated with large, economic uranium deposits. In addition, uranium mobilization for the granite of the Owl Creek Mountains probably predates formation of

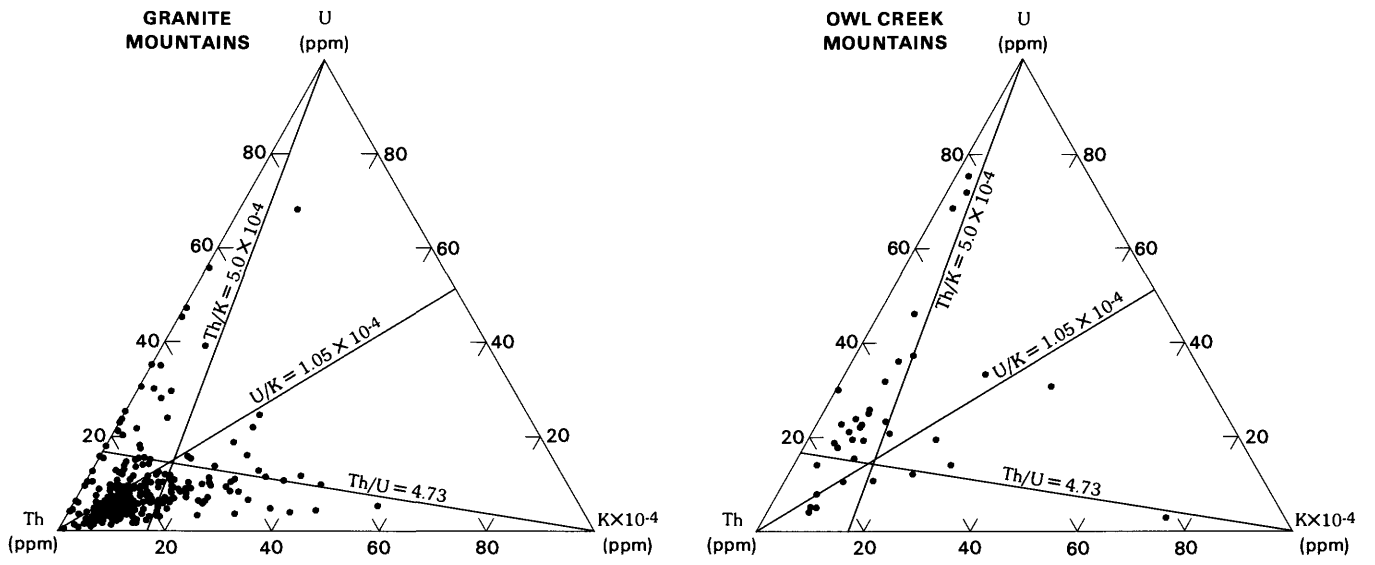

FIGURE 6.—Ternary diagrams for uranium, thorium, and potassium contents for granites from the Owl Creek and Granite Mountains (modified from Stuckless, Bunker, and others, 1981).

the Tertiary sedimentary rocks that host the uranium ore deposits of central Wyoming. As a result, the granite may provide a reasonable uranium source for only those mineralized zones that are located within the fractured portion of the granite.

CONCLUSIONS

Uranium-thorium-lead systematics for granite from the Owl Creek Mountains show that samples unaffected by hydrothermal alteration yield a lead-lead age of 2,730 ± 35 Ma. Large variations in the initial $^{208}Pb/^{204}Pb$ ratio preclude obtaining an age in the thorium-lead system. These variations, like those in initial $^{87}Sr/^{86}Sr$, can be correlated with whole-rock $\delta^{18}O$ values. Hydrothermally altered samples are displaced from both the lead-lead isochron and thorium-lead reference isochron. The direction of displacement is consistent with lead loss that may have occurred during alteration of potassium feldspar to muscovite. A maximum age of 2,600 Ma is indicated for alteration. This age, in combination with the minimum age of 2,300 obtained by the rubidium-strontium whole-rock isochron method, indicates the existence of a previously unknown Early Proterozoic event.

The large variations in initial $^{208}Pb/^{204}Pb$ ratios indicate a large but reasonable variation in $^{232}Th/^{204}Pb$ ratios in the source region of the granite. In contrast, μ values for the source region were fairly uniform such that initial $^{206}Pb/^{204}Pb$ and $^{207}Pb/^{204}Pb$ ratios can be calculated. A minimum μ value of 11.64 indicates a uranium-enriched protolith for the granite.

A concordia plot for the unaltered granite samples yields intercepts of 2,695 ± 20 and 120 ± 40 Ma. The upper intercept agrees with the age obtained by lead-lead and rubidium-strontium whole-rock isochron methods, and the data are colinear within the limits of analytical precision. Therefore, the uranium-lead system appears to have remained closed from the time of intrusion to approximately Laramide time. During early Laramide time or shortly before, mineralized samples gained 50–10,000 percent uranium, and at the same time, most surface and shallow drill-core samples lost 60–80 percent of their uranium. Thus the granite is interpreted to be both source and host for uranium mineralization.

The high degree of uranium mobility in the granite of the Owl Creek Mountains is reasonable in view of the uranium sites within the granite. Much uranium is located along cleavages and grain boundaries of biotite and magnetite where it would be readily accessible to oxidizing ground water. A similar distribution has been noted for uranium in granite associated with large uranium deposits (Stuckless and others, 1977; Nash, 1979). Furthermore, leached granite samples appear to have less uranium associated with biotite and magnetite than samples that contain near-equilibrium amounts of uranium and radiogenic lead.

In spite of the fact that there is much evidence for uranium mobility for the granite of the Owl Creek

Mountains from results of uranium-thorium-lead systematics, Q-mode factor analysis, and petrographic observations, this granite is not associated with large economic deposits. The lack of economic association is thought to be due to the relatively small area of leached granite, the limited depth of leaching, and the fact that mobilization of uranium appears to predate formation of Tertiary sediments that host most of the uranium deposits of central Wyoming.

REFERENCES

Doe, B. R., and Delevaux, M. H., 1980, Lead-isotope investigations in the Minnesota River Valley—Late-tectonic and post-tectonic granites: Geological Society of America Special Paper 182, p. 105–112.

Doe, B. R., Stuckless, J. S., and Delevaux, M. H., 1982, The possible bearing of the granite of the UPH deep drill holes, northern Illinois, on the origin of Mississippi Valley ore deposits: Journal of Geophysical Research, v. 88, p. 7335–7345.

Doe, B. R., and Zartman, R. E., 1979, Plumbotectonics I, the Phanerozoic, *in* Barnes, H. L., ed., Geochemistry of hydrothermal ore deposits: New York, John Wiley and Sons, p. 22–70.

Henry, D. J., Mueller, P. A., and Wooden, J. L., 1981, Early Archean granulite supracrustal assemblages, eastern Beartooth Mountains, Wyoming: Geological Society of America Abstracts with Programs, v. 13, p. 471.

Ludwig, K. R., 1979, Age of uranium mineralization in the Gas Hills and Crooks Gap Districts, Wyoming, as indicated by U-Pb isotope apparent ages: Economic Geology, v. 74, p. 1654–1668.

Manton, W. I., 1973, Whole rock Th-Pb age for the Masuke and Dembe-Divula complexes, Rhodesia: Earth and Planetary Science Letters, v. 19, p. 83–89.

Maysilles, J. H., Nichols, I. L., and Seidel, D. C., 1977, Extracting uranium from a Wyoming granite: U.S. Bureau of Mines Report of Investigations 8219, 15 p.

Nash, J. T., 1979, Uranium and thorium in granitic rocks of northeastern Washington and northern Idaho, with comments on uranium resource potential: U.S. Geological Survey Open-File Report 79–233, 39 p.

Nkomo, I. T., Stuckless, J. S., Thaden, R. E., and Rosholt, J. N., 1978, Petrology and uranium mobility of an early Precambrian granite from the Owl Creek Mountains, Wyoming: Wyoming Geological Association Guidebook, 30th annual field conference, p. 335–348.

Rogers, J. J. W., and Adams, J. A. S., 1969a, Uranium, *in* Wedepohl, K. H., ed., Handbook of geochemistry, v. 2, no. 4: Berlin, Springer-Verlag, p. 92–B to 92–O.

———1969b, Thorium, *in* Wedepohl, K. H., ed., Handbook of geochemistry, v. 2, no. 4: Berlin, Springer-Verlag, p. 90–1 to 90–O.

Rosholt, J. N., Zartman, R. E., and Nkomo, I. T., 1973, Lead isotope systematics and uranium depletion in the Granite Mountains, Wyoming: Geological Society of America Bulletin, v. 84, p. 989–1002.

Stacey, J. S., and Kramers, J. S., 1975, Approximation of terrestrial lead isotope evolution by a two-stage model: Earth and Planetary Science Letters, v. 26, p. 207–221.

Steiger, R. H., and Jäger, E., 1977, Subcommission geochronology—Convention on the use of decay constants in geo- and cosmochronology: Earth and Planetary Science Letters, v. 36, p. 359–362.

Stuckless, J. S., Bunker, C. M., Bush, C. A., Doering, W. P., and Scott, J. H., 1977, Geochemical and petrologic studies of a uraniferous granite from the Granite Mountains, Wyoming: U.S. Geological Survey Journal of Research, v. 5, p. 61–81.

Stuckless, J. S., Bunker, C. M., Bush, C. A., and VanTrump, George, Jr., 1981, Radioelement concentrations in Archean granites of central Wyoming: U.S. Geological Survey Open-File Report 81–948, 40 p.

Stuckless, J. S., and Nkomo, I. T., 1978, Uranium-lead isotope systematics in uraniferous alkali-rich granites from the Granite Mountains, Wyoming: Implications for uranium source rocks: Economic Geology, v. 73, p. 427–441.

———1980, Preliminary investigations of U-Th-Pb systematics on uranium-bearing minerals from two granitic rocks from the Granite Mountains, Wyoming: Economic Geology, v. 75, p. 289–295.

Stuckless, J. S., Nkomo, I. T., and Doe, B. R., 1981, U-Th-Pb systematics in hydrothermally altered granites from the Granite Mountains, Wyoming: Geochimica et Cosmochimica Acta, v. 45, p. 635–645.

Stuckless, J. S., and VanTrump, George, Jr., 1982, A compilation of radioelement concentrations in granitic rocks of the contiguous United States: Proceedings of the IAEA/OECD Symposium on Uranium Exploration Methods, p. 191–208.

Wedepohl, K. H., 1974, Lead—abundance in common magmatic rock types—Crustal abundance, *in* Wedepohl, K. H., ed., Handbook of geochemistry, v. 2: Berlin, Springer-Verlag, p. 82–E–1 to 82–E-18.

Wooden, J. L., Muellers, P. A., and Bowes, D. R., 1981, Archean crustal evolution in the Beartooth Mountains, Montana–Wyoming: Geological Society of America Abstracts with Programs, v. 13, p. 585.

Yellich, J. A., Cramer, R. T., and Kendall, R. G., 1978, Copper Mountain, Wyoming, uranium deposit—rediscovered: Wyoming Geologic Association Guidebook, 30th annual field conference, p. 311–327.

York, Derek, 1969, Least-squares fitting of a straight line with correlated errors: Earth and Planetary Science Letters, v. 5, p. 320–324.

Zielinski, R. A., Lipman, P. W., and Millard, H. T., Jr., 1977, Minor-element abundances in obsidian, perlite, and felsite of calc-alkalic rhyolites: American Mineralogist, v. 62, p. 426–437.

Zielinski, R. A., Peterman, Z. E., Stuckless, J. S., Rosholt, J. N., and Nkomo, I. T., 1981, The chemical and isotopic record of rock-water interaction in the Sherman Granite, Wyoming and Colorado: Contributions to Mineralogy and Petrology, v. 78, p. 209–219.

*U.S. GOVERNMENT PRINTING OFFICE: 1986-676-047:26031